



NTNU – Trondheim
Norwegian University of
Science and Technology

Multiple Holdup Solutions and the Effect of Interface Level Gradients

Even Andersen

Master of Science in Product Design and Manufacturing

Submission date: June 2012

Supervisor: Ole Jørgen Nydal, EPT

Norwegian University of Science and Technology
Department of Energy and Process Engineering

MASTEROPPGAVE

for

Stud.techn. Even Andersen

Våren 2012

Multiple holdup solutions and the effect of interface level gradients

Flere løsninger for lagdelt strøm: effekt av nivåendringer

Background

The two fluid model is the basis for most commercial engineering tools used to estimate liquid content and pressure drop in production pipelines. This model has been found to have multiple holdup solutions for inclined gas-liquid flows where the liquid volume flow rate is less than about 1% of the gas flow rate. In this case, the two fluid model has three solutions, one corresponding to friction dominated flow (low holdup solution) and two corresponding to gravity dominated flow (back flow along the wall and a high holdup solution). Physical arguments exclude the middle holdup solution. However, the possible coexistence of the low and high holdup solution has been the subject of considerable discussion in the scientific community.

Objectives

The objectives of the work are to investigate the following hypothesis: The holdup of a pipe segment operated in the multiple holdup solution will be determined by the holdup of the downstream pipe segment which has a different inclination and is operated in the single holdup solution region.

Tasks

The thesis will consist of the following tasks:

1) *Steady state simulations with CFD software*

Two dimensional flow: Assume fully developed steady state flow between to infinite planes.

- I. Assume zero gradients at the outlet and investigate if multiple holdup solutions are possible for two different liquid loadings 1 % and 0.1 %. Flow rates, physical and geometrical parameters will have to be decided by discussion.
- II. Study the effect of the holdup of the downstream pipe segment by imposing hydraulic gradients on the low and high holdup solution at the outlet.

Three dimensional flow: Assume fully developed steady state flow in a cylindrical geometry (pipe) and repeat I and II for this flow configuration.

2) *Transient simulations with CFD software*

If time allows, the dynamics associated with the high and low holdup solution are to be investigated. Experiments indicate that the low holdup solution should be relatively smooth while large waves are expected on the high holdup solution. The aim will be to perform one simulation at

statistically steady state for both the high and low holdup solution. The interfacial waves and secondary flows in the cross section are of special interest.

” - ”

Senest 14 dager etter utlevering av oppgaven skal kandidaten levere/sende instituttet en detaljert fremdrift- og eventuelt forsøksplan for oppgaven til evaluering og eventuelt diskusjon med faglig ansvarlig/veiledere. Detaljer ved eventuell utførelse av dataprogrammer skal avtales nærmere i samråd med faglig ansvarlig.

Besvarelsen redigeres mest mulig som en forskningsrapport med et sammendrag både på norsk og engelsk, konklusjon, litteraturliste, innholdsfortegnelse etc. Ved utarbeidelsen av teksten skal kandidaten legge vekt på å gjøre teksten oversiktlig og velskrevet. Med henblikk på lesning av besvarelsen er det viktig at de nødvendige henvisninger for korresponderende steder i tekst, tabeller og figurer anføres på begge steder. Ved bedømmelsen legges det stor vekt på at resultatene er grundig bearbeidet, at de oppstilles tabellarisk og/eller grafisk på en oversiktlig måte, og at de er diskutert utførlig.

Alle benyttede kilder, også muntlige opplysninger, skal oppgis på fullstendig måte. For tidsskrifter og bøker oppgis forfatter, tittel, årgang, sidetall og eventuelt figurnummer.

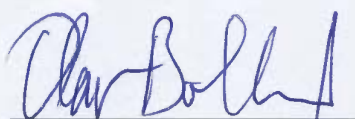
Det forutsettes at kandidaten tar initiativ til og holder nødvendig kontakt med faglærer og veileder(e). Kandidaten skal rette seg etter de reglementer og retningslinjer som gjelder ved alle (andre) fagmiljøer som kandidaten har kontakt med gjennom sin utførelse av oppgaven, samt etter eventuelle pålegg fra Institutt for energi- og prosesssteknikk.


Risikovurdering av kandidatens arbeid skal gjennomføres i henhold til instituttets prosedyrer. Risikovurderingen skal dokumenteres og inngå som del av besvarelsen. Hendelser relatert til kandidatens arbeid med uheldig innvirkning på helse, miljø eller sikkerhet, skal dokumenteres og inngå som en del av besvarelsen.

I henhold til ”Utfyllende regler til studieforskriften for teknologistudiet/sivilingeniørstudiet” ved NTNU § 20, forbeholder instituttet seg retten til å benytte alle resultater og data til undervisnings- og forskningsformål, samt til fremtidige publikasjoner.

Besvarelsen leveres digitalt i DAIM. Et faglig sammendrag med oppgavens tittel, kandidatens navn, veileders navn, årstall, institutt navn, og NTNUs logo og navn, leveres til instituttet som en separat pdf-fil. Etter avtale leveres besvarelse og evt. annet materiale til veileder i digitalt format.

NTNU, Institutt for energi- og prosesssteknikk, 16. januar 2012


Olav Bolland
Instituttleder


Ole Jørgen Nydal
Faglig ansvarlig/veileder

Medveileder: Peter Sassan Johansson, Statoil Forskningscenter

Abstract

Simulations on liquid loads and flow rates which the Taitel-Dukler model predicts to have multiple solutions have been performed with ANSYS Fluent and LedaFlow. Both steady state and transient results in one, two and three dimensional flows are reported in this work. The hypothesis that the holdup of a pipe operated in the multiple solution region will be determined by the downstream holdup is investigated. Some results indicate that the hypothesized interface level gradients effects are correct.

The Fluent steady state simulations had mass imbalance issues in addition to being both grid and geometry dependent, but produced results consistent with the independent Fluent transient simulations. The one dimension LedaFlow solver illustrated the effect shear stress modeling have on the multivalued solution region. The solver chose the intermediate solution for some flow rates, which by physical arguments can be excluded. The novel solver LedaFlow Q3D produced transient results displaying the wavy surface of the high holdup solutions. The results from the different models are deviating, but it is hard to predict which results are most the accurate since no comparison with experimental results have been conducted.

Sammendrag

Simuleringer med væskelaster and stømningsrater som ifølge Taitel-Dukler modellen vil gi flere løsninger er utforsket med ANSYS Fluent and LedaFlow. Både stasjonære og transiente resultater i en, to og tre dimensjoer er rapportert. Hypotesen om at holdupen for ett rør som er operert i flerløsningsområdet blir bestemt av holdupen nedstrøms er utforsket. Noen av resultatene indikerer at de hypotisererte effektene av nivåendringer er korrekt.

Fluent stasjonær simuleringene hadde problemer med masse ubalanse og var avhengig av både grid og geometri, men produserte resultat som var konsistent med de uavhengige Fluent transiente simuleringene. Den en dimensjonale LedaFlow løseren viste hvilken effekt skjærkraft modellering har på flerløsningsområdet. Løseren valgte den mellomliggende løsningen for noen strømningsrater, en løsning som kan bli ekskludert som følge av fysiske argumenter. Den nye simulatoren LedaFlow Q3D produserte transiente resultater som viser den bølgete overflaten til de høye holdup løsningene. Avvik i resultatene fra de forskjellige modellene er observert, men det er vanskelig å anslå hvilke resultater som er mest nøyaktig siden det ikke har blitt gjort en sammenligning med eksperimentelle resultater.

Preface

I requested an assignment within multiphase flows of Dr. Sigurd Næss from Statoil Flow Assurance, and he put me in touch with Dr. Peter Sasson Johansson from Statoil Research Centre. Johansson proposed the thesis and became the co-supervisor with Prof. Ole Jørgen Nydal from NTNU as the formal advisor representing the University.

The thesis consists of a special flow feature existing in stratified multiphase flow. Several multiphase flow simulators have been used to produce results on this particular flow, which has been both a challenging and a rewarding experience.

I would like to thank my supervisors for their guidance during my work with the thesis. Johansson's feedback on the work has been very helpful. Many have made contributions to my work. I would like to thank Dr. Sjur Mo and Dr. Alireza Ashrafi from SINTEF Materials and Chemistry assisting with the LedaFlow simulations as well as feedback. I would also like to thank Dr. Stein Tore Johansen (SINTEF) and Dr. Carl Birger Jenssen (Statoil). Their assistance is appreciated.

Even Andersen, June 11, 2012. Trondheim

Contents

Background and Objective	i
Abstract	iii
Sammendrag	iii
Preface	iv
Contents	v
Nomenclature	vi
List of Figures	viii
1 Theory	1
1.1 Introduction	1
1.2 Studies in Literature	2
1.3 Two-Fluid Based Model	4
1.4 Volume-of-Fluid Model	7
1.5 Quasi-Three-Dimensional Model	11
2 Results and Analysis	13
2.1 Geometry and Mesh	13
2.2 Taitel & Duckler's Two-Fluid Model	15
2.3 LedaFlow 1D Steady State	17
2.4 Fluent 2D Steady State	20
2.5 Fluent 2D Transient	27
2.6 Fluent 3D Steady State	31
2.7 LedaFlow Q3D Transient	34
3 Discussion	43
4 Conclusion	47
Appendices	50
A - Turbulence	50
B - LedaFlow Profile Model	61
C - User Defined Functions	61
D - Data	61
Bibliography	73

Nomenclature

LL	Liquid loading = U_{sl}/U_{sg} (-)
U_{sl}	Superficial liquid velocity = Q_l/A (m/s)
U_{sg}	Superficial gas velocity = Q_g/A (m/s)
Q	Volume flow rate (m^3/s)
A	Area (m^2)
ρ	Density (kg/m^3)
u	Velocity (m/s)
γ	Velocity shape factor (-)
g	Gravitational constant (m/s^2)
t	Time (s)
p	Pressure (N/m^2)
τ	Shear stress (N/m^2)
β	Inclination (rad)
f	Friction factor (-)
Re	Reynolds number (-)
μ	Molecular viscosity (kg/ms)
D_h	Hydraulic diameter (m)
h	Average wave height (m)
α	Volume fraction (-)
V	Volume (m^3)
σ	Surface tension (N/m)
g	Subscript: Gas phase
l	Subscript: Liquid phase
i	Subscript: Interface
'	Superscript: Local
"	Superscript: Fluctuating
L	Superscript: Binary phase indicator
LSI	Superscript: Large-scale interfaces

List of Figures

1.1	Illustrative velocity profiles	1
1.2	Multiple holdup solutions	3
1.3	Slice averaging	11
2.1	Ideal geometries	13
2.2	Basic meshes	14
2.3	TD model. LL=0.1%. Holdup and pressure gradient	16
2.4	TD model. LL=0.01%. Holdup and pressure gradient	16
2.5	LedaFlow 1D. LL=0.1%. Holdup and pressure gradient	18
2.6	LedaFlow 1D. LL=0.01%. Holdup and pressure gradient	18
2.7	LedaFlow 1D. Combined. Holdup and pressure gradient	18
2.8	Fluent 2D. Liquid level versus holdup for pipe and channel	20
2.9	Fluent 2D. Mass imbalance	21
2.10	Fluent 2D. Mesh refinement	21
2.11	Fluent 2D. Fully developed regions	23
2.12	Fluent 2D. Critical flow rate on low mesh	23
2.13	Fluent 2D. LL=0.1%. Holdup and pressure gradient. Steady	24
2.14	Fluent 2D. LL=0.01%. Holdup and pressure gradient. Steady	24
2.15	Fluent 2D. Combined. Holdup and pressure gradient. Steady	24
2.16	Fluent 2D. LL=0.1%. Interface level gradient	25
2.17	Fluent 2D. LL=0.01%. Interface level gradient	25
2.18	Fluent 2D. LL=0.1%. Velocity profiles high holdup	26
2.19	Fluent 2D. LL=0.01%. Velocity profiles high holdup	26
2.20	Fluent 2D. LL=0.1%. Velocity profiles low holdup	26
2.21	Fluent 2D. LL= 0.1% Holdup versus time. Geo#1	28
2.22	Fluent 2D. LL= 0.01% Holdup versus time. Geo#1	28
2.23	Fluent 2D. LL= 0.01% Holdup versus time. Geo#2	28
2.24	Fluent 2D. LL= 0.1%. Holdup and pressure gradient. Transient	29
2.25	Fluent 2D. LL= 0.01%. Holdup and pressure gradient. Transient	29
2.26	Fluent 2D. Velocity profiles. Snapshot of wave top and bottom	29
2.27	Fluent 2D. LL= 0.1%. Velocity profiles	30
2.28	Fluent 2D. LL= 0.01%. Velocity profiles	30
2.29	Fluent 2D. Domain emptying	31

2.30	Fluent 2D. Domain emptying. Snapshot Geo#1	31
2.31	Fluent 3D. LL=0.1%. Liquid holdup and pressure gradient	32
2.32	Fluent 3D. LL=0.01%. Liquid holdup and pressure gradient	33
2.33	Fluent 3D. Holdup profiles high holdup	34
2.34	Fluent 3D. Velocity profiles high holdup	34
2.35	Fluent 3D. Velocity profile low holdup	34
2.36	LedaFlow Q3D. LL=0.1%. Holdup. Snapshot of domain. Geo#1	35
2.37	LedaFlow Q3D. LL=0.01%. Holdup. Snapshot of domain. Geo#1	36
2.38	LedaFlow Q3D. LL=0.01%. Holdup. Snapshot of domain. Geo#2	37
2.39	LedaFlow Q3D. LL=0.1%. Holdup versus time. Geo#1.	37
2.40	LedaFlow Q3D. LL=0.01%. Holdup versus time. Geo#1.	38
2.41	LedaFlow Q3D. LL=0.01%. Holdup versus time. Geo#2.	38
2.42	LedaFlow Q3D. LL=0.1%. Holdup and pressure gradient	39
2.43	LedaFlow Q3D. LL=0.01%. Holdup and pressure gradient	39
2.44	LedaFlow Q3D. Snapshot of wave top and bottom	41
2.45	LedaFlow Q3D. Actual velocity profile	41
2.46	LedaFlow Q3D. LL=0.1%. Velocity profile. Geo#1	42
2.47	LedaFlow Q3D. LL=0.01%. Velocity profile. Geo#1	42
2.48	LedaFlow Q3D. LL=0.01%. Velocity profile. Geo#2	42

Chapter 1

Theory

1.1 Introduction

Flow in a pipe or a channel with two or more fluids, such as liquid and gas, can take on several flow regimes depending on the flow rates of the fluids. These regimes are generally classified as either stratified, annular, slug or dispersed flows. This work is on stratified gas-liquid flows that are inclined slightly upwards with very low liquid to gas volume flow rates (liquid load, LL). The fraction of the volume of the pipe filled with liquid to the total pipe volume (liquid holdup, or just holdup) and the pressure gradients for a range of flow rates will be of particular interest.

There will be flow rates for upward gas-liquid flows that produce shear stresses on the interface that are much greater in magnitude than the contribution of the gravitational body forces. The result is a flow with a low liquid holdup. Reducing the flow rate will alter the magnitude of these two forces in favor of gravity. At one point, some of the liquid will begin to flow backwards along the wall, increasing the liquid holdup significantly. These two described flow situations are illustrated to the right, with the liquid and gas colored blue and red, respectively. The flow with the lowest holdup will be referred to as *friction dominated* and the flow with highest holdup as *gravity dominated*.

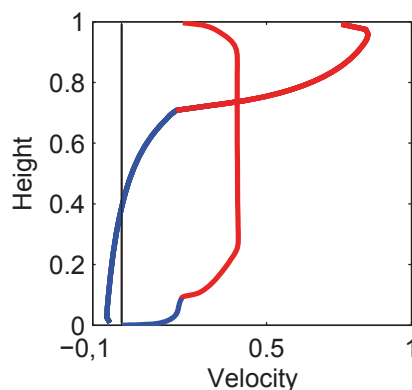


Figure 1.1: Illustrative velocity profiles. *Friction dominated* with lowest holdup. *Gravity dominated* with highest holdup and back-flow along the wall.

Any given flow rate will have *one* solution corresponding to one liquid holdup. However, the situation for the very low liquid loadings investigated in this work deviates from the norm. The model equations will have multiple solutions for flow rates in a certain region. One solution corresponding to friction dominated flow, and two solutions corresponding to gravity dominated flows with back-flow along the wall.

1.2 Studies in Literature

Some of the earliest work on stratified two-phase flows started with Lockart and Martinelli in 1949 [27], and has since been a major area of fluid mechanics. One of the most significant papers on the subject was written by Taitel and Dukler in 1976 [31] in which they introduced a two-fluid model that could predict liquid holdup, pressure gradients, flow regimes and flow regime transitions. Their two-fluid model will be referred to as the TD model in this work. Only some years later in 1987 did Baker and Gravestock [9] first point out that this model predicts non-unique solutions for given flow rates in upward inclined flows.

It became important to determine if more than one solution could be physically realizable, if they possibly could coexist, and which solution the model will choose in this multivalued solution region.

Landman [23] presented a few years later a theoretical investigation on this issue, in which he showed that the multiple holdups in upward stratified flows are not an artifact of the TD model. He discovered that the exact solution for the simpler laminar two phase flow in an inclined rectangular closed duct predicts similar behavior.

Figure 1.2 displays the appearance of such multivalued solution regions predicted by the TD model. From his stability analysis he concluded that the lowest holdup solution that is displayed as the blue line in Figure 1.2 is the most stable, the highest holdup (green) will be unstable, and the intermediate holdup (red) either stable or unstable. As a criteria for instability he used ill-posedness and Kelvin-Helmholtz (K-H) instability that considers exponential growth of perturbations around the steady state solution.

Barnea and Taitel published many papers the following years with structural and interfacial stability stratified flows [10], [12], [14], [13], and among them a paper specifically on the multiple solutions for upwards gas-liquid flows [11]. The stability of the steady state solutions were examined, using linear and non-linear analysis, and they concluded that the low holdup solution is always stable, the intermediate solution is always linearly structurally unstable, and the highest holdup solution is almost always unstable both to structural and K-H instability which they interpreted as an indication that this solution does not exist.

Even though the linear structural stability is based on a spatially uniform model that is not consisted with mass conservation due to the removal of the

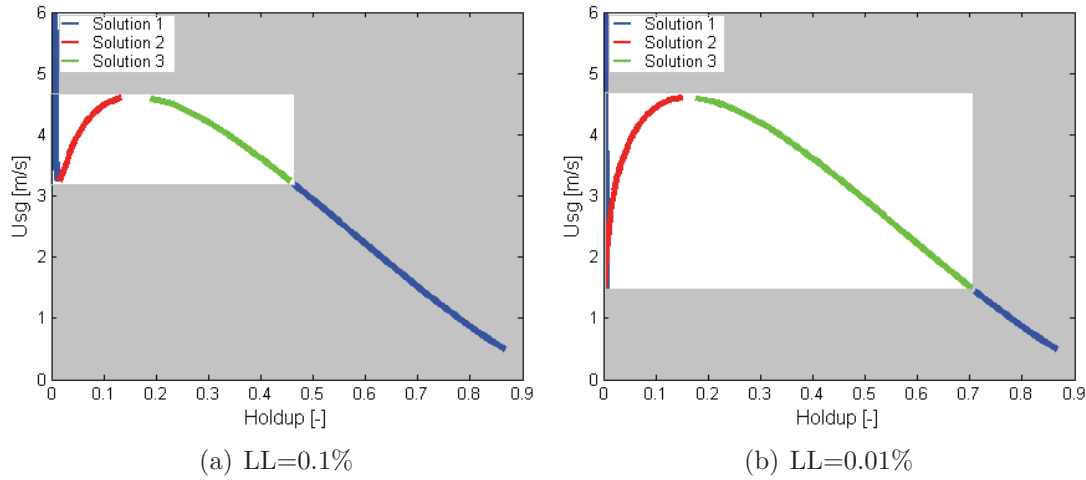


Figure 1.2: Multiple holdup solutions from TD model. Flow rate on the vertical axis and liquid holdup on the horizontal axis.

convective term, physical reasoning can illuminate the nature of the intermediate solution. As Johansson [21] pointed out; the holdup for the intermediate solution will increase with increasing gas velocities (see Figure 1.2), and can therefore be considered unphysical since the information on increasing gas velocities has to be transported vertically through the liquid layer.¹

In 1992 Brauner and Maron [16] published a more general liquid-liquid stability analysis, but still valid for stratified gas-liquid flows. Following the stability analysis, in which a velocity shape factor² has been introduced in the convective term in the momentum equation, will produce interesting information on the multiple holdup region as Johansson has shown in [21]. These shape factors will not influence the steady state conditions but it has been shown that they can have significant impact on the dynamic stability of the TD model. Particularly if they become very large for the liquid phase, which is the case for gravity dominated flows with low liquid loading when the up- and downstream flux are almost equal. The stability method used is that of viscous K-H and well-posedness which requires real characteristics of the TD model for a solution to be well-posed. If imaginary characteristics are found it is assumed that the stratified flow regime is not possible, implying that there must be a transition to another flow regime such as slug or dispersed flow. Large shape factors typically makes ill-posed solutions well-posed, arguing for the existence of the high holdup solution. Estimating the value of shape factors though, is no easy task. Currently no good estimation approach has been found and it is therefore usually set to unity in multiphase flow simulators.

¹An extended explanation of the argument of inconsistency can be found on page 17

²For the definition and use of velocity shape factor see Eq. 1.2 and 1.4 on page 5

The paper by Ullmann, Zamir, Gat and Brauner from 2003 [33] experimentally proved for the first time that multiple holdups are possible for co-current flows, just as they previously had found for countercurrent flow [34]. They obtained at least two different, stable holdups in liquid-liquid upward flow for the same operational conditions, and showed that different operational protocol results in different holdups, hence, hysteresis³ phenomena are involved.

Other experiments such as the one presented by Smith et.al in 2003 [30], found that the data generally supported the published theoretical works that recommend that one accept the solution yielding the lowest liquid holdup. No hysteresis was observed in the calculated multiple solution region.

Statoil together with Total have performed ramp-up and ramp-down experiments of gas-liquid flow with very low liquid loading to investigate hysteresis [21]. This experiment, when published, will add much needed experimental data on multiple solutions, as the available data is scarce. In addition to experiments Johansson [21] used the simulation program OLGA by SPT Group [4] to identify the multiple solution region predicted by this model. The same fluid properties is used throughout this work to facilitate a possible comparison between the multiphase flow simulators.

Johansson [21] believes as Sira (2007) [29] that the holdup of the downstream pipe segment may determine whether the low or high holdup solution is the preferred solution in the multivalued solution region. In this work several multiphase flow models will be tested with respect to find multiple solutions, and the effect of these interface level gradients (downstream holdup) on the multivalued solution region.

1.3 Two-Fluid Based Model

The TD model is a one dimensional representation of an actual pipe or channel flow. The cross-section averaging generates a plug⁴ velocity and pressure for each phase, leaving only temporal and axial variations. The shear stresses, which are based on the cross-sectional variations, therefore have to be introduced explicitly. The shear stress modeling have to take into account the effects of turbulence in both phases, the waves on the interface between them, and cross-sectional variations such as back-flow along the wall. The result is that it is very difficult to find general models that are sufficiently good for all flow situations.

In multiphase flows with low liquid loading, such as in the multivalued solution region, the physics of droplets might be the dominant mechanism for transporting the liquid. In these cases a droplet field has to be included where the entrainment

³Hysteresis is the dependence of a system not only on its current environment but also on its past environment.

⁴In plug flow, the velocity and pressure of the fluid is assumed to be constant across any cross-section of the pipe perpendicular to the axis of the pipe.

modeling is essential. Both OLGA [4] and LedaFlow 1D [3] have extended the TD model and included this among other phenomena in their models. It will add complexity to the governing equations, but to keep this 1D presentation simple and to the point, the model equations by Brauner and Moalem Maron in [16] will be presented. More information on OLGA is given in [15], and LedaFlow 1D in [20] [18], [22] and [6].

Model Equations

The continuity equations state that the amount of mass can only change by the amount that passes in or out of the region through the boundary.

$$\frac{\partial}{\partial t}(\rho_g A_g) + \frac{\partial}{\partial x}(\rho_g A_g u_g) = 0, \quad \frac{\partial}{\partial t}(\rho_l A_l) + \frac{\partial}{\partial x}(\rho_l A_l u_l) = 0 \quad (1.1)$$

The momentum equations describe unsteady and convective acceleration on the left hand side, while the right hand side consists of the surface and body forces.

$$\begin{aligned} \frac{\partial}{\partial t}(\rho_g A_g u_g) + \frac{\partial}{\partial x}(\rho_g A_g \gamma_g u_g^2) = \\ - \tau_g S_g + \tau_i S_i + \rho_g A_g g \sin \beta - \frac{\partial}{\partial x}(A_g P_g) + P_{ig} \frac{\partial A_g}{\partial x} \end{aligned} \quad (1.2)$$

$$\begin{aligned} \frac{\partial}{\partial t}(\rho_l A_l u_l) + \frac{\partial}{\partial x}(\rho_l A_l \gamma_l u_l^2) = \\ - \tau_l S_l - \tau_i S_i + \rho_l A_l g \sin \beta - \frac{\partial}{\partial x}(A_l P_l) + P_{il} \frac{\partial A_l}{\partial x} \end{aligned} \quad (1.3)$$

where the lowercase g and l indicates the phases gas and liquid. A , S , U , τ , τ_i are the cross-sectional area, the wetted perimeter, the axial velocity, the wall shear stress and the interfacial shear stress. P_{ig} and P_{il} are the interface pressures for the respective phases and may be different due to surface tension effects.

The shape factors, γ_g and γ_l are defined in terms of the local velocity profiles, $u'_{g,l}$.

$$\gamma_g = \frac{1}{A_g u_g^2} \int_0^{A_g} u_g'^2 dA_g, \quad \gamma_l = \frac{1}{A_l u_l^2} \int_0^{A_l} u_l'^2 dA_l \quad (1.4)$$

As discussed in the previous section, very large shape factors can have an impact on the stability of the high holdup solution. Currently no valid approach as to estimating these values has been proposed, and their value are therefore set to one in LedaFlow and OLGA.

Solutions for liquid holdup and pressure gradients are highly dependent on the shear stress modeling. They are conventionally defined as

$$\tau_g = \frac{f_g}{2} \rho_g u_g |u_g|, \quad \tau_l = \frac{f_l}{2} \rho_l u_l |u_l|, \quad \tau_i = \frac{f_i}{2} \rho_g (u_g - u_l) |u_g - u_l| \quad (1.5)$$

The friction factors, f_g and f_l , should take into account effects such as turbulence and secondary flows in the pipe. The interfacial friction factor, f_i , also has to account for waves on the interface between the phases etc. Regardless of their value it should be noted that the shear stress modeling results in non-linear functions. A region of multiple solutions is expected for all reasonable multiphase flow models.

There are several methods of obtaining the friction factors. Taitler and Dukler in their two fluid model uses the Fanning's friction factors

$$f_g = C_g \text{Re}_g^{-m}, \quad f_l = C_l \text{Re}_l^{-n} \quad (1.6)$$

with the values for C_g , C_l , m and n depending on geometry and flow regime (laminar or turbulent based on the phase Reynolds numbers). By assuming a smooth interface and much larger gas velocity than interface velocity, the modeling of the interface shear stress τ_i is reduced to $\tau_i = \tau_g$.

The gas and liquid Reynolds numbers Re_g and Re_l , and the gas and liquid hydraulic diameters D_{hg} , D_{hl} are defined in the following manner

$$\text{Re}_g = \frac{\rho_g u_g D_{hg}}{\mu_g}, \quad \text{Re}_l = \frac{\rho_l u_l D_{hl}}{\mu_l}, \quad (1.7)$$

$$D_{hg} = \frac{\alpha_g \pi D^2}{S_g + S_i}, \quad D_{hl} = \frac{\alpha_l \pi D^2}{S_l} \quad (1.8)$$

and used in this form for all the models discussed here.

OLGA on the other hand, calculates a turbulent and laminar friction factor for each phase and uses the maximum.⁵ The turbulent friction factors are

$$f_{tg} = 0.0055 \left[1 + \left(\frac{2 \cdot 10^4 \epsilon}{D_{hg}} + \frac{10^6}{\text{Re}_g} \right)^{1/3} \right]$$

$$f_{tl} = 0.0055 \left[1 + \left(\frac{2 \cdot 10^4 \epsilon}{D_{hl}} + \frac{10^6}{\text{Re}_l} \right)^{1/3} \right] \quad (1.9)$$

where ϵ is the absolute pipe roughness. The laminar friction factors are given as

$$f_{lg} = 64/\text{Re}_g, \quad f_{ll} = 64/\text{Re}_l \quad (1.10)$$

A value for the average wave height is obtained by assuming that mass flow forces in the gas balance the the gravitational and surface tension forces. This average wave height determines the nature of the surface (smooth or wavy), and allows different friction factors for the interface to be calculated. If the surface is smooth the standard friction factors presented above are used with zero pipe roughness. If it is wavy then the minimum values of the following friction factors

⁵Might be changes in the current version of the software since this is based on [15] from 1991

are used

$$f_i = \frac{h_w}{D_{hi}}, \quad f_i = 0.02(1 + K v_l) \quad (1.11)$$

where h_w is the mentioned average wave height and K is a empirically determined coefficient.

LedaFlow uses Håland's explicit formula as an approximation of the implicit Colebrook-White equation for the gas-wall and liquid-wall friction factors for Reynolds numbers indicating turbulent flow [22]

$$\frac{1}{\sqrt{f_g}} = -3.6 \log_{10} \left[\frac{6.9}{\text{Re}_g} + \left(\frac{k}{3.7 D_{hg}} \right)^{1.11} \right] \quad (1.12)$$

$$\frac{1}{\sqrt{f_l}} = -3.6 \log_{10} \left[\frac{6.9}{\text{Re}_l} + \left(\frac{k}{3.7 D_{hl}} \right)^{1.11} \right] \quad (1.13)$$

where k the relative roughness. No more information is published on the LedaFlow 1D model . One approach to model the interface shear stresses that should be noted are based on the momentum equations and can be found in [6]. The shear modeling varies from model to model. The effect of an increase in the interfacial friction will be that the region of multiple solutions will be found for lower flow rates. Some deviations are therefore expected between different models.

1.4 Volume-of-Fluid Model

The difference when increasing the dimensions represented in a flow model is that local variations replaces modeling at the cost of increased computational resources. These variations can be decisive in the physical understanding of phenomena such as droplets and interfacial waves.

ANSYS Fluent [2] has a two or three dimensional volume of fluids model (VOF model) that can solve several multiphase flow regimes, among them stratified two phase flow. This model differs from two fluid models in the sense that it solves a single set of momentum equations with interpolated mixture properties. In other words both phases share the same velocity field. It is an Eulerian method where the control volumes are fixed in space and the free surface between the phases are tracked. The tracking of this surface is based on the distribution of the two phases α_g and α_l . The sum of volume fractions is always one, and the surface will be in computational cells where the volume fraction of the phases is between the extremes of 0 and 1.

Simplifications will be made on the modeling equations as they appear in the ANSYS Fluent's Theory Guide [1] to present the essence of the model.

Fluid flow equations

The physical properties of the mixing phase used in the model equations are defined in the following manner

$$\rho = \alpha_l \rho_l + (1 - \alpha_l) \rho_g, \quad \mu = \alpha_l \mu_l + (1 - \alpha_l) \mu_g \quad (1.14)$$

where α_l and α_g are the volume fraction of liquid and gas respectively, and are calculated in the following manner

$$\frac{\partial \alpha_l}{\partial t} + \nabla \cdot (\alpha_l \vec{u}) = 0, \quad \alpha_g = 1 - \alpha_l. \quad (1.15)$$

Together with the the continuity equation

$$\frac{\partial(\rho)}{\partial t} + \nabla \cdot (\rho \vec{u}) = 0 \quad (1.16)$$

and the momentum equations

$$\frac{\partial(\rho \vec{u})}{\partial t} + \nabla \cdot (\rho \vec{u} \vec{u}) = -\nabla p + \nabla \cdot \left[\mu \left(\nabla \vec{u} + \nabla \vec{u}^T \right) \right] + \rho \vec{g} \quad (1.17)$$

they form the basis of the model.

General setup

- A constant surface tension coefficient is set and is equal for all the simulations in this work. This value is used in the continuum surface force model (CSF model), which in turn includes the effects of surface tension as a source term in the momentum equations.
- All the grid resolutions in this work are insufficient to include the effects of turbulence without any modeling. Comparisons of different models lead to the choice of modeling turbulence with the *SST* $k - \omega$ model, as it gave the least deviations from the RSM model results. It merges the advantageous aspects of the $k - \epsilon$ and $k - \omega$ models into one single model, providing a good performance to computational time ratio. With its enhanced wall treatment the turbulence model takes into account the non-dimensional wall distance y^+ , and will therefore be valid for all the different grid resolutions in this work. More on the nature of turbulence and the models Fluent offers can be found in Appendix A. The turbulent properties (k and ω) set as boundary conditions are equal to the values in a fully developed domain obtained from a test case on the respective grid and flow.
- Standard values for under-relaxation factors were used in the results. These factors set the weighting of the previous and the current values forming

the values for the next iteration step. They can help the solver if it "get stuck", and were heavily experimented with in the initial stages of this work to reach converged solutions with satisfying residuals. The residuals is a measure on how much the solver changes a value between each iteration. Modifying the inter-relaxation-parameters did not improve the convergence of the iterations.

- There are also pre-process options such as choice of geometry and how to mesh it⁶. The phases have to be introduced into the domain at the boundaries, preferably through separate inlets in order to minimize the necessary domain. If a combined inlet is used for the simulations, as in this work, the liquid phase will be mixed with the gas, never sedimenting to form a liquid layer along the bottom wall. The disadvantage with separate inlets is that when it is desirable to investigate flows with different inlet sizes, then there has to be *one* mesh for every size. A way to avoid this issue is to introduce the phases on one single boundary through a user defined function (UDF) that can function as two separate inlets, thereby greatly improving the flexibility of the mesh-simulation connection. Sizes and velocities, phases volume fractions and pressures can all be defined on the boundaries. UDFs have been used diligently throughout the Fluent simulations and an example of a 2D and 3D UDF are given in Appendix C.
- Custom Field Functions can also be used, for instance to initialize the domain with a desired velocity profile for a rapid steady state convergence, or an ideal initial state for a transient simulation. The experience obtained in this work with small meshes is that it will generally not be productive to spend much time initializing the domain close to the expected solution.
- Reference values are based on the fluid with the smallest properties for the value in question and the pressure location is consistently located close to the top of the outlet boundary. The gravity is decomposed in order to account for the upward inclination instead of an upward inclined geometry. This will simplify the post-process treatment of the extracted properties, since Fluent's coordinate system is absolute and does not follow the direction of the pipe as it does in LedaFlow.

Solution Methods

- *Pressure-Velocity Coupling.* A projection method is used that solves a pressure correction equation based on the constraint of continuity in the velocity field. Due to the equations nonlinear and coupled nature, an iterative process of the entire set of model equations will be performed until the

⁶The geometries and meshes are presented in Chapter 2.1 on page 13

solution converges. This is best performed with the PISO algorithm for transient simulations, and has also been used for steady state.

- *Spatial Discretization.* The least-squares gradient method was used because it will for the meshes be the least expensive while still providing the same accuracy in the results.
- *Pressure Discretization.* When the body forces are large (high holdup simulations), the body force weighted scheme is used. Including the implicit body forces provides more stability to a scheme that has divergence issues when using segregated algorithms such as PISO. This was only experienced in the first few iterations and solved by running a few transient time steps for a better initialization in the steady state simulations. For the low holdup simulations the PRESTO! discretization scheme will lead to a faster convergence.
- *Momentum and Turbulent Discretization.* First order upwind and second order upwind discretization schemes are used for transient and steady simulations, respectively. Higher order schemes can minimize numerical diffusion, but decrease the convergence rate. The first order scheme is therefore conventionally used for a quick initial solution convergence, and then replaced by a higher order scheme and subsequently converged again. Similar results were generated (first vs second order) when this method was applied on the steady state simulations.
- *Volume Fraction Discretization.* The geometric reconstruction scheme is the ultimate scheme when solving for the volume fraction, as it provides a surface between the phases with no numerical diffusion. For the steady state simulations the compressive scheme is used, yielding an accurate and fairly crisp surface.
- *Temporal Discretization.* The explicit scheme is generally recommended whenever the dynamics of flow is of interest and the geometric reconstruction scheme for the volume fraction is only available with the explicit scheme. While explicit time discretization has a stricter stability criteria than implicit, initial simulations showed that a small time step also was needed to correctly resolve the physics in the domain and to reach the desired residual criteria. It is recommended for the Courant-Friedrichs-Lewy (CFL⁷) condition to be no more than 0.25. This value of CFL=0.25 was used with variable time stepping.

⁷CFL= $u_{cell}\Delta t/\Delta x$, where Δx is the cell size and Δt the time step

1.5 Quasi-Three-Dimensional Model

In industrial problems the span in time and length scales poses a major problem for 3D multi-fluid approaches. They are based on direct simulation of interface evolution, which is computationally demanding and can, with great reduction in computational time, be replaced by a multi-scale approach. This approach has to handle large-scale interfaces (LSI) representing waves, coexisting with transport of bubbles and droplets, including deposition and entrainment. The way LedaFlow-Q3D models the transport phenomena at interfaces is a unique feature, resulting in a hybrid model of the multi-fluid and VOF modeling techniques that can include effects of both dispersed and separated flows. [26]

The full 3D transport equations belonging to the same phase are combined together to create *phase equations*, e.g. for two phase; liquid, gas, liquid droplets in gas and gas bubbles in liquid. For three phase flows there would be three continuous and six dispersed fields.

To further reduce the computational time without losing too much of the important physics related to the pipe geometry, the domain will be averaged over transversal slices shown in Figure 1.3. This allows pipe-flow simulations to be calculated on a 2D computational mesh, hence a quasi-three-dimensional model (Q3D).

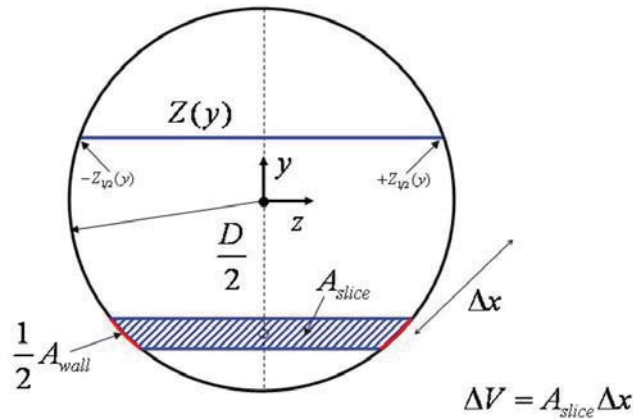


Figure 1.3: Illustration of the degenerated slices over which the transport equations are averaged, $Z(y)$, and of the three-dimensional slice volume over which averaged transported equations are integrated in the discretization, ΔV . [25]

Model Equations

In order to save space only the phase equations for the gas phase will be presented here. These consist of the continuity equation for the gas field

$$\frac{\partial(\alpha_g \rho_g)}{\partial t} + \nabla \cdot (\alpha_g \rho_g \vec{u}_g) = 0 \quad (1.18)$$

and the gas momentum equations

$$\begin{aligned} \frac{\partial(\alpha_g \rho_g \vec{u}_g)}{\partial t} + \nabla \cdot (\alpha_g \rho_g \vec{u}_g \vec{u}_g) = & -\alpha_g \nabla P + \alpha_g \rho_g \vec{g} - \left[\alpha_g^L \frac{\alpha_l \rho_l}{t_{p,droplet}} + \alpha_l^L \frac{\alpha_g \rho_g}{t_{p,bubble}} \right] (\vec{u}_g - \vec{u}_l) \\ & + \left[\alpha_g^L \frac{\rho_l}{t_{p,droplet}} \overline{u_g''} - \alpha_l^L \frac{\rho_g}{t_{p,droplet}} \overline{u_l''} \right] + \tau^{LSI} A^{LSI} + S_i + \alpha_g^L \alpha_g \nabla \cdot \vec{\tau}_g \\ & + \alpha_l^L \alpha_g \nabla \cdot \vec{\tau}_l + \alpha_g^L \alpha_g \vec{\tau}_g^{wall} \frac{A_{wall}}{\Delta V} + \alpha_l^L \alpha_g \vec{\tau}_l^{wall} \frac{A_{wall}}{\Delta V} \end{aligned} \quad (1.19)$$

where all the terms are slice-averaged over the pipe width. \vec{u}_g'' is the deviation between the local three-dimensional velocity component and the slice-averaged value. α_g^L and α_l^L are either zero or unity depending on if the dispersed field is droplets or bubbles. $t_{p,droplet}$ is a characteristic time a droplet uses from the moment it is released from the surface until it reaches the velocity of the surrounding gas. τ^{LSI} is the shear stresses that arise from a wavy surface or other large scale effects. For the complete model with all terms explained in detail, see [25]

A filter based $k-l$ turbulence model is used that resolves the large scale features, but models flow features smaller than the applied filter size. More information on the LSI and model details can be found in [25], [26], [19], [8], [17] and [7], along with Q3D obtained results on several flow structures.

A fixed bubble/droplet size will be used in this work, but it is possible to turn on the dynamic particle size model. The solution method in LedaFlow Q3D is based on finite-volume approach, with 1st-order discretization in space and time. The temporal discretization is semi-implicit, but other than that no further information on solution methods are presented here.

Chapter 2

Results and Analysis

2.1 Geometry and Mesh

The ideal physical geometries for all the simulations are presented in figure 2.1. Both geometries have an upward inclination of 3° , but they differ at the downstream segments¹. Where Geo#1 has a pipe segment with higher inclination, Geo#2 will switch straight to a downhill pipe segment. These two geometries have been chosen in order to investigate the effect of interface level changes on the multiple solutions. We know that a for a pipe segment downstream of greater inclination such as in Geo#1, the region of multiple solutions will be different. For the conditions in which the 3° pipe segment has non-unique solutions, the 5° segment will only have one solution (gravity dominated) that corresponds to a higher holdup. For a downhill segment as in Geo#2 there will also be only one solution (friction dominated) corresponding to a lower holdup.

For better simulations the sharp edges have been replaced with bends for both Fluent and LedaFlow. It is clear from Table 2.1 that not all the simulations have been run on the ideal geometries from Figure 2.1, but the reasons for this will

¹Flow from left to right, so downstream will be to the right on the figures

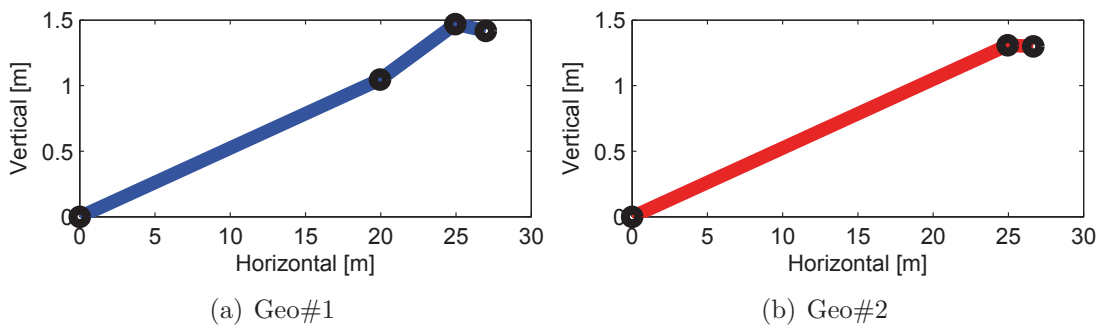


Figure 2.1: The ideal geometries to investigate interface level gradients

Simulation	Geometry	Description	Mesh	Description
LedaFlow	Section 2.3			
1D	0.0685m x 25m	Geo#1	1 x 800	Uniform
1D	0.0685m x 25m	Geo#2	1 x 800	Uniform
Fluent	Section 2.4			
2D High Mesh	0.0685m x 5m	Incl. const	60 x 200	Uniform
2D Low Mesh	0.0685m x 0.685m	Incl. const	200 x 800	Y-bias
Fluent	Section 2.5			
2D Transient	0.0685m x 25m	Geo#1	60 x 800	Uniform
2D Transient	0.0685m x 25m	Geo#2	60 x 800	Uniform
Fluent	Section 2.6			
3D High Mesh	0.0685m x 5m	Incl. const	5700 x 200	Normal
3D Low Mesh	0.0685m x 0.685m	Incl. const	5250 x 800	Bias
LedaFlow	Section 2.7			
Q3D	0.0685m x 25m	Geo#1	25 x 600	Y-bias
Q3D	0.0685m x 25m	Geo#2	25 x 600	Y-bias
LedaFlow	Appendix B			
Profile Model	0.0685m	Profile	75 x 1	Uniform
Profile Model	0.0685m	Profile	2000 x 1	Uniform

Table 2.1: Grid Properties. For the geometry and grid columns, the vertical or cross-section dimension is given first followed by the axial dimension.

follow in the respective sections.

Illustrations of the grids have been given in Figure 2.2. The aspect ratios are the same except for the 3D mesh with bias used to find the low holdup, but better resolved than displayed. For figure 2.2(a) 25 times greater, figure 2.2(b) 9 times, and figure 2.2(c) 25 times greater than displayed. Only structured meshes are used in this work as they are superior to unstructured and easy to create for simple geometries.

One way to reduce the grid size for the 3D simulations is to introduce a

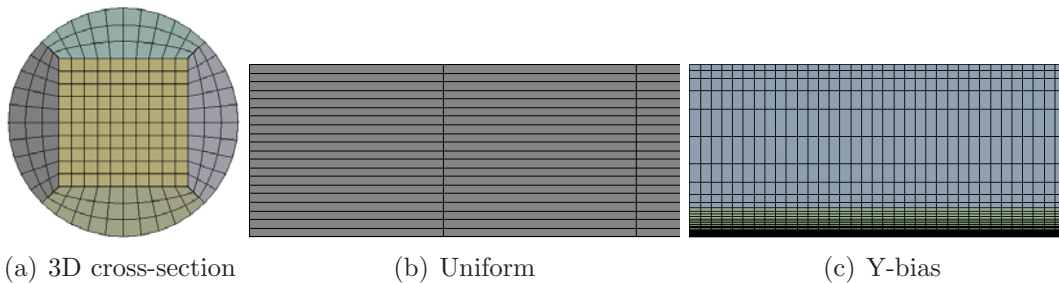


Figure 2.2: Illustrations of the basic meshes. The aspect ratios are as in this figure but the grid resolution is better.

symmetry plane (yz -plane, where z is the axial and y the vertical direction). A symmetry plane was not used since transient simulations generally do not have symmetry across the symmetry line unless the flow field is averaged over a sufficiently long period of time. The two transient 3D simulations (one on high holdup, one on low) were too heavy for my computational resources and unfortunately did not yield usable results before this project was due. The idea was to investigate secondary flows, wave behavior, in addition to comparing pressure gradients and liquid holdup with steady state results.

The fluid properties that has been used for the gas and liquid phase throughout this work are given in Table 2.2

Property	Gas	Liquid
Density, ρ	48 kg/m ³	817 kg/m ³
Viscosity, μ	3.4E-5 kg/(ms)	1.8E-3 kg/(ms)
Surface tension, σ	0.022 N/m	

Table 2.2: The fluid properties used throughout this work.

2.2 Taitel & Duckler's Two-Fluid Model

The TD model was the first to predict non-unique solutions and the multiple holdup region that is found from this model portray the region of interest the best. The solver made by Johansson [21], was used for the two liquid loadings of 0.1% and 0.01% for flow rates in the multivalued solution region yielding liquid holdups and pressure drops. Both liquid loads were found to have multiple solutions for flow rates in the range of $U_{sg} \in [3.2\text{m/s}, 4.60\text{m/s}]$ with $LL=0.1\%$ for flow rates $U_{sg} \in [1.45\text{m/s}, 4.60\text{ m/s}]$ for $LL=0.01\%$

The holdup figures are the same as displayed in Figure 1.2 with flow rate on the vertical axis, but this time with a logarithmic horizontal axis for the holdup. The best way to present the information in the figures is to consider the properties as they change with the flow rates. Start in the upper left corner of Figure 2.3(a) or 2.4(a) and follow the friction dominated low solution as it grows with decreasing flow rates. Eventually this blue line ends and the change in holdup is a discrete jump from the blue line on the left to the blue line on the right, indicating that the flow has suddenly become gravity dominated with back-flow along the wall. The holdup will subsequently continue to grow as the flow rate is decreased along the blue line to the right. The green and red lines are the alternate solutions in the multivalued solution region and correspond to gravity dominated flows.

The fluids will experience friction from the walls resulting in a negative pres-

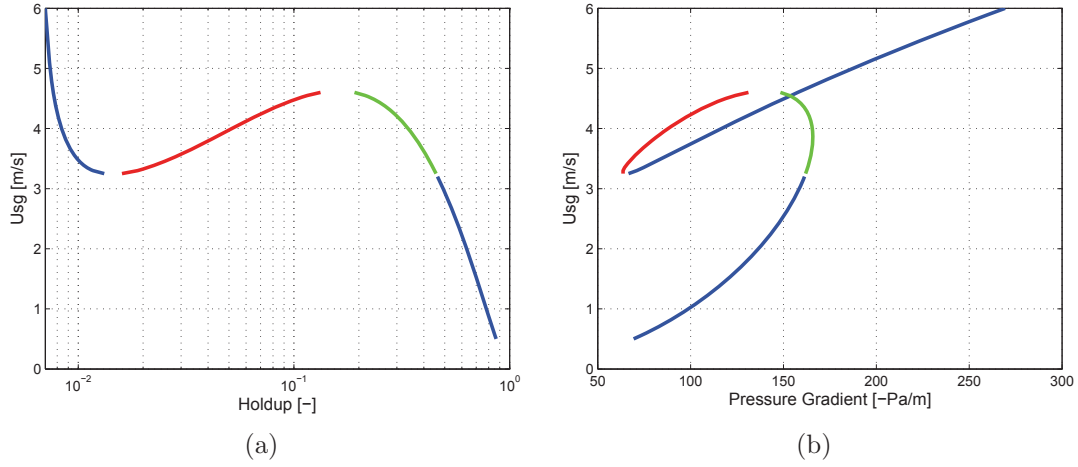


Figure 2.3: LL=0.1%. Holdup and Pressure Gradient

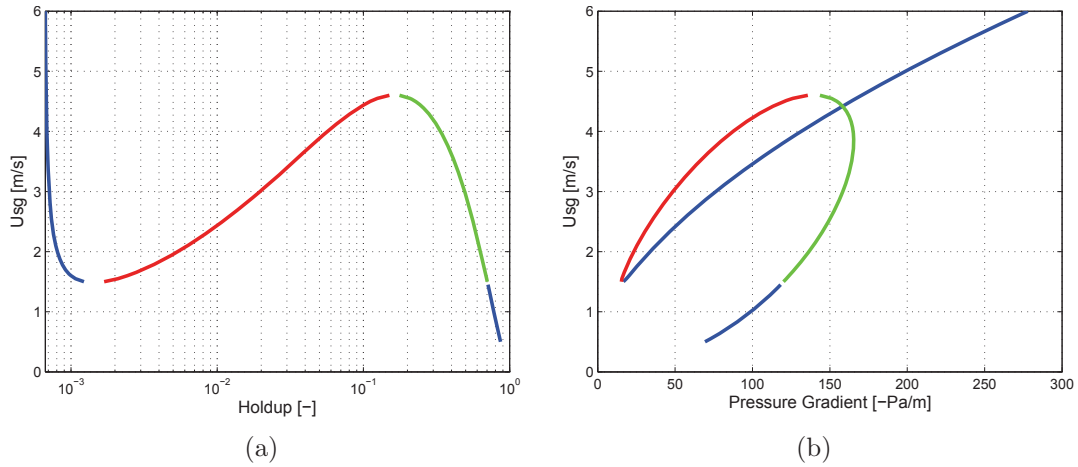


Figure 2.4: LL=0.01%. Holdup and Pressure Gradient

sure gradient² in the axial direction. This will be described as a pressure drop in this work. For an explanation of the pressure drop figures, follow the same approach used to explain the holdup figures. The corresponding start for Figures 2.3(b) and 2.4(b) will be in the upper right corner. We can see a decreasing pressure drop as the flow rate is reduced. It will continue to do so until the holdup value takes on a much larger value, in turn reducing the area occupied by the gas which results in an increased the gas velocity (from Eq. 1.1, $\frac{d\dot{A}_g}{dx} = -\frac{du_g}{dx}$). The pressure drop then suddenly increases before it continues its decrease with further reductions in flow rate.

The red and green lines, together with the blue line on the left for flow rates where these two lines exists, represents the multiple holdup solutions. The in-

²Sign of the pressure gradient in the unit for the figures. For the connection between the phases' velocity and magnitude of the pressure gradient see Eq. 1.2 and 1.5.

intermediate solution represented by the red line will be rejected with basis in the argument presented by Johansson [21]. To further explain this argument consider the boundaries for the liquid layer. The bottom will be the fixed boundary represented by the wall, and the top will be a variable boundary represented by the surface. The shear stresses experienced by the liquid close to the surface will be increased with an increased gas velocity. This information on the increased liquid velocity on the surface has to travel through a velocity gradient from the top down towards the wall. For a gravity dominated flow, like the intermediate solution, with no change in the gravity force in the axial direction, a reduction in the liquid level is the only possible consequence. Only with a larger axial gravity component (increased pipe inclination), or a variable wall boundary is it possible for an increase in the liquid level with increasing gas velocities.

The high holdup solution represented by the green line is still an alternate solution in the multivalued solution region, but the question is when this solution will be the preferred solution. There are some situations that potentially can promote the high holdup solution. Consider a situation with low flow rates. The holdup will then be in the single valued region with a high holdup. If the flow rate is then ramped up into the multivalued solution region, the pipe will then have surplus fluid and through an increased interfacial shear due to larger gas flow velocities, will transport this liquid downstream until an equilibrium again is found for the shear and gravitational forces. This equilibrium level would in this case be the high holdup solution if it is a physical candidate.

Also coming into play will be the geometry of the downstream pipe segment. If this segment is operated in the single valued region with either a low or high holdup solution, then these interfacial level changes can impact the region upstream operated in the multivalued solution region. A high holdup downstream could facilitate the high holdup solution in the multivalued region, and vice versa, regardless of the initial condition. More on this in the following sections.

2.3 LedaFlow 1D Steady State

Even though this work's main focus is on two and three dimensional flows, the LedaFlow 1D model is included since one dimensional models does not require much effort nor computational resources while still providing the most illustrative results. LedaFlow with its intuitive user interface allowed me to generated the results presented in this section quickly, justifying the side track.

There are two pipe geometries that will be investigated, Geo#1 and Geo#2, illustrated in Figure 2.1. The plots that will be presented will show gas flow rates versus liquid holdup and versus pressure gradient just as in the previous and all the following sections. Figures 2.5 and 2.6 show the two liquid loadings separately and figure 2.7 combines them with a logarithmic holdup axis.

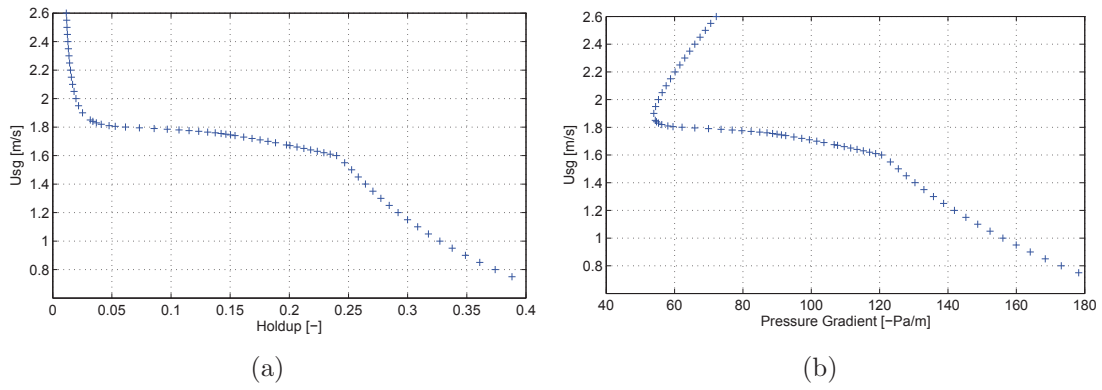


Figure 2.5: LL=0.1%. Holdup and Pressure Gradient

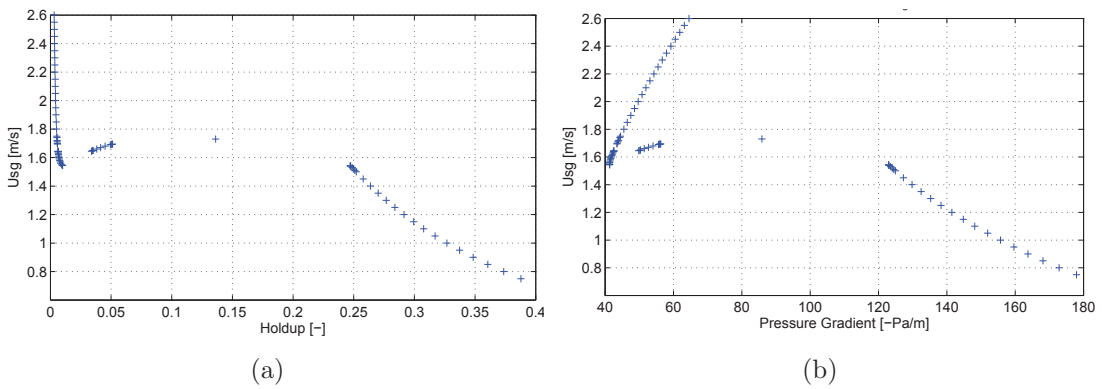


Figure 2.6: LL=0.01%. Holdup and Pressure Gradient

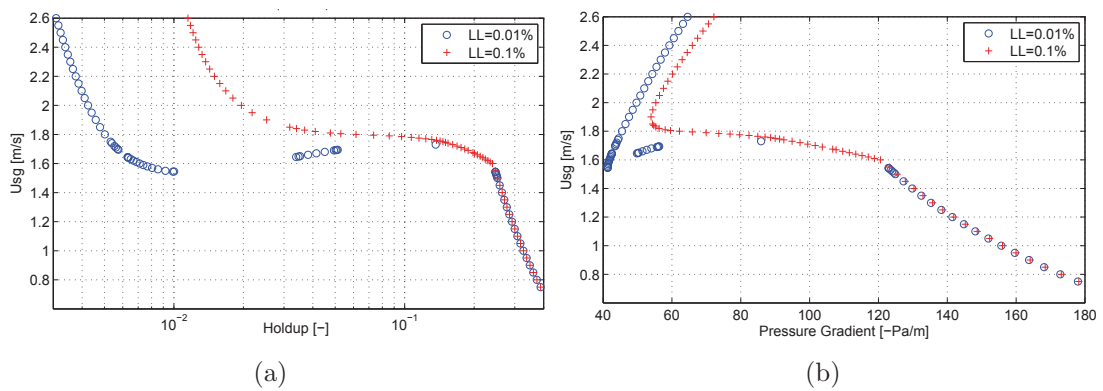


Figure 2.7: Combined. Holdup and Pressure Gradient

The results on Geo#1 were equal to Geo#2, i.e. the downstream interfacial gradient has no impact on the holdup in a potential multivalued solution region.

Most illustrating is Figure 2.7, comparing the two liquid loadings. As the large liquid loading demonstrate a continuous transition from low to high holdup at $U_{sg}=1.8\text{m/s}$, the smallest liquid loading has a distinct discrete jump between the low and high holdup. This jump occurs at a $U_{sg}=1.543\text{m/s}$. It can also be seen that the solver in the region around $U_{sg}=1.65\text{m/s}$ will produce an intermediate holdup solution.

This is a clear indication that we have found the region of multiple solutions for the smallest liquid load, but not for the largest liquid load. It should be noted that no multiple solutions have been found for any flow rates in these simulations, but this is due to the solvers choice of solution rather than a single solution from the models equations. See Appendix D, listing all the flow rates with its unique holdup and pressure drop.

When comparing the results from the TD model and LedaFlow 1D it becomes clear that the results differs, but the main trend is the same. The modeled interface shear stress in LedaFlow appears to be much stronger when considering the largest liquid load, since the flow rate where the flow changes from friction to gravity dominated is lowered (TD model: $U_{sg}=3.2\text{m/s}$. LedaFlow: $U_{sg} = 1.8\text{m/s}$). Higher interfacial friction also leads to no multiple solutions for the large liquid loading.

The smallest liquid loading predicts a discrete jump for $U_{sg} = 1.543\text{m/s}$, which is close to the one predicted from the TD model of $U_{sg} = 1.45\text{m/s}$, indicating that the shear stresses on the interface are only slightly lower for that given flow rate. Some flow rates above this value also indicate multiple solutions, as it would appear that the solver has chosen the intermediate solution instead of the low holdup solution.

Results for the friction dominated solutions shows a holdup almost ten times larger for $LL=0.1\%$ than for $LL=0.01\%$ for both models. LedaFlow predicts these holdups to increase more with decreasing flow rates than the TD model, in addition to predicting an overall higher holdup level for the friction dominated flows.

The gravity dominated flows in Leda have holdups much lower than predicted from the TD model, but at least shows the same trend unlike when comparing the pressure gradients for low flow rates. In the TD model the pressure drop will decrease with lower flow rates, but LedaFlow predicts an increase of pressure drop with lower flow rates. This inconsistency will briefly be reviewed. Practically only the gas phase will contribute to pressure drop for the gravity dominated flows, with its significantly larger velocity. For flow rate between $U_{sg} \in [1.45\text{m/s}, 0.75\text{m/s}]$, the area occupied by the gas phase has been reduced for the TD model

by 38%³, and for LedaFlow by 18%⁴. This implies that the TD model has twice the increase in velocity as LedaFlow with decreasing flow rates. This would for equal shear stress modeling lead to a faster growing pressure drop as the flow rate is reduced for the TD model than LedaFlow, but this is not the case as presented. It then has to come down to the shear stress modeling, showing just how important they are at accurately predicting the flow. It has been shown that the shear stresses are larger for a wavy than a smooth stratified surface, so the inclusion of wave effects in the LedaFlow modeling is a potential candidate in order to explain this deviation.⁵

2.4 Fluent 2D Steady State

The 2D Fluent simulations differ from all the other simulations of this work in the following way: Instead of a pipe geometry, the flow is now between two infinitely wide plates. This geometry is a rectangular duct with no effects from other walls than the top and bottom walls. This will effect the region of multiple solutions and the results cannot be compared quantitatively with pipe flow. The conversion between liquid level and liquid holdup for these two geometries is given in Figure 2.8.

Procedure

The results in this section were generated on two different meshes, see Figures 2.2(b) and 2.2(c). There are several reasons for this. A prerequisite of obtaining good simulation results is that all the important aspects of the flow are sufficiently resolved. This is a challenge for the low holdup solution that has a liquid height of about 0.1% of the pipe height. The VOF model is also particularly demanding for proper grid resolution in close proximity of the surface. For the small liquid loading this converts to, if a uniform grid is used, a height-wise grid number of several thousands. This small cell-height along with constraints on the cell aspect ratio, converts to length-wise grid number in the order of several

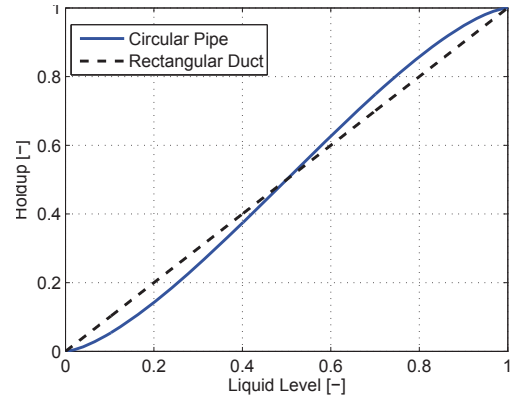


Figure 2.8: Liquid level versus liquid holdup for pipe and channel

³Numbers from Appendix D $\frac{H_{gas,1.45} - H_{gas,0.75}}{H_{gas,1.45}} = \frac{(1-0.711) - (1-0.821)}{(1-0.711)} = 0.38$

⁴Numbers from Appendix D $\frac{H_{gas,1.45} - H_{gas,0.75}}{H_{gas,1.45}} = \frac{(1-0.258) - (1-0.388)}{(1-0.258)} = 0.18$

⁵The shear stresses are a non-linear function of the velocity.

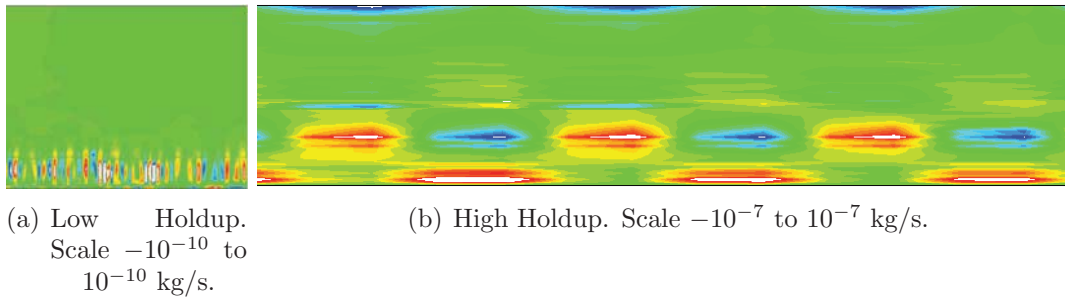


Figure 2.9: Mass Imbalance for $U_{sg}=1.75\text{m/s}$ for both Low- and High Mesh.

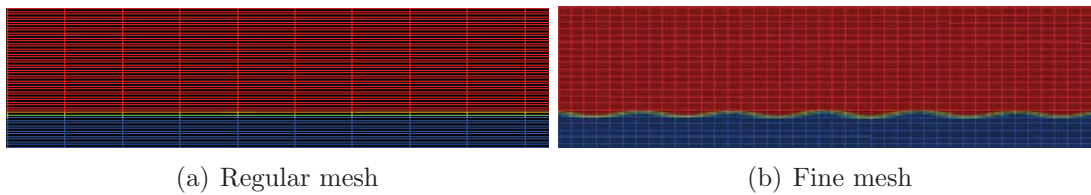


Figure 2.10: Holdup on regular and fine mesh. $U_{sg}=1.7\text{m/s}$

hundreds of thousands of cells if Geo#1 or Geo#2 were to be meshed this way. This is clearly not a viable approach. In order to reduce the computational demands a grid bias that decreases the cell sizes with increasing height is used. In addition the length-wise geometry has been reduced to ten times the diameter of the pipe. This length is long enough so that the evaluated region is unaffected by the inlet and outlet boundary conditions. This is illustrated in Figure 2.11. The the liquid phase is also sufficiently resolved while keeping the grid size down. This mesh will be referred to as the "Low Mesh", and displayed in Figure 2.2(c). No investigation of interface level changes has been performed on the Low Mesh, as the length is too short to study its effects. The results generated on this mesh have all converged, but the continuity equation has larger residuals than desired. This is a general feature of the steady state simulations. The mass imbalance is given as a contour plot in Figure 2.9(a).

It would be far from optimal to find the high holdup solutions on the Low Mesh, due to longer domain influence of the boundary conditions, and the fact that the grid resolution would only lead to heavier simulations with slower convergence. Ideally these simulations should be performed on the exact same mesh as the transient simulations, based on Geo#1 or Geo#2, where the interfacial level changes are due to actual pipe inclination changes downstream. Strangely though, the steady state solver could not converge to a solution on these meshes. The high holdup solution simulations were therefore performed on a pipe with constant inclination (no bends) with a length equal to a fifth of Geo#1, hereby referred to as the "High Mesh" displayed in Figure 2.2(b). The surface level change effects have to be introduced from a pressure profile on the outlet using a

UDF. Height- and length-wise grid resolution were chosen to be equal to that of the transient simulations for consistency. Comparisons with a mesh with 8 times the resolution showed for $U_{sg}=1.7\text{m/s}$ a 1.9% lower holdup, but the main difference is the surface displayed in Figure 2.10. No high holdup solution was found for a grid with 64 times the resolution, strongly stating that these simulations are grid dependent. All solutions obtained on the High Mesh were converged, but with the same continuity residual issue as for the Low Mesh shown in Figure 2.9(b) .

It should also be noted that I have been unable to recreate the low and high holdup solutions with longer domains with equal size grid-cells. This could imply that the model choices made were unfortunate, but further experimentation, with all modeling variations, different mesh resolutions and boundary conditions, did not result in converged solutions. Visually the solutions on the longer Low Mesh would have liquid patches instead of a continuous layer, where the patches would move, become larger and breakup as the solver iterations increased. Domains empty of the liquid phase were also observed. The high holdup simulations on Geo#1 struggled with the higher inclination region downstream, repeating a process of filling and emptying, in turn also effecting the holdup in the region upstream during the iteration process. For the longer High Mesh simulations the liquid layer would form patches and moving around never converging on a solution. The reasons for this have not been understood. These issues, along with a failed attempt at creating a "profile model" for the VOF simulations⁶, were a significant time drain during the initial stages of this work.

Strangely Fluent did not provide pressure gradient values anywhere in the domain, so these values had to be obtained by extracting the static pressures along two lines and subsequently subtracting and dividing by the length between them. Great care has been taken in ensuring that the correct flow rate for each phase was introduced into the domain. The local velocity at the inlet for each phase will be calculated as a function of the flow rate divided by the dimensionless phase inlet area for the respective phases. The velocities should yield the desired flow rates independent of the phase area at the inlet for an infinitely resolved surface, but due to the relative low number of grid points, there will be deviations from the correct value in the order of several percents for the liquid phase. An adjusting factor has therefore been multiplied into the expressions. This was a time consuming approach, but at least inaccuracy in the results will not originate from erroneous inlet conditions.

Results

All the simulations displayed in Figures 2.13, 2.14 and 2.15, have an inlet and outlet liquid level equal to the liquid level in the fully developed region. In other

⁶The "profile model" attempt failed mainly due to no periodic B.C. and the problems that arose with the workaround involving negative values on a velocity inlet (velocity outlet).

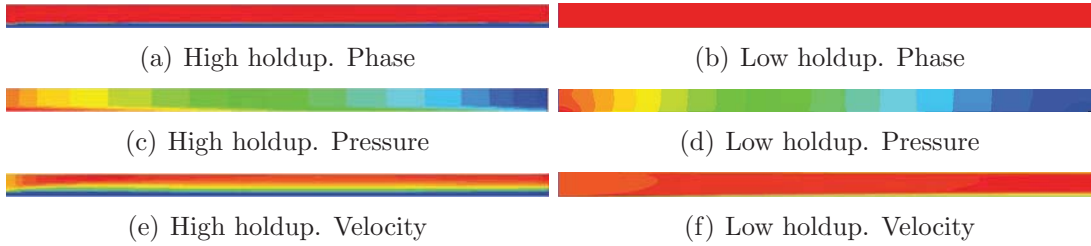


Figure 2.11: $LL=0.1\%$ $U_{sg}=1.7\text{m/s}$. The scaling is not important here, as these figures are used to illustrate that the values extracted were from fully developed converged simulations. The length to height ratios have been manipulated.

words, no interface level change effect downstream will influence the solutions. The domain used to extract the holdup and pressure gradients on the Low Mesh and High Mesh are illustrated in Figure 2.11 for one flow rate.

We can see the same trend as for LedaFlow 1D, but the multiple solution region is increased. From the results generated on the two separate grids we can see a multiple holdup region for $U_{sg} \in [1.5 \text{ m/s}, 1.8 \text{ m/s}]$ for both liquid loads (see Figure 2.15). Just as for the 1D pipe flow; the friction dominated solutions displays holdups ten times larger for the largest liquid load and with practically the same values. One difference though is that the 2D open channel predicts less change in holdup with flow rates.

No intermediate solutions can be identified, but the high holdup solutions can be found for the same flow rates as low holdups, i.e. multiple solutions. The gravity dominated holdups are practically equal for the two liquid loadings. This was also predicted by the TD model, but they started to differ as they moved into the multivalued solution region. The pressure drops for the 2D open channel are a bit lower than predicted by LedaFlow for the pipe, but displays the same trend.

It was quite clear when the High Mesh did not have a high holdup solution, because it switched to a low holdup. The situation on the Low Mesh was different in that it did not completely switch to a high holdup when the flow rate was lowered. This is due to the short domain. Instead there was a bulb buildup that moved around the domain as the simulation never converged. This is shown in Figure 2.12 for the large liquid loading, but the feature was also there for the small liquid load.



Figure 2.12: $LL=0.1\%$. The situation for the Low Mesh when no friction dominated solution was found. Blue is liquid, red is gas. Only a section illustrated.

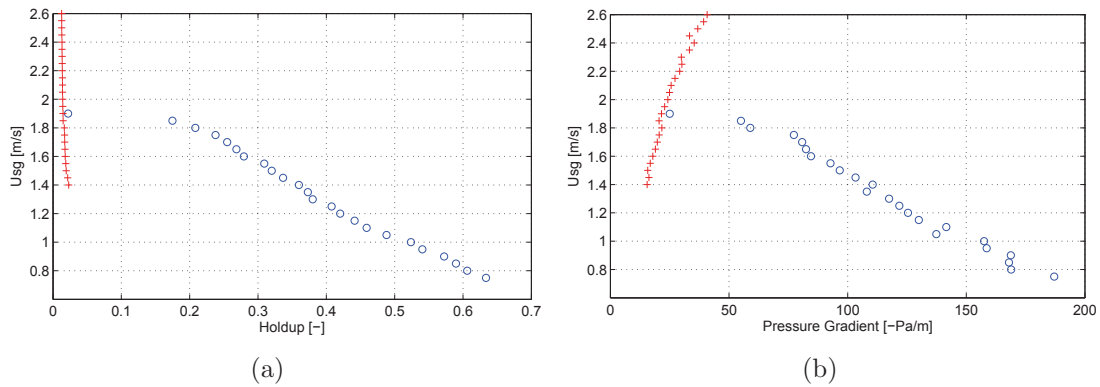


Figure 2.13: LL=0.1%. Holdup and Pressure Gradient. Blue are holdups generated on the High Mesh, and red are holdups generated on the Low Mesh.

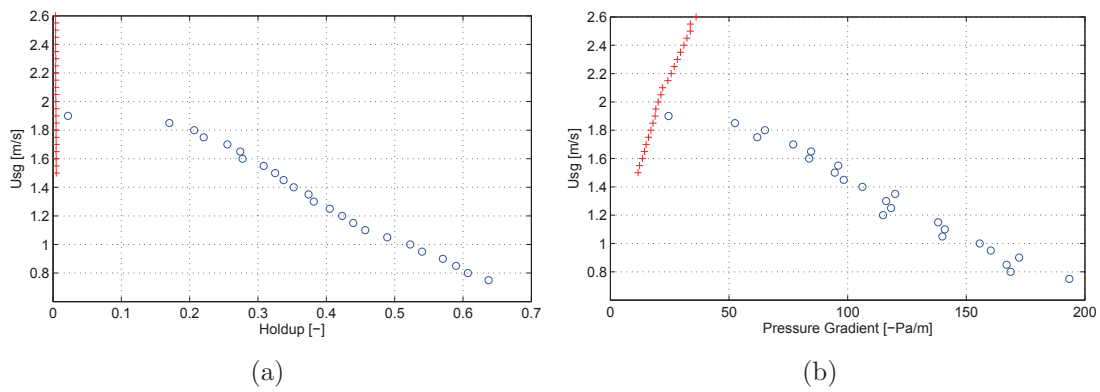


Figure 2.14: LL=0.01%. Holdup and Pressure Gradient. Blue are holdups generated on the High Mesh, and red are holdups generated on the Low Mesh.

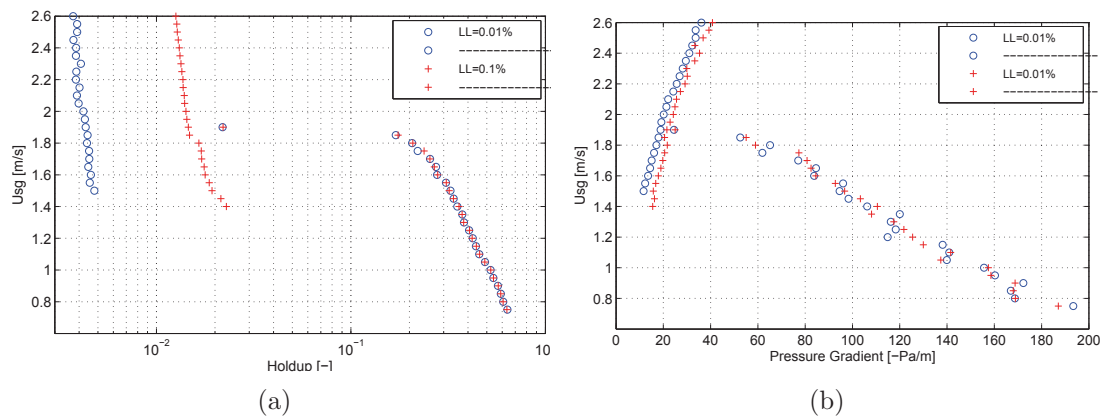


Figure 2.15: Combined. Holdup and Pressure Gradient

Interface Level Gradients

Two different pressure profiles were used on the outlet to force an interface level change close to the outlet. For the gravity dominated solutions a higher hydrostatic gradient downstream had no effect compared to a straight surface all the way out of the domain, i.e. no hydrostatic gradient. A higher hydrostatic gradient was not investigated for the friction dominated solution due to the short domain.

The second pressure profile was created to yield a low holdup at the outlet. This had no effect on the low friction dominated solution which was as expected, but it did have an impact on the gravity dominated solution. Due to the identified multiple solutions, it was expected that for *one* flow rate there would be a discrete jump from the friction dominated to the gravity dominated solutions. This flow rate was expected to be close to the lowest flow rate where friction dominated solutions exist ($U_{sg}=1.5\text{m/s}$). This was not the case though, as can be seen in Figures 2.16 and 2.17 with the interface level change located further upstream with increasing flow rates. A conservative conclusion would be to say that the gravity to friction dominated switch due to interfacial level changes occurred for flow rates $U_{sg}=1.55\text{m/s}$ for the highest liquid load, and $U_{sg}=1.6\text{m/s}$ for the lowest liquid load.

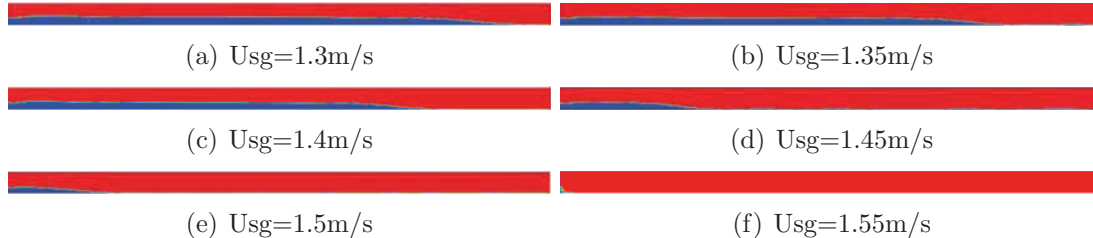


Figure 2.16: $LL=0.1\%$. Low Hydrostatic Gradient. The vertical dimension is three times the actual. Blue is liquid, red is gas.

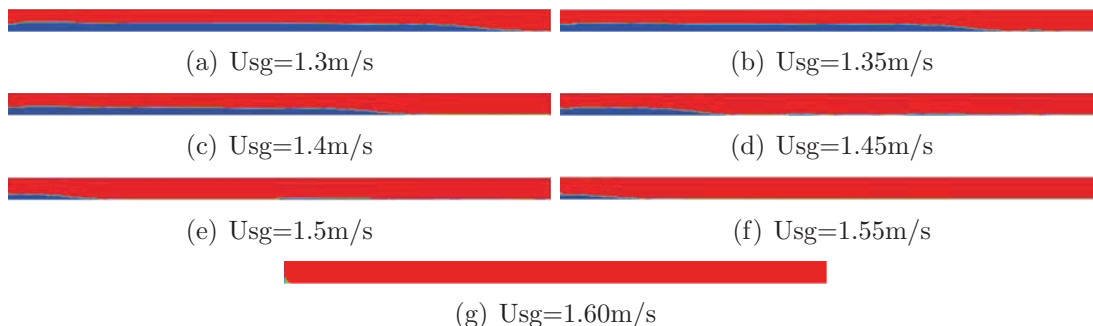
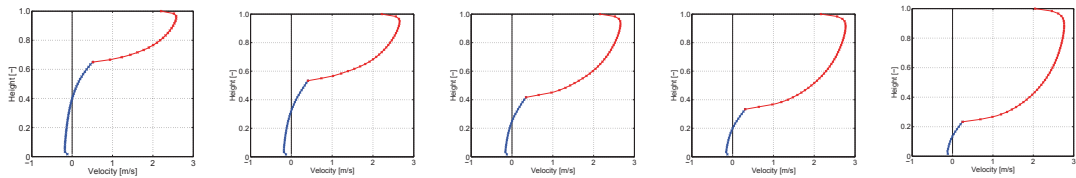


Figure 2.17: $LL=0.01\%$. Low Hydrostatic Gradient. The vertical dimension is three times the actual. Blue is liquid, red is gas.

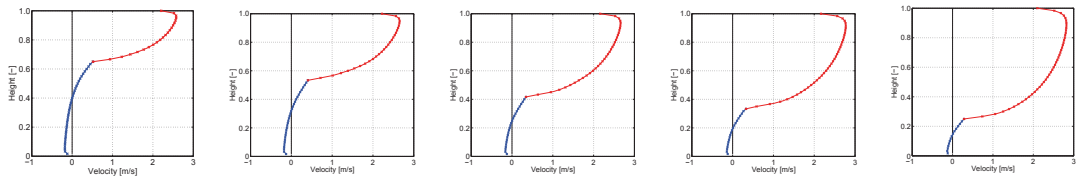
Velocity Profiles

The velocity profiles illustrate the influence of flow rates on the gas and liquid velocities. There is practically no difference in Figures 2.18 and 2.19 displaying the velocity profiles for the high holdups. This is expected since both liquid loads have similar holdup and pressure gradients. However, when friction dominates the flow, as in Figure 2.20(c), a clear difference in the liquid holdups can be found. These velocity profiles are very illustrating of the actual flow in the domain because they have the physically correct discrete change in the velocity gradient between the phases unlike the transient flow profiles in the next section where a wavy surface has been averaged.



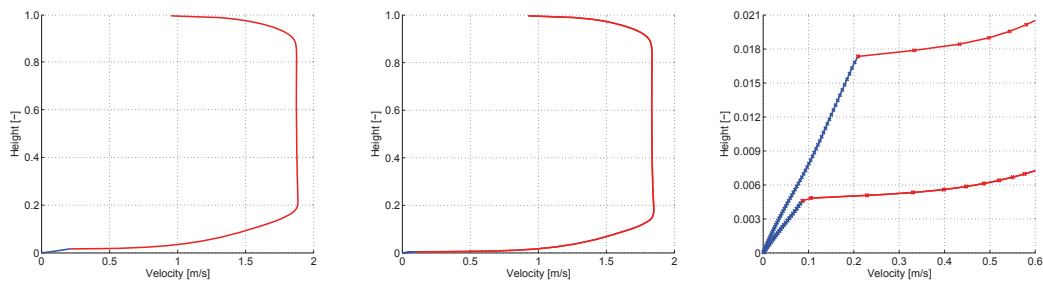
(a) $U_{sg}=0.75\text{m/s}$ (b) $U_{sg}=1.00\text{m/s}$ (c) $U_{sg}=1.25\text{m/s}$ (d) $U_{sg}=1.50\text{m/s}$ (e) $U_{sg}=1.75\text{m/s}$

Figure 2.18: LL= 0.1%. Velocity Profiles



(a) $U_{sg}=0.75\text{m/s}$ (b) $U_{sg}=1.00\text{m/s}$ (c) $U_{sg}=1.25\text{m/s}$ (d) $U_{sg}=1.50\text{m/s}$ (e) $U_{sg}=1.75\text{m/s}$

Figure 2.19: LL= 0.01%. Velocity Profiles



(a) LL=0.1%. $U_{sg}=1.75\text{m/s}$ (b) LL=0.01%. $U_{sg}=1.75\text{m/s}$ (c) Zoom Inlets

Figure 2.20: LL=0.01%. Velocity Profiles. Low Holdup

2.5 Fluent 2D Transient

Twelve transient gravity dominated Fluent channel simulations were made to supplement the steady state simulations and investigate the dynamic nature of the flow in the geometries presented in Figure 2.1. The gas enters in the upper half of the inlet, while the bottom half functions as a wall apart from a small slot at the bottom where the liquid enters. This setup has no back-flow on the inlet, but still retains high liquid height close to the inlet due to recirculation.

To find the holdup as it varies with time, the liquid height is averaged in the central region of the channel that is unaffected by the inlet and the downstream inclination change. If the region had been sufficiently long then there should be no variations for a statistically steady state solution. This region, $l \in [5\text{m}, 15\text{m}]$, was not long enough to remove the fluctuations, but it appears to be statistically steady states for the superficial gas velocities of 1.7m/s, 1.8m/s and 1.9m/s. For 2.0m/s, the emptying of the channel starts at the inlets and pushes the liquid through the pipe, indicating a low holdup solution. The grid does not resolve the bottom region sufficiently to find the low holdup value for the transient simulations.

As can be seen from Figure 2.21 the holdup enters from above in the initial stages. This is due to the initialization of the domain. Both the low liquid flow rate and small grid size prevented simulations of the filling process for the channel within the time period of this work. It was found, however, that if the domain has a holdup value greater than the statistically steady state value, the excess liquid is removed with a few large slugs reaching statistically steady state in less than one minute.

Some of the simulations have been calculated without surface tension effects for a period of time in order to investigate if this added surface unsteadiness on the somewhat coarse grid resolution that was used. However, no effect of surface tension was observed. The first 150 seconds are calculated with no surface tension and are illustrated by the red lines, and the last 50 seconds have been performed with surface tension effects included, shown as blue lines (See Figures 2.22 and 2.23). Figures 2.22(a) and 2.22(c) show a strange behavior after the surface tension effects are included, but when reviewing the domains before and after the decrease in holdup, the only observed difference was a large wave that moved out of the domain. It seems that no new large waves enters the domain, but it is not possible to spot a change in the general behavior with regards to wave amplitude or length.

The holdup and pressure drop values are time averaged from about 50s and onwards to the end. The holdups are similar to those found for steady state for both geometries. Pressure drops were a bit higher indicating that the steady state model did not accurately estimate the effects of the wavy surface.

The time averaged profiles will not have a sudden change in velocity gradient between the phases. This is due to the unsteady surface between the phases and

the VOF-model's shared velocity field. Figure 2.26 illustrates this with a wave top and wave bottom that when averaged will yield this unphysical result. Still, a time averaged velocity profile can give some information on the flow if this unsteady surface effect is kept in mind. See Figures 2.27 and 2.28. Increasing the flow will impact the areas occupied by the phases, but the maximum velocity in the domain appears to be constant and close to the one found by the steady state solutions. It was also interesting to see that there will be back-flow close to the wall even during wave tops, just as it is shown in the next section in Figure 2.44.

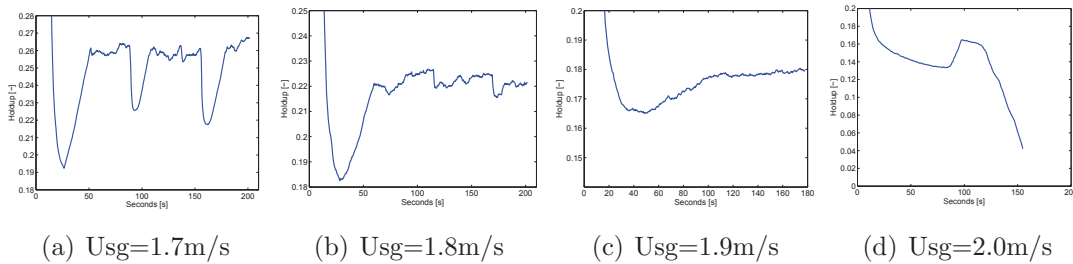


Figure 2.21: LL= 0.1%. Geo#1. Holdup $l \in [5m,15m]$.

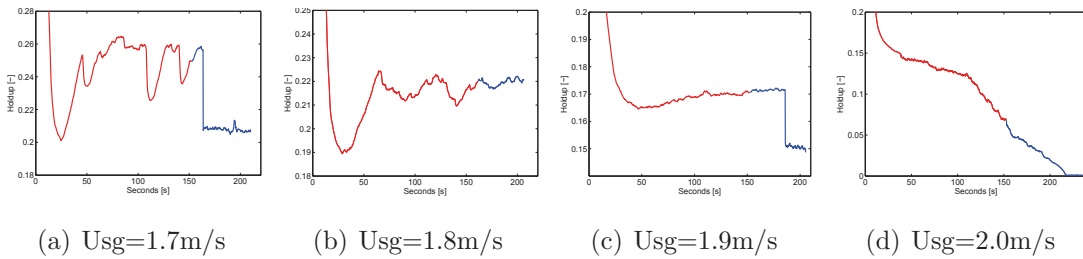


Figure 2.22: LL= 0.01%. Geo#1. Holdup $l \in [5m,15m]$. Red is without surface tension, blue is with.

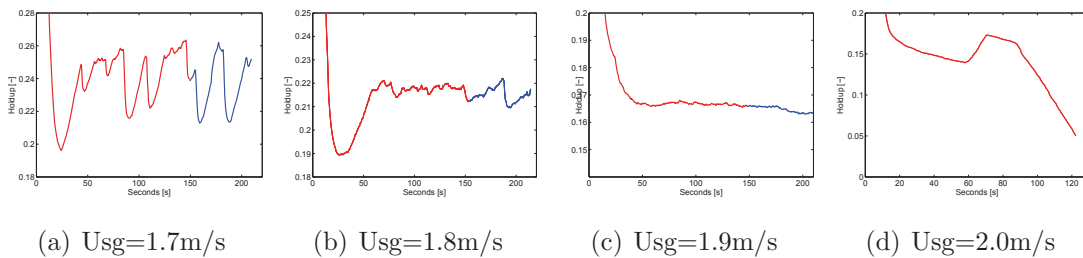


Figure 2.23: LL= 0.01%. Geo#2. Holdup $l \in [5m,15m]$. Red is without surface tension, blue is with.

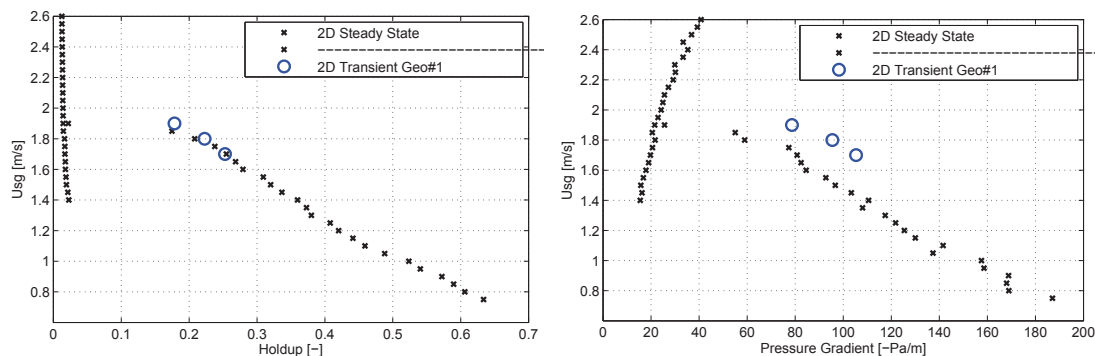


Figure 2.24: LL= 0.1%. Holdup and Pressure Gradient

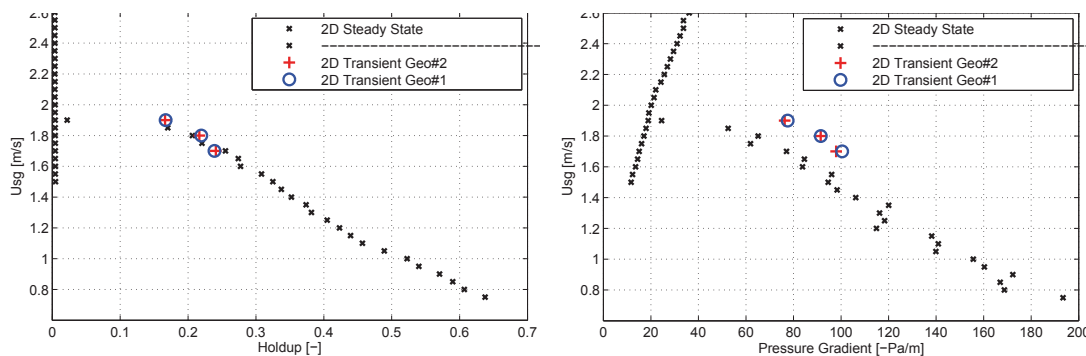


Figure 2.25: LL= 0.01%. Holdup and Pressure Gradient

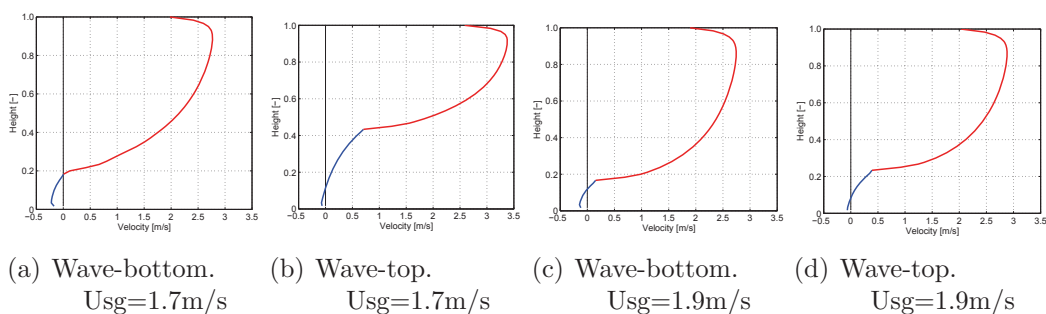


Figure 2.26: LL= 0.01%. Snapshot of velocity profile for wave tops and bottoms.

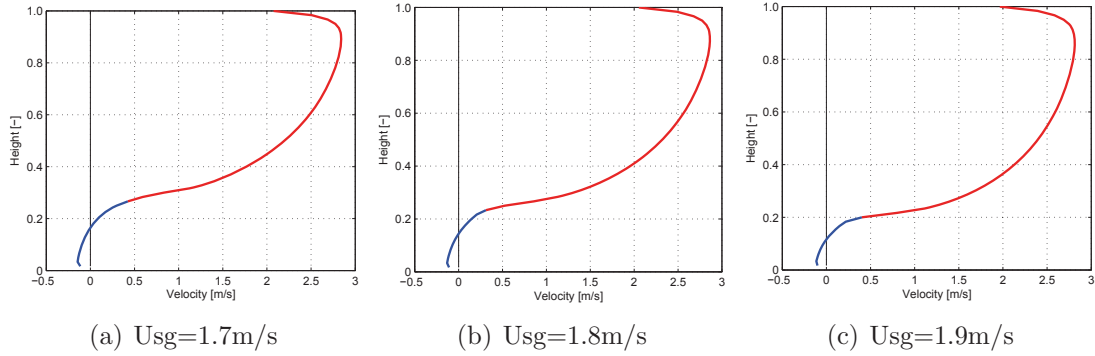


Figure 2.27: LL= 0.1%. Velocity Profile

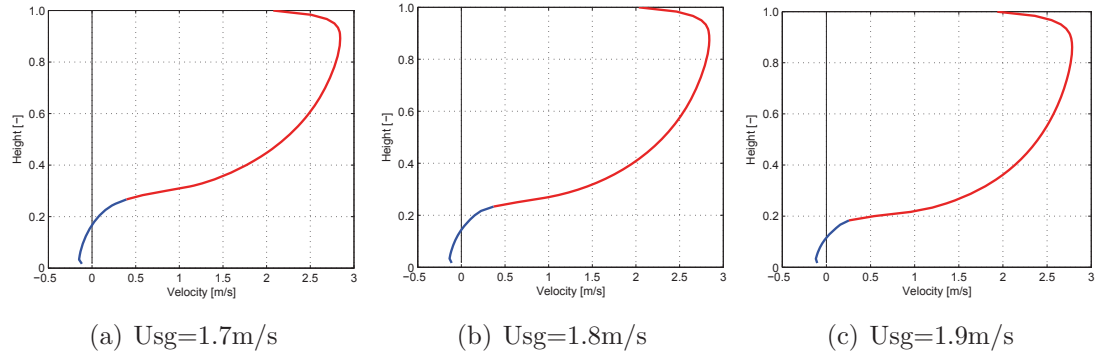


Figure 2.28: LL= 0.01%. Velocity Profile

Emptying process of Geo#1 and Geo#2

During the writing process of this work some of the transient simulations were continued in order to investigate a possible emptying of the channel for the two geometries. The mass flow at the inlet and outlet is given in Figure 2.29 as a function of time. The figures have accurate mass flow values where the value at every time step is averaged into one for every two seconds, but the fluctuation is greater than the figures indicate. The time averaged mass fluxes on the outlet were 0.2754kg/s for Figure 2.29(a), 0.1602kg/s for Figure 2.29(b) and 0.0523kg/s for Figure 2.29(c). Fluctuations for them all were between 1kg/s and 0kg/s . Due to the differences in the mass flow in and out of the domain, an emptying process of the region $l \in [5\text{m}, 15\text{m}]$ for Geo#2 estimated to last about 8 minutes for $U_{sg}=1.9\text{m/s}$ and 25 minutes for $U_{sg}=1.7\text{m/s}$.

Most interesting were the results on Geo#1 where a consistent high hydrostatic gradient was expected in the highest inclination pipe segment downstream in addition to little or no emptying rate. This was not the case. This steeper segment was emptied and large irregular waves originating far upstream in the

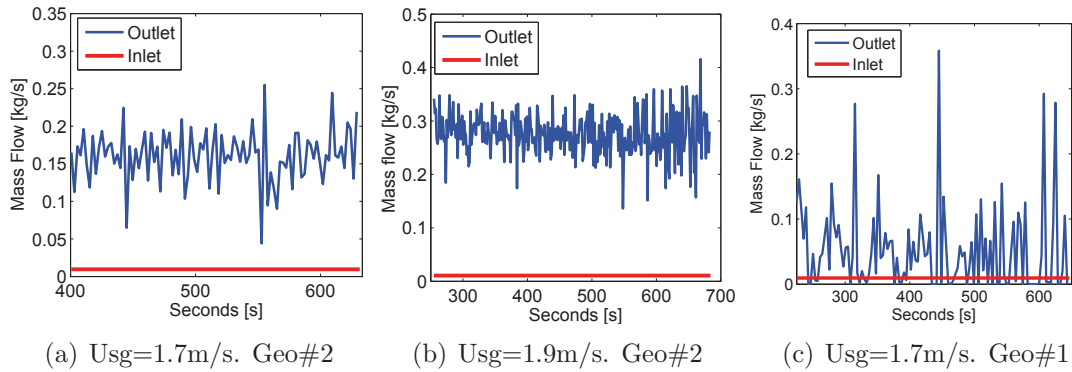


Figure 2.29: LL= 0.01%. Mass flow at the inlet and the outlet.

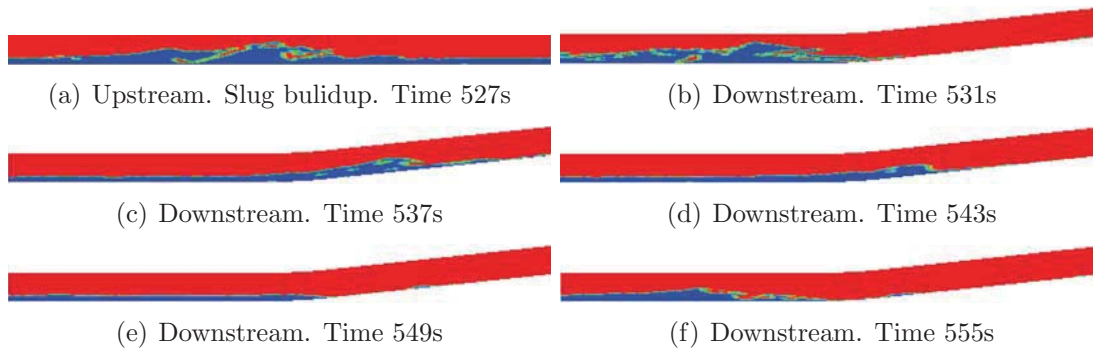


Figure 2.30: LL= 0.01%. Geo#1. Usg= 1.7m/s.

multivalued solution region had enough momentum to climb the segment before most of the liquid rolled back, but some of the fluid reached the outlet and exited the domain (see Figure 2.30). The average of this liquid mass flux was larger than the one entering, and an estimated emptying for the region $x \in [5m, 15m]$ in will then occur in 42 minutes.

All these estimated times of emptying are based on an equal emptying rate until the channels are empty, which might be far from the actual situation. Further investigations are needed to reach any conclusions regarding the emptying, but a trend has been identified.

2.6 Fluent 3D Steady State

The Fluent 3D pipe simulations feature the same mass imbalance issues as the channel simulations. Adjusting factors in the UDF were used for every 3D simulation, similarly as for the 2D simulations. Both liquid loadings have been investigated and are presented in Figures 2.31 and 2.32. The 3D results exhibit higher holdup values for the lowest flow rates with stronger dependence on flow rate compared to LedaFlow 1D. This slope appears to be linear for both liquid

loadings until no gravity dominated flow can be maintained. The 3D results have lower holdup than LedaFlow 1D for $U_{sg}=1.5\text{m/s}$ and above. The low holdup solutions have only been investigated for the largest liquid loading, shown in Figure 2.31(b). These friction dominated solutions have much lower holdups than found in LedaFlow 1D. The pressure drop is lower for both liquid loadings and for both friction and gravity dominated holdup solutions. No investigation on grid and geometry dependency have been performed.

Multiple holdup solutions were found for flow rates $U_{sg}\in[1.35\text{m/s}, 1.75\text{m/s}]$ for $LL=0.1\%$. The friction dominated solutions were obtained on the Low Mesh with bias, and the gravity dominated on the High Mesh. No friction dominated solutions were obtained on the smallest liquid load due to resolution demands for a properly resolved liquid layer. The friction dominated solution has from the previous simulations been found for the smallest liquid loading for flow rates equal or lower than for 0.1% liquid loading. Surely multiple solutions exists for the smallest liquid load too, even though only the gravity dominated holdups were found due to too coarse grid.

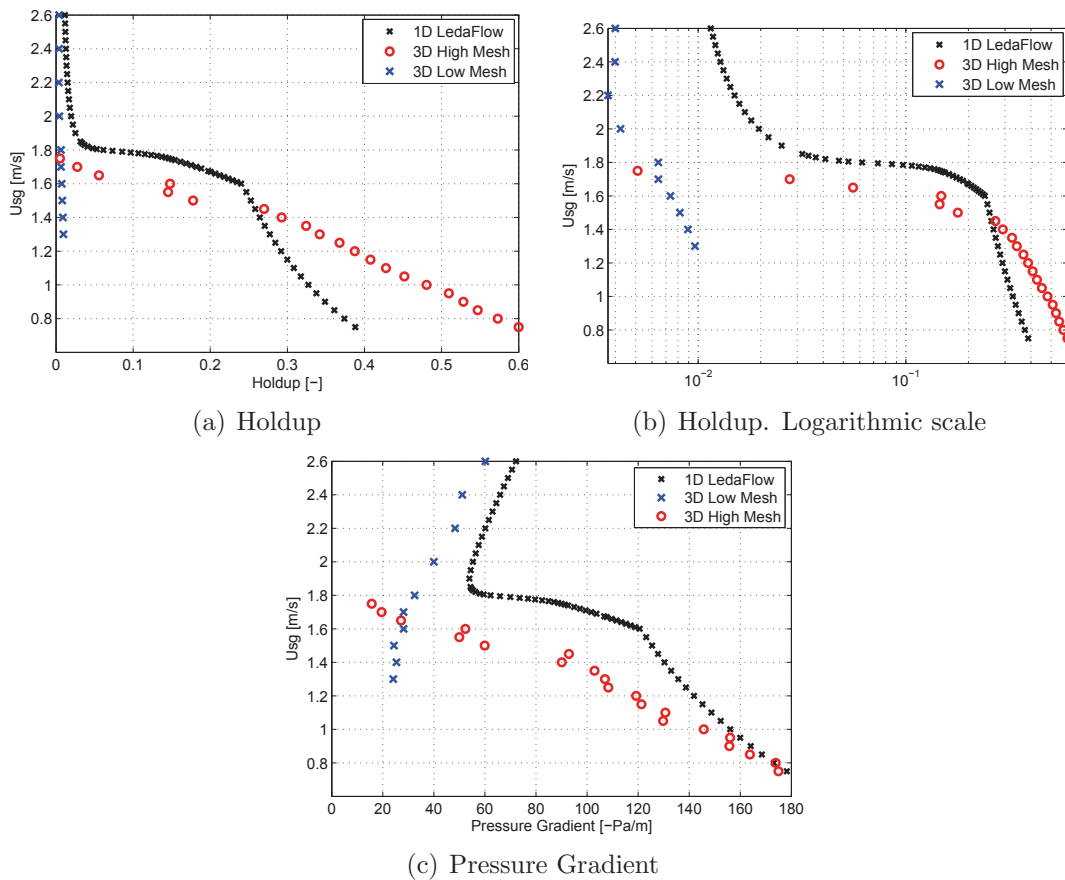


Figure 2.31: $LL=0.1\%$. Liquid Holdup and Pressure Gradient

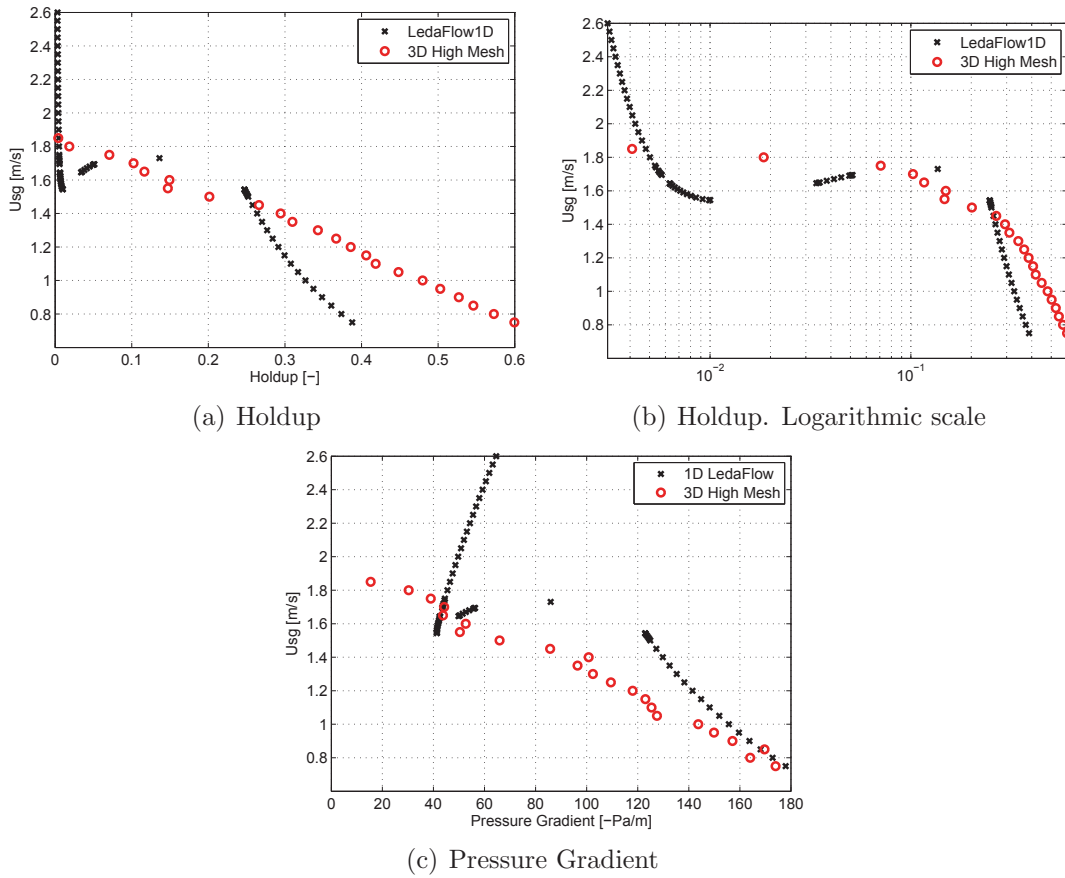


Figure 2.32: LL=0.01%. Liquid Holdup and Pressure Gradient

Interface Level Change

The same procedure with the pressure profiles on the outlets were performed on the 3D pipe simulations as for the 2D channel, but these profiles did not result in the same conditions on the outlet. The surface was lowered from the situations with no hydrostatic gradients, but far from the level that corresponds to a low holdup solution. Interface level gradients gave no significant changes for the gravity dominated holdup in the multiple holdup region.

Velocity and Holdup Profiles

When comparing the high holdup solution of the liquid loadings it becomes clear that they produce very similar results. The 0.1% liquid loading covers the left half of the circle and the 0.01% liquid loading the right half. When considering the holdup values in the region next to $U_{sg}=1.5\text{m/s}$ in Figures 2.31 and 2.32, the deviation between the liquid loadings in Figure 2.33(d) appears to be due to inaccurate solutions. It appears from the velocity profiles that the maximum

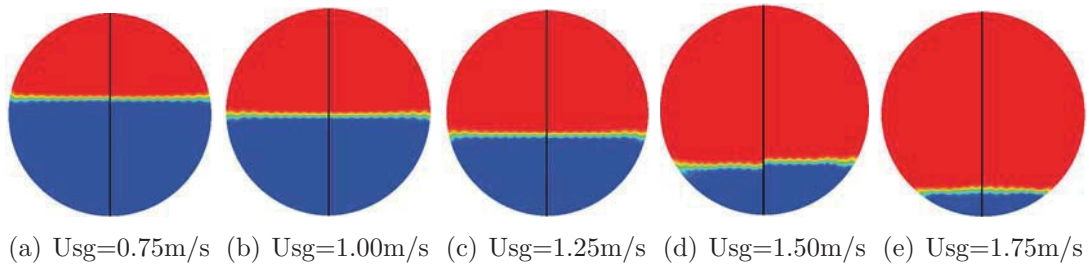


Figure 2.33: LL= 0.1% on the left half, LL= 0.01% on the right half.

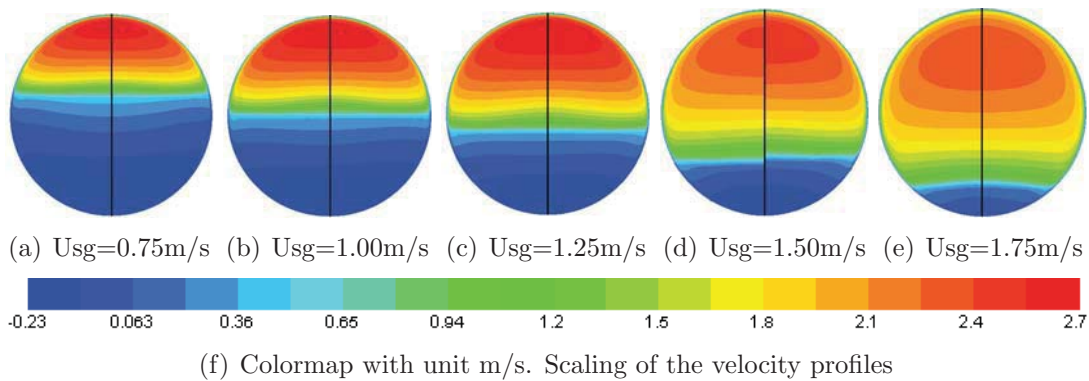


Figure 2.34: LL= 0.1% on the left half, LL= 0.01% on the right half.

velocities are highest for the lower flow rates.

A velocity profile for the friction dominated holdup solution is given in Figure 2.35. It should also be noted that the phase and velocity profiles for both friction and gravity dominated flows do not show significant variations in the horizontal direction except for the region close to the wall due to friction. This might not be the situation for transient flows with waves on the surface. The next section will integrate over horizontal slices, and the wall friction will be modeled. A 3D transient simulation is therefore proposed as future work to investigate the effects of the secondary flows in the cross-section.



Figure 2.35: LL= 0.1%. $U_{sg}=1.7\text{m/s}$

2.7 LedaFlow Q3D Transient

Investigations have been performed on both geometries presented Figure 2.1 for both liquid loads, but with the main focus on the smallest liquid load. It is clear from the snapshots of the pipes in Figures 2.36, 2.37 and 2.38, that the interface is wavy and the wave amplitude decreases with increasing flow rates.

A statistically steady state was obtained for all the flow rates presented in the figures, except for one, displayed in Figure 2.37(j). This simulation was

included to illustrate that the region of gravity dominated flows have a boundary condition dependency. The inlet for all the simulations are split into one gas and one liquid part. The liquid area fraction of the inlet has been set to a quarter, but Figure 2.37(j) has a larger liquid area fraction that covers half of the inlet. Because of this difference the pipe will be emptied starting at the inlet and moving downstream for $U_{sg}=2.0$ m/s. The simulations with the liquid area covering a quarter of the inlet can have higher flow rates without being emptied from the inlet and downstream. See Figure 2.37(i). Further investigations showed that an even smaller liquid area fraction of the inlet ($1/20$) produce similar behavior as one quarter of the inlet area.

If the flow rate is further increased from $U_{sg}=2.2$ m/s the pipe will be emptied in the same manner as Figure 2.37(j) independent of inlet variations, revealing that the gravity dominated solution is no longer sustainable.

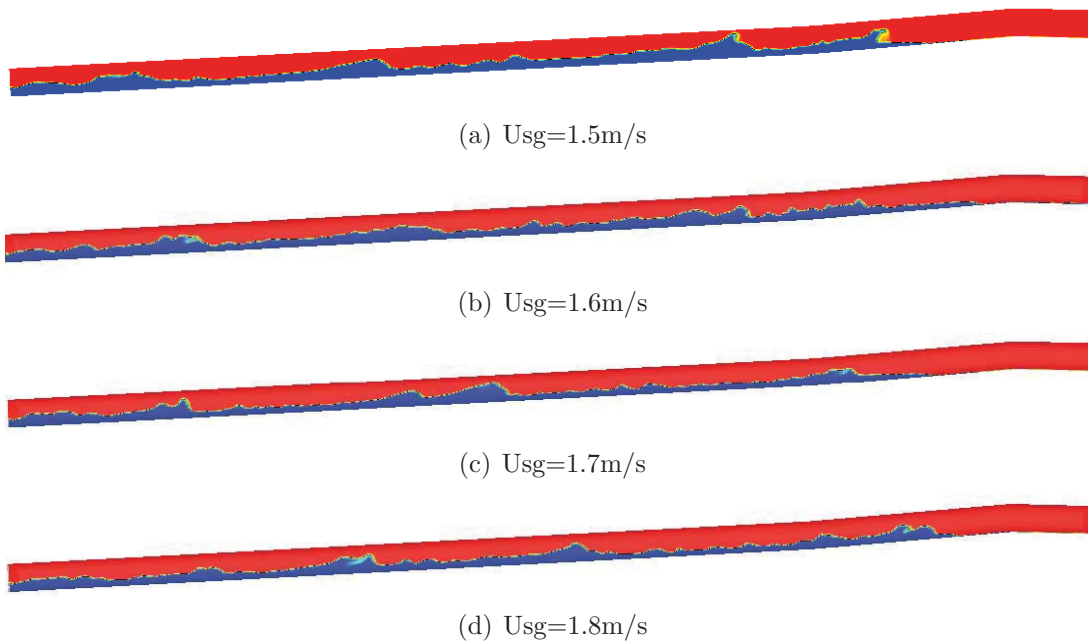


Figure 2.36: $LL=0.1\%$. Geo#1. Snapshot of holdup. The diameters illustrated are stretched by a factor of ten. Blue areas are filled with liquid and red ones with gas.

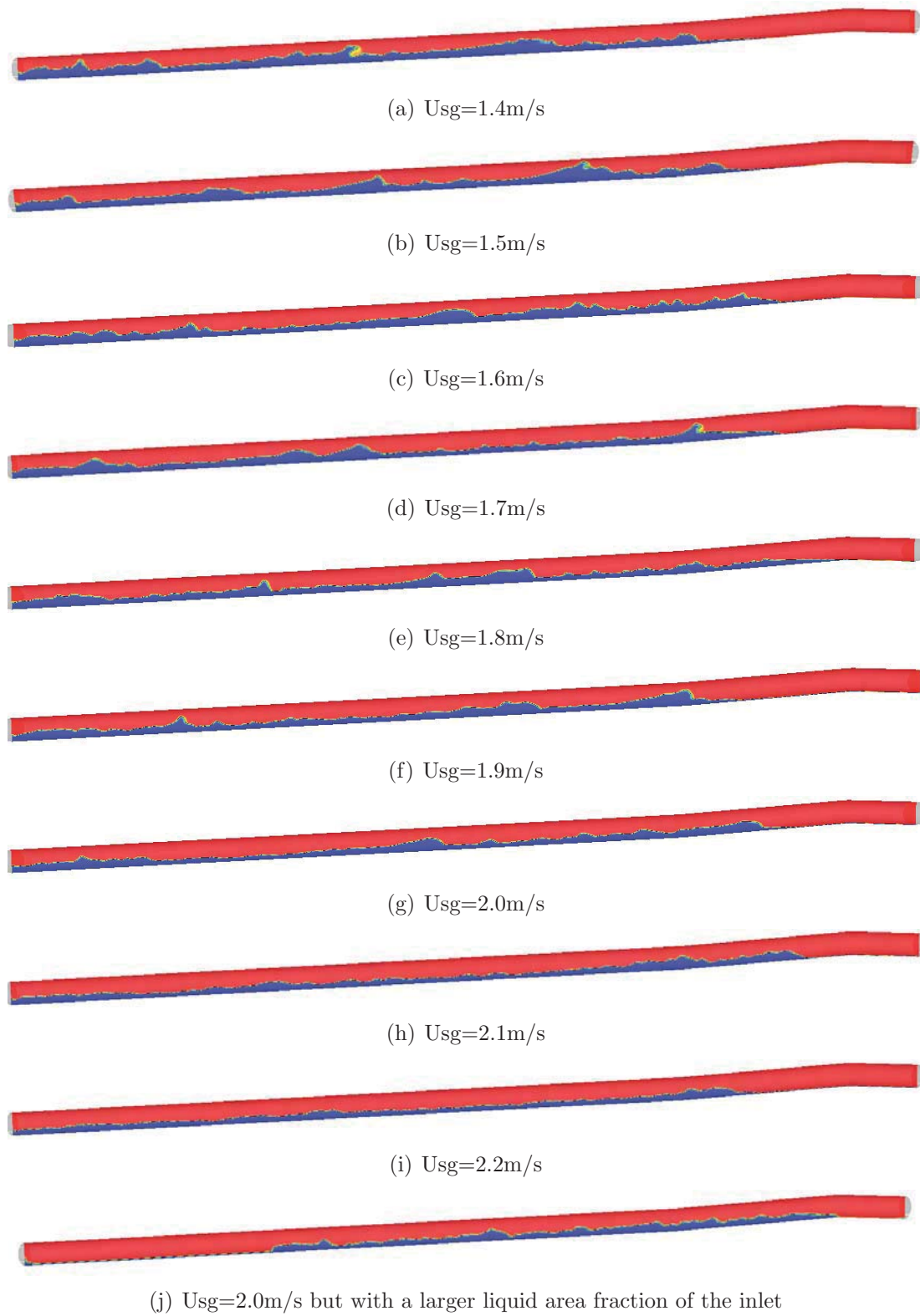


Figure 2.37: $LL=0.01\%$. Geo#1. Snapshot of holdup. The diameters illustrated are stretched by a factor of ten. Blue areas are filled with liquid and red ones with gas.

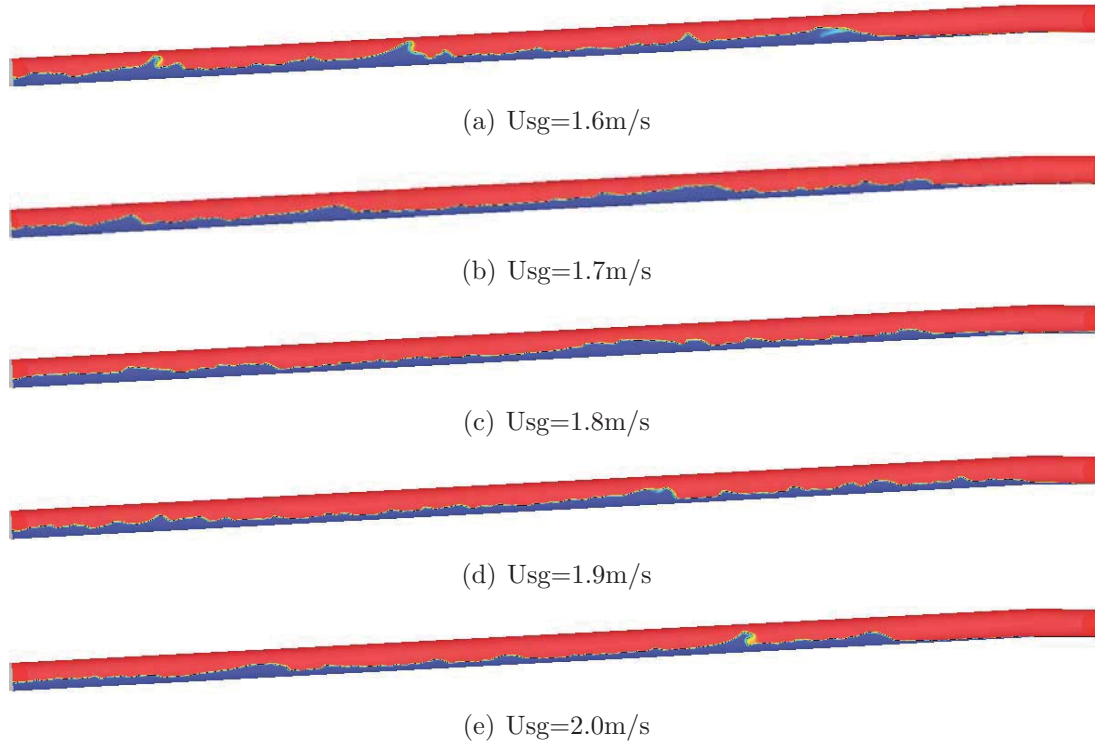


Figure 2.38: LL=0.01%. Geo#2. Snapshot of holdup. The diameters illustrated are stretched by a factor of ten. Blue areas are filled with liquid and red ones with gas.

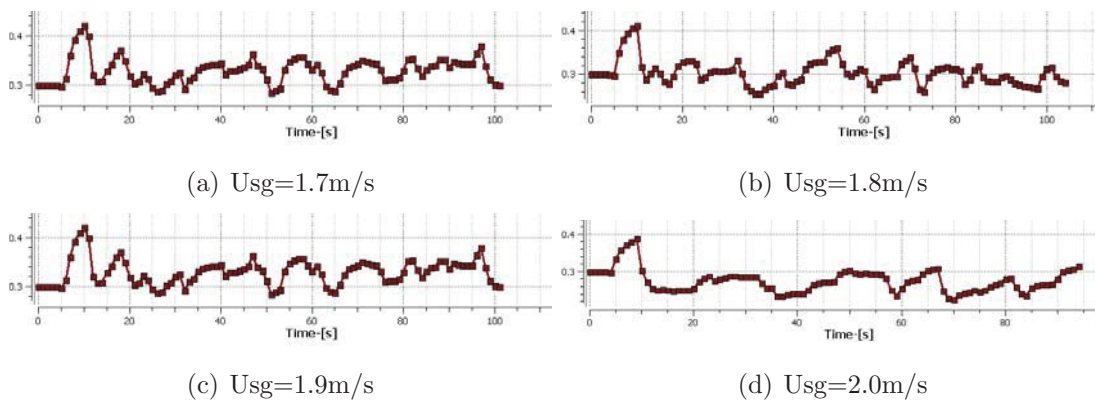


Figure 2.39: LL=0.1%. Liquid Holdup axial averaged $l \in [5\text{m}, 15\text{m}]$. Geo#1

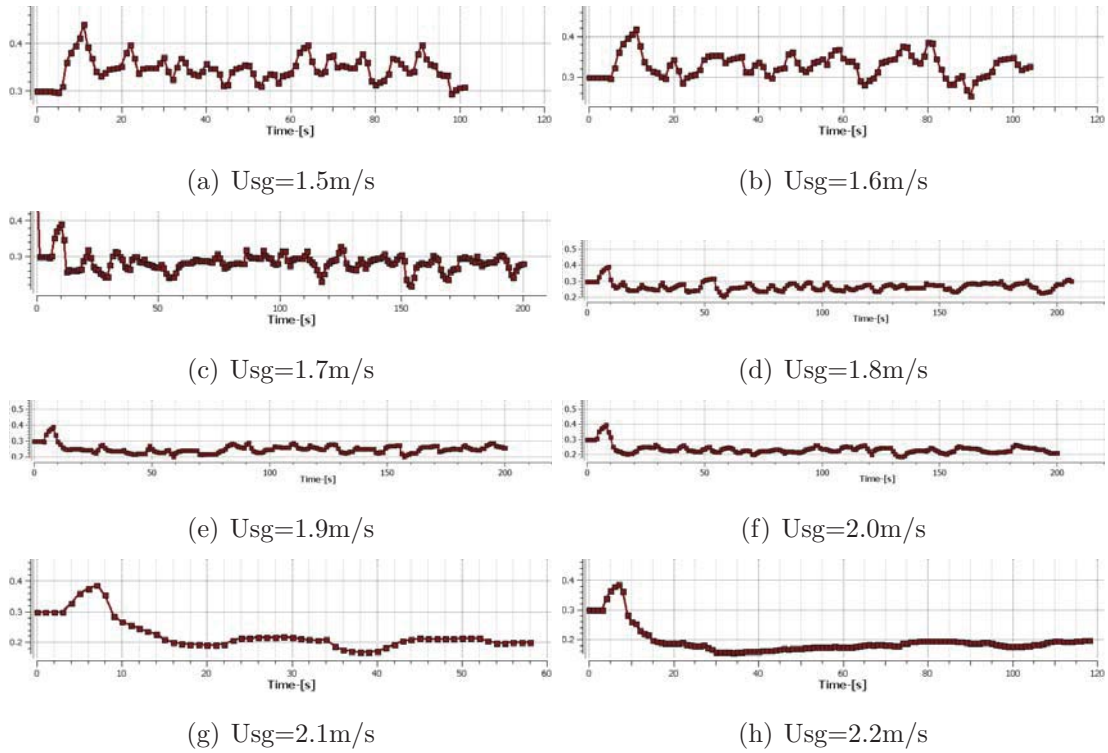


Figure 2.40: $LL=0.01\%$. Liquid Holdup axial averaged $l \in [5m, 15m]$. Geo#1

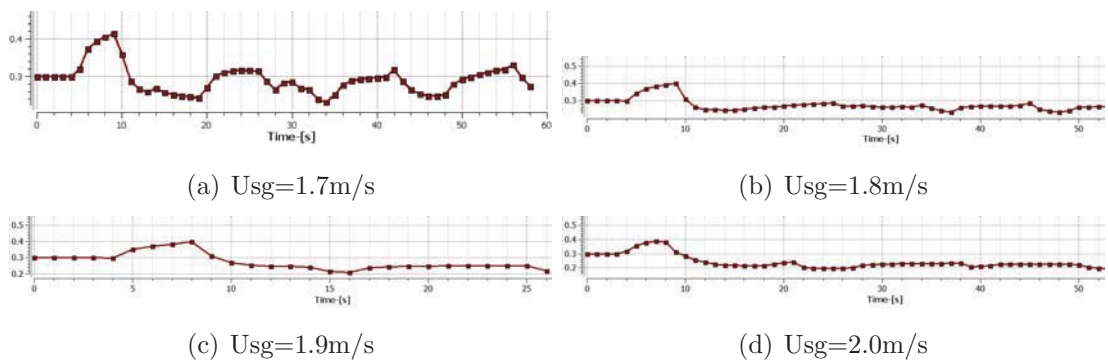


Figure 2.41: $LL=0.01\%$. Liquid Holdup axial averaged $l \in [5m, 15m]$. Geo#2

Plots have also been added similar to the ones for the transient channel simulations, with the liquid holdup spatially averaged in the pipe region that is unaffected by the inlet and outlet boundaries. See Figures 2.39, 2.40 and 2.41. All of them appear to be statistically steady. It has been verified that the interface level change effects are still present, i.e. Geo#1 has enough liquid in the steepest region downstream.

The lower flow rates have larger fluctuations within the averaged region than the higher flow rates due to greater waves on the interface. The time span for each of the simulations differs and could preferably be longer, but time limitations did not allow improvements. It is believed that the time averaged will acceptably represent the statistically steady state holdup.

The flow at any point in space and time is fully transient, but after space- and

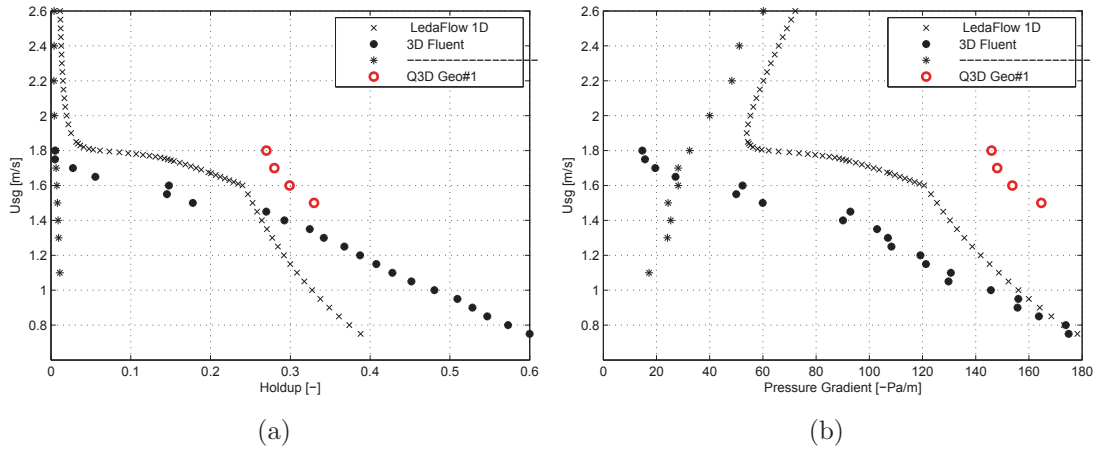


Figure 2.42: LL=0.1%. Liquid Holdup and Pressure Gradient

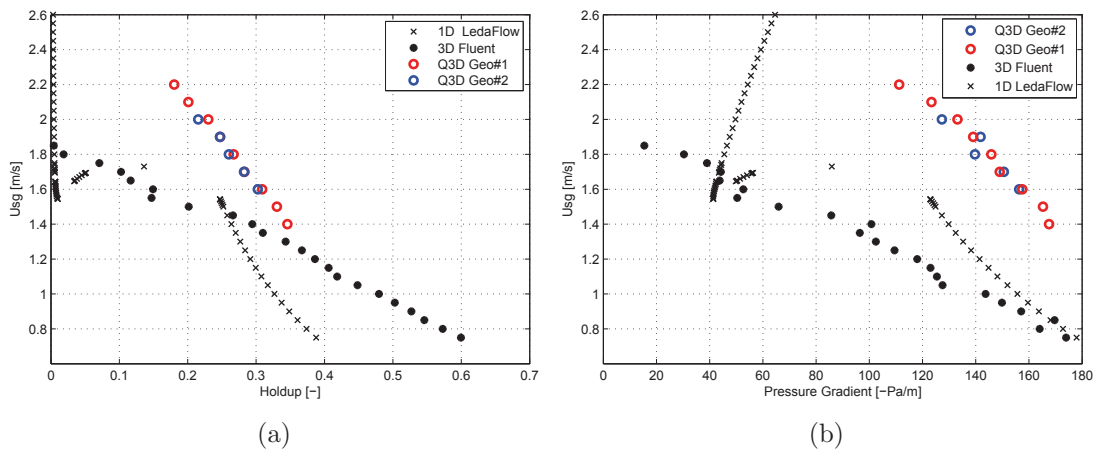


Figure 2.43: LL=0.01%. Liquid Holdup and Pressure Gradient

temporal averaging the flow domain will be compared to the steady state results from LedaFlow 1D and Fluent 3D (see Figures 2.42 and 2.43). This averaged domain will be from axial length $l \in [5\text{m}, 15\text{m}]$ and from $t = 30$ s to the end.

It is interesting to see that the holdup on both geometries and for both liquid loadings are higher than for the steady state simulations. With the higher holdup value it is natural to expect a higher pressure drop since the gas phase occupies a smaller fraction of the pipe and therefore has to travel faster. This is consistent with the situation displayed in the Figures 2.42(b) and 2.43(b), but a higher pressure drop can also arise from other factors such as a wavy surface.

An investigation on the maximum flow rate at which the gravity dominated solution could be found was only performed for the lowest liquid loading. The Q3D simulations found high holdup solutions for flow rates larger than the steady state Fluent 3D, and much larger than LedaFlow 1D.

It would be helpful to compare with a full 3D transient simulation on the geometries from Figure 2.1, or better yet, experimental results.

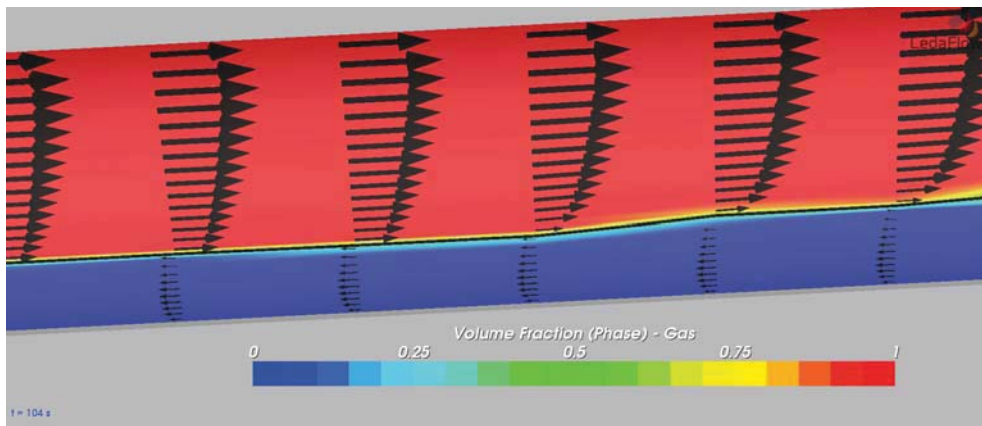
No investigation of the emptying process of the pipe in the multivalued solution region has been performed.

Velocity and Phase Profiles

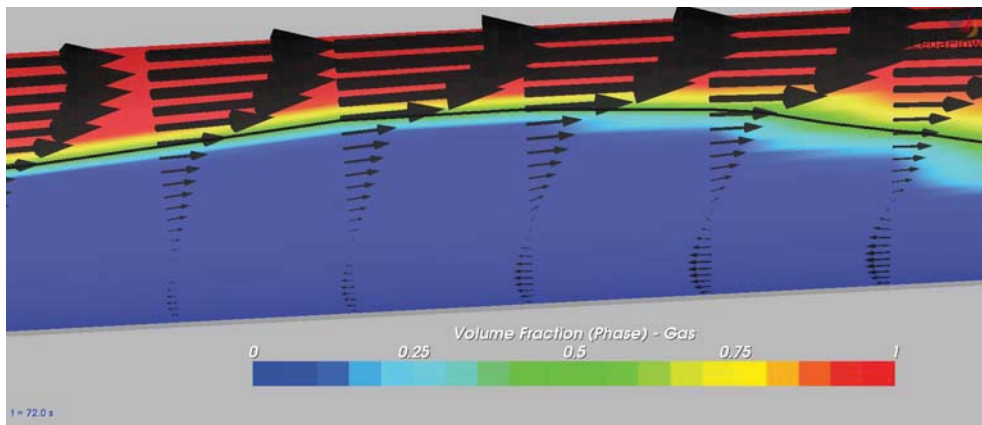
In Figure 2.44 phase contours with an over-layer of velocity vectors are displayed for a wave top and a wave bottom. These illustrations were generated in the LedaFlow Q3D user interface. The easy-to-use program with streamlined model-setup, solver, result viewer and post-processing capabilities was appreciated during this work with a limited available time period.

The spacial and temporal averaged velocity profiles are presented, just as for the transient channel flow. And like the channel flow there will be some difficulties when averaging a wavy flow. However, instead of issues with a shared velocity field, each phase will have both continuous and dispersed fields that impose their own difficulties (see Figure 2.45). Information on the averaged holdup is not included in this velocity field, and the liquid velocity in the region usually occupied by the gas can appear confusing, and vice versa. In order to illustrate why the liquid phase has an average velocity of 5m/s close to the top of the pipe, consider the only time the liquid was in this region; as droplets in the continuous gas phase during a wave top for only a brief moment.

In order to produce illustrations similar to the velocity profiles of the previous sections, the velocity of the liquid in the region below the averaged holdup value, and the gas velocities above have been used (see Figures 2.46, 2.47 and 2.48). The effect of this is that the profiles are not consistent with the average mass flow of each phase, since much of the transport of the liquid will occur close to the surface, and therefore, due to the waves, in regions above the averaged holdup. They all show the same trend as seen in the previous sections.



(a) Wave bottom



(b) Wave top

Figure 2.44: Vector field on top of phase contours

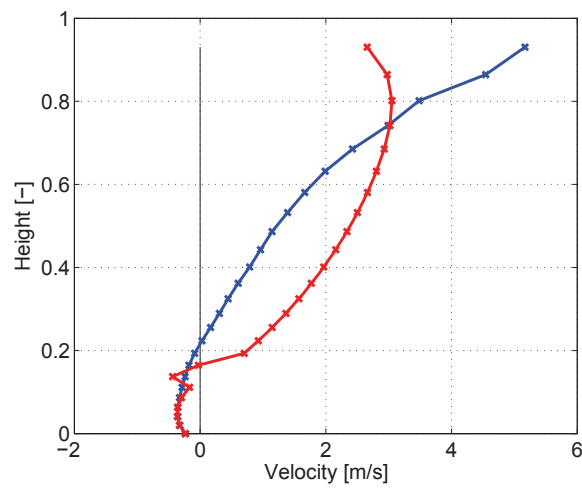


Figure 2.45: Actual velocity profile. $U_{sg}=1.8\text{m/s}$. Gas is red and liquid is blue.

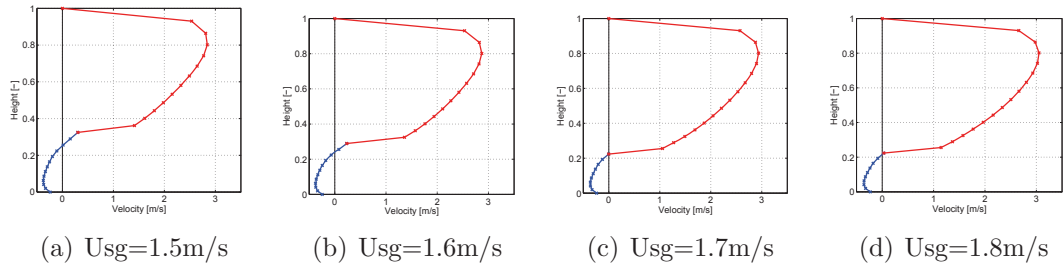


Figure 2.46: LL=0.1%. Geo#1. Averaged velocity profiles

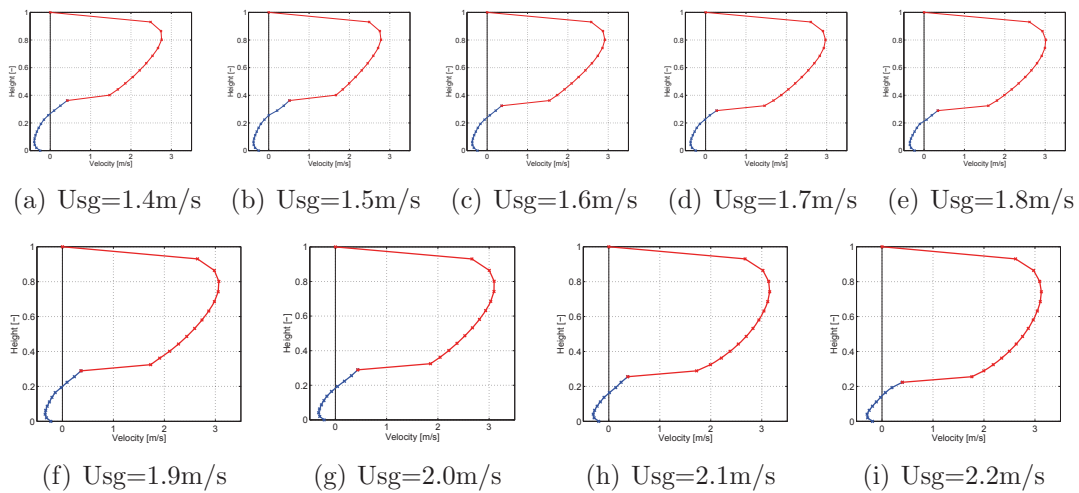


Figure 2.47: LL=0.01%. Geo#1. Averaged velocity profiles

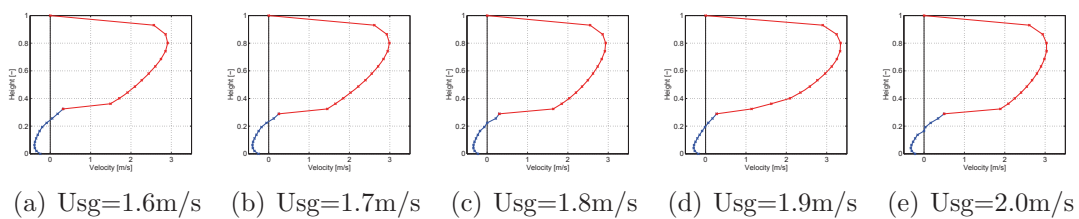


Figure 2.48: LL=0.01%. Geo#2. Averaged velocity profiles

Chapter 3

Discussion

Taitel Dukler model

Multiple holdup solutions are illustrated for both liquid loadings in Figures 2.3 and 2.4. These results formed an illustrative basis of what to expect in terms of holdup and pressure drops for the other models in the multivalued solution region.

LedaFlow 1D steady state

The LedaFlow 1D results indicated that the multivalued solution region is dependent on the modeling of the shear stresses. No multiple solutions were obtained since we were not able to modify how the solver finds the solutions. However, the simulations with the smallest liquid loading indicated a multivalued solution region, since there were random discrete jumps from the low friction dominated solution to the intermediate gravity dominated solution and from the gravity dominated intermediate solution to the low friction dominated solution as the flow rate varied. The intermediate solution has been discarded by physical reasoning in this work. Anyways, LedaFlow's 1D solver behavior is unacceptable and the LedaFlow team should review their solver for flows with very low liquid load. The multivalued solution region was found at lower flow rates than for the TD model. The LedaFlow model is more in accordance with experiments [21].

Interface level gradients did not affect the multivalued solution region. However, it is not believed that the LedaFlow steady state solver accounts for interface level gradients. If this is the case, no effects will be seen.

Fluent 2D steady state

The channel simulations featured multiple solutions with the friction and gravity dominated solutions obtained on different meshes. It should be noted that the results are highly grid *and* geometry dependent. This reduces the confidence in the results.

The effect of interface level gradients was investigated, imposed through pressure profiles corresponding to high and low holdup solutions. The physical expected impact in steady state simulations was that the friction dominated solutions would be favored for a low holdup downstream, and a gravity dominated solution for a high holdup downstream.

A low holdup on the outlet was investigated for the gravity dominated solutions. An illustration of what to expect can be provided by the LedaFlow 1D smallest liquid loading holdup which illustrates a discrete jump from high to low holdup solution as the flow rate was marginally increased into the multivalued solution region. For flow rates below the multivalued solution region, no interface level change effects are expected (through the whole channel) as there is only one solution. For flow rates within the multivalued solution region, however, the solver is expected to choose the low holdup solution over the previously obtained high holdup solution. While it was shown that no high holdup solutions existed for flow rates in the multivalued solution region, the behavior for flow rates below was unexpected. Here, an interface level gradient was located further upstream with higher flow rates (see Figures 2.16 and 2.17). The reason for this has not been understood.

A high holdup on the outlet has no effect on the gravity dominated solutions, as expected. Due to the length of the domain used to produce results on the friction dominated low holdup solution, no such investigation has been performed on the low holdup. It would be interesting to see the effect of a high holdup downstream for a flow initialized with a converged friction dominated holdup solution. This is proposed as future work if a multiphase simulator can converge a low holdup solution for a longer geometry than the one used in this work.

The velocity profiles turned out as expected with back-flow along the wall for the gravity dominated solutions and a discrete change in velocity gradient on the surface. The effect of an increased flow rate was an increased area occupied by the gas. Interestingly, the maximum velocity did not change with increasing flow rate.

Fluent 2D transient

The transient channel simulations supplemented the gravity dominated steady state solutions. The time averaged holdups were close to the ones found from the steady state simulations, thereby removing much of the uncertainty in the steady state results. The surface was wavy for the simulated gravity dominated flows and similar to the transient pipe flows simulated with LedaFlow Q3D. This unsteady surface is a potential candidate to explain the higher pressure drops since the steady state solver has to model the effects of a wavy surface.

The time averaged velocity profiles are not physically correct due to the effects of an unsteady surface, but they display the same trend as the steady state channel flow with a maximum velocity that is independent of the flow rate.

An investigation of mass flux into and out of the domain was performed for the geometries displayed in Figure 2.1. If the hypothesized interface level gradient effects are a physical phenomenon, then they should lead to an emptying of the domain for a transient simulation with a high holdup solution in the multiple solution region when a low holdup solution is imposed downstream. This emptying would begin downstream and propagate upstream, represented by the mechanism where potential gravitational energy of the liquid is converted into kinetic energy of the liquid, i.e. the friction dominated low holdup solution.

This expected emptying rate was found, and the trend was that higher flow rates had higher emptying rates. This also makes sense because it has more potential to carry away surplus liquid while still maintaining a friction dominated holdup.

The geometry with a steeper downstream segment, and therefore a predicted high holdup in this segment, should according to the hypothesis maintain the high holdup solution in the domain. This was not the case as Figure 2.29 displays. More liquid exited the domain throughout the whole period investigated. This emptying trend should be further investigated on other inclinations and segment length before a conclusion can be reached, but if this trend is correct, then there will in theory never exist a statistical steady state high holdup solution in the multivalued solution region. Only a temporary solution while the pipe is undergoing an emptying process.

Fluent 3D steady state

Multiple holdup solutions were found for the large liquid load, and even though the friction dominated solutions were not obtained for the smallest liquid loading, it is expected that a multivalued solution region exists here as well. The gravity dominated holdup changes almost linearly with the flow rates, a trend that has only been identified for Fluent 3D steady state. The pressure drops are consistently lower than predicted by LedaFlow 1D.

The investigation of interface level gradients were not satisfactory due to the reduced impact the pressure profiles on the outlet had on the holdup. With no prominent interface level gradient the same procedure as performed for the 2D channel flow did produce similar effects.

LedaFlow Q3D transient

The holdups and pressure drops found for the gravity dominated solutions were higher than predicted by the steady state LedaFlow 1D and Fluent 3D. Snapshots of the pipe displays the irregular wavy surface for different flow rates. As predicted for the Fluent 2D transient channel flow, the amplitude of the waves appears to decrease with increasing flow rates.

LedaFlow Profile Model

In addition to the results presented in this chapter, there is one more model in LedaFlow that was tested for flow rates in the multivalued solution region. The results from this LedaFlow Profile Model were poor and have therefore been moved to Appendix B. Two grid resolutions were tested, but no explanation on how the results were obtained or discussion on the results will be given.

Overall

It is difficult to reach any conclusion as to which of the simulators generates the most accurate results without any experimental data to compare with.

Much time was spent to force the steady state simulations to produce usable results. With mass imbalance in addition to grid and geometry dependence, it becomes clear that simulating the effects of the interface level gradients might not be suited for the Fluent steady state solver.

Transient multidimensional simulations are better on investigating the hypothesized interface level gradient effects, but due to the span in length and time scales such simulations become computationally demanding really fast. Experiments are therefore proposed as future work, due the higher level of confidence inherent in experimental results.

User Experience

Fluent's versatility to some degree deteriorates the user friendliness, when comparing it to a program specialized on a particular flow. The pre-process consisting of generating a geometry, meshing and setting up a solver was easier and quicker with the LedaFlow, as should be expected from this specialized program. Some post-processing features of were also very helpful, and sincerely missed in Fluent. The simple option of changing the aspect ratio of diameter and axial length, allows for viewing of the entire pipe at once. There is a workaround in Fluent, but it is complicated and involves external programs. The time evolution of the desired flow property was easy to view during the transient simulations in LedaFlow with refreshing information as the solver progressed. This is not possible inside the Fluent, but extracted transient information can be viewed in CFD-Post. This program function quite differently from Fluent, which means more time must be spend learning instead of doing.

One of the features I missed in LedaFlow was the feeling of control that the easy viewing of residuals that Fluent provides. Another feature is the user defined functions which Fluent relies so heavily upon to be flexible. While it is true that LedaFlow manages fine without them, it would not be a nice feature to have to increase the flexibility and versatility.

Chapter 4

Conclusion

- The one dimensional Taitel-Dukler model predicted multiple holdup solutions for both the liquid loadings investigated in this work. LedaFlow 1D predicted a continuous transition from low to high holdup for $LL=0.1\%$, which indicates that there will not be multiple solutions for this liquid loading (according to the LedaFlow 1D model). A discrete jump is predicted in the transition region for $LL=0.01\%$, which is a clear sign of multiple solutions. The intermediate solution is also chosen by the LedaFlow 1D solver for some flow rates. This solution is rejected in this work due to physical reasoning¹. The deviances between the one dimensional models are mainly due to differences in shear stress modeling. No effects of interface level gradients were found. This is likely to be caused by the LedaFlow steady state model not accounting for interface level gradients. The OLGA 7 steady state model accounts for hydraulic level gradients and shows such dependence [21].
- The Fluent steady state simulations had mass imbalance issues as well as being both grid and geometry dependent, but produced results consistent with the independent Fluent transient simulations. Multiple holdup solutions have been found for both liquid loadings using two different meshes; one for the friction dominated low holdup and one for the gravity dominated high holdup solution. The effect of a low holdup downstream produced a low holdup in the multivalued solution region for the 2D channel simulations. The effect of a high holdup downstream on a multivalued solution region initialized with a low holdup solution has not been investigated due to computational cost, constraints and difficulties. The holdup downstream for the steady state 3D pipe simulations was less responding to the pressure profile imposed at the outlet, so no effect of interface level gradients has been found in the upstream multivalued solution region.

¹An extended explanation of the argument of inconsistency can be found on page 17

- The transient Fluent 2D channel simulations investigated the mass flux in and out of the geometries displayed in Figure 2.1. If the hypothesized interface level gradient effects are correct, then a pipe with the high holdup solution in the multivalued solution region should be emptied for a transient simulation with a low holdup solution imposed downstream. This emptying would begin downstream and propagate upstream. This expected emptying rate was found, and the trend was that higher flow rates had higher emptying rates. Interestingly, also the pipe with a steeper downstream region had larger mass flux out than into the domain. It may very well be that the section with high inclination is too short to stop surging waves from the 3° section entering the downward section. This emptying trend should be further investigated on other inclination combinations and section length before a conclusion can be reached. This work, however, does not support the possible existence of the high holdup solution in the multivalued solution region.
- LedaFlow Q3D produced transient simulations on gravity dominated holdup solutions in the multivalued solution region. The holdups and pressure drops were higher than predicted by the steady state LedaFlow 1D and Fluent 3D. Snapshots of the pipe displays the irregular wavy surface for different flow rates. The amplitude of the waves appear to decrease with increasing flow rates.

Appendices

A - Turbulence

This work is taken from [5].

Turbulence is a flow regime where properties such as pressure and velocity fluctuates randomly in time and space. It is no longer a steady and predictable flow, i.e laminar flow, due to the ratio between inertial and viscous forces. When this ratio, represented by the Reynolds number $Re_x = \frac{Ux}{\nu}$, gets sufficiently high the viscous forces are no longer able to dampen the convective fluctuations and the flow becomes unstable and chaotic i.e. turbulent. The legendary physicist Richard Feynman stated that turbulence is one of the biggest unsolved problems of classical physics. Unfortunately in fluid dynamics laminar flow is the exception, rather than the rule. But even though turbulence still is much of a mystery, some characteristics about it's spatial structure can be described: [35, p. 400]

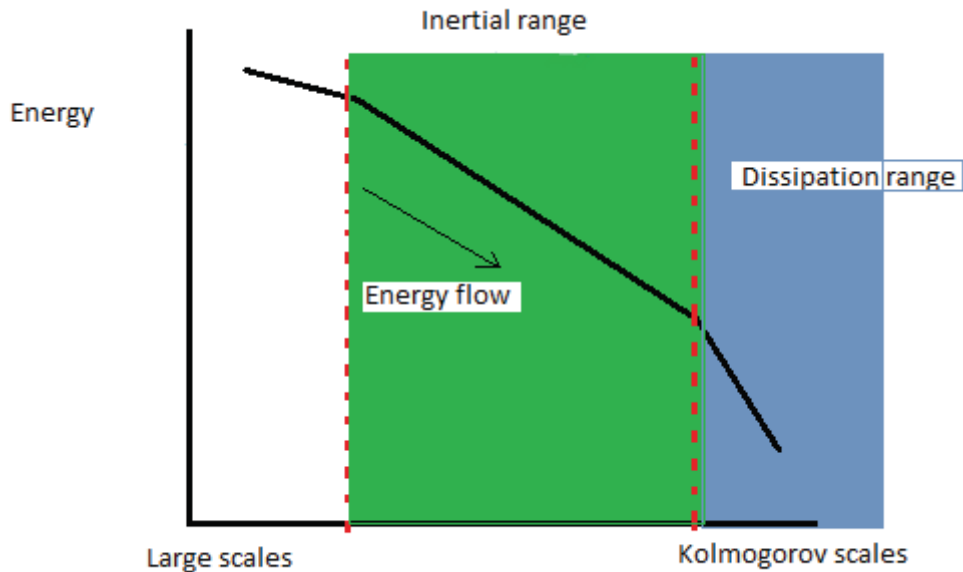
- *Fluctuations* in pressure, velocity and temperature in all three directions. Turbulence is a 3D phenomenon.
- *Eddies* of varying size intermingle and fill the shear layer.
- *Random* variations in fluid properties.
- *Self-sustaining* motion. Produces new eddies to replace those lost by viscous dissipation.
- *Mixing* is much stronger than in the case of laminar (molecular) action. Ambient laminar fluid is entrained in a turbulent flow.

Even though it does not exist any theoretical model describing turbulence, it is believed that the Navier-Stokes equations contain the information if the resolution of the calculation domain is high enough. The domain has to capture every motion from the large scales to the smallest Kolmogorov micro-scales. [32, p. 20] A relation between large and small length scales can be found:

$$\frac{L}{\eta_k} = Re^{\frac{3}{4}} \quad (\text{A.1})$$

$$\left(\frac{L}{\eta_k}\right)^3 = Re^{\frac{9}{4}} \quad (\text{A.2})$$

As we can see, grid nodes in three dimensions are proportional to $Re^{\frac{9}{4}}$, so Direct Numerical Simulation (DNS) of turbulence demands extreme amounts processing power and is at this time reserved for academic research with supercomputers. Instead of using DNS to the Navier-Stokes equations without any modeling one can employ filtering. The equations are solved in their natural form down to the grid scales; and then all smaller scales are modeled. This is called Large Eddy Simulation, LES.



Large Eddy Simulation

In LES, large eddies are resolved directly, while small eddies are modeled. Large eddy simulation thus falls below DNS in terms of the fraction of the resolved scales. The rationale behind LES can be summarized as follows:

- Momentum, mass, energy, and other properties are transported mostly by large eddies.
- Large eddies are more problem-dependent. They are dictated by the geometries and boundary conditions of the flow involved.
- Small eddies are less dependent on the geometry, tend to be more isotropic, and are consequently more universal.
- The chance of finding a universal turbulence model is much higher for small eddies.

Resolving only the large eddies allows a coarser mesh and larger time steps in LES than in DNS. However, LES still requires substantially finer meshes than those typically used for RANS (next section) calculations. In addition, LES has to be run for a sufficiently long flow-time to obtain stable statistics of the flow being modeled. As a result, the computational cost involved with LES is normally orders of magnitude higher than that for steady RANS calculations in terms of memory (RAM) and CPU time. Therefore, high-performance computing (e.g., parallel computing) is a necessity for LES, especially for industrial applications. The main shortcoming of LES lies in the high resolution requirements for wall

boundary layers. Near the wall, even the “large” eddies become relatively small and require a Reynolds number dependent resolution. This limits LES for wall bounded flows to very low Reynolds numbers (10^4) and limited computational domains.

Figure A shows how the scales are separated in the different models. DNS resolves all scales, LES models the area marked in blue, while RANS-based methods model the area marked by blue and green.

Reynolds Averaged Navier-Stokes Equations

This section utilizes *Einstein’s summation convention*, which is a notational convention where if two index variables appear twice in the same term, this implies a summing over all its possible values. We switch notations for the RANS equations as it is the most common representation in the literature. As an example consider the vector \vec{V} :

$$\vec{V} = u\vec{e}_1 + v\vec{e}_2 + w\vec{e}_3 = \sum_{i=1}^3 u_i\vec{e}_i \quad (\text{A.3})$$

and $u_i \frac{\partial u_j}{\partial u_i}$

$$u_i \frac{\partial u_j}{\partial u_i} = u_i \left(\frac{\partial u}{\partial x} + \frac{\partial v}{\partial y} + \frac{\partial w}{\partial z} \right) \quad (\text{A.4})$$

In 1895 Reynolds introduced the idea of time averaging the Navier-Stokes equation, by using Reynolds decomposition:

$$u_j = \bar{u}_j + u'_j \quad (\text{A.5})$$

Here we see the velocity components decomposed into a mean (time-averaged) \bar{u}'_j and a fluctuating value u_j with $j = 1, 2, 3$. The decomposition is analogous for pressure and other scalar quantities: $\phi = \bar{\phi} + \phi'$. The time average for any variable V is defined as:

$$\bar{V} = \frac{1}{T} \int_{t_0}^{t_0+T} V dt$$

And for the fluctuations we have:

$$\overline{u'_j} = \frac{1}{T} \int_{t_0}^{t_0+T} u'_j dt = 0 \quad (\text{A.6})$$

This decomposition is inserted into the Navier-Stokes equations yields:

$$\frac{\partial \rho}{\partial t} + \frac{\partial}{\partial x_i} (\rho u_i) = 0 \quad (\text{A.7})$$

$$\frac{\partial}{\partial t}(\rho u_i) + \frac{\partial}{\partial x_j}(\rho u_i u_j) = -\frac{\partial p}{\partial x_i} + \frac{\partial}{\partial x_j} \left[\mu \left(\frac{\partial u_i}{\partial x_j} + \frac{\partial u_j}{\partial x_i} - \frac{2}{3} \delta_{ij} \frac{\partial u_k}{\partial x_k} \right) \right] + \frac{\partial}{\partial x_j} (-\overline{\rho u'_i u'_j}) \quad (\text{A.8})$$

The momentum equations looks exactly like the non-averaged except for $\frac{\partial}{\partial x_j} (-\overline{\rho u'_i u'_j})$.

$$\tau_{ij}^t \equiv -\overline{\rho u'_i u'_j} = -\rho \begin{pmatrix} \overline{u'^2} & \overline{u'v'} & \overline{u'w'} \\ \overline{v'u'} & \overline{v'^2} & \overline{v'w'} \\ \overline{w'u'} & \overline{w'v'} & \overline{w'^2} \end{pmatrix} \quad (\text{A.9})$$

This term, the Reynolds stress tensor, actually comes from the left hand side convection term, and represents the mean transport of fluctuating momentum by turbulent velocity fluctuations. Mean flow momentum is transformed into turbulence through equation A.9. [32, p. 32] But instead of treating the term as a momentum flux, we can consider it as a divergence of stress, where the diagonal normal stress components creates a “turbulent pressure” while the symmetric off-diagonals create shear stresses. Therefore the term is put on the right hand side as a stress tensor, τ_{ij} , but we still have to quantify the 6 new unknowns which came out of this decomposition. This is known as the closure problem in turbulence modeling, as we have 4 equations (continuity and 3 momentum equations) and 10 unknowns (p, u, v, w and the Reynolds stresses). This leads us to Boussinesq’s eddy viscosity hypothesis.

Boussinesq’s Eddy Viscosity Hypothesis

The most common way of solving the closure problem is to use the Boussinesq hypothesis, which relates Reynolds stresses to a turbulent viscosity ν_t and the mean velocity gradients:

$$-\overline{\rho u'_i u'_j} \equiv \mu_t \left(\frac{\partial u_i}{\partial x_j} + \frac{\partial u_j}{\partial x_i} \right) - \frac{2}{3} \left(\rho k + \mu_t \frac{\partial u_k}{\partial x_k} \right) \delta_{ij} \quad (\text{A.10})$$

Where δ_{ij} is the Kronecker delta .

$$\delta_{ij} = \begin{cases} 1 & \text{if } i=j \\ 0 & \text{if } i \neq j \end{cases} \quad (\text{A.11})$$

If we assume incompressible flow:

$$-\overline{\rho u'_i u'_j} \equiv \mu_t \left(\frac{\partial u_i}{\partial x_j} + \frac{\partial u_j}{\partial x_i} \right) - \frac{2}{3} \rho k \delta_{ij} \quad (\text{A.12})$$

When inserted into the momentum equation A.8 we get:

$$\frac{\partial u_i}{\partial t} + u_j \frac{\partial u_i}{\partial x_j} = -\frac{1}{\rho} \frac{\partial p}{\partial x_i} + \frac{\partial}{\partial x_j} \left[(\nu + \nu_t) \left(\frac{\partial u_i}{\partial x_j} + \frac{\partial u_j}{\partial x_i} \right) \right] \quad (\text{A.13})$$

This somewhat crude approach to the eddy viscosity has some large impacts on the flow. In our equation above the eddy viscosity ν_t is a scalar, i.e. it has no sense of direction. Which means that the turbulence is *isotropic*, equal in every direction, which clearly is wrong. Nevertheless, the assumption of isotropic turbulence can yield good results for shear flows dominated by only one component of the turbulent shear stresses, such as wall boundary layers, mixing layers, jets etc. The two most used turbulence models which calculate ν_t as a scalar value are the k - ϵ model and the k - ω model.

Two-Equation Turbulence Models

The Standard k - ϵ Model

By dimensional analysis we see that

$$\nu_t = \left[\frac{m^2}{s} \right], k = \left[\frac{m^2}{s^2} \right], \epsilon = \left[\frac{m^2}{s^3} \right] \quad (\text{A.14})$$

and therefore

$$\nu_t = C_\mu \frac{k^2}{\epsilon} \quad (\text{A.15})$$

where C_μ is calibrated to keep the turbulent production equal to the dissipation.

Two transport equations are now solved, one for k and one for ϵ . [1, section 4.3.1.2]

$$\frac{\partial}{\partial t}(\rho k) + \frac{\partial}{\partial x_i}(\rho k u_i) = \frac{\partial}{\partial x_j} \left[\left(\mu + \frac{\mu_t}{\sigma_k} \right) \frac{\partial k}{\partial x_j} \right] + G_k + G_b - \rho \epsilon - Y_M + S_k \quad (\text{A.16})$$

and

$$\frac{\partial}{\partial t}(\rho \epsilon) + \frac{\partial}{\partial x_i}(\rho \epsilon u_i) = \frac{\partial}{\partial x_j} \left[\left(\mu + \frac{\mu_t}{\sigma_\epsilon} \right) \frac{\partial \epsilon}{\partial x_j} \right] + C_{1\epsilon} \frac{\epsilon}{k} (G_k + C_{3\epsilon} G_b) - C_{2\epsilon} \rho \frac{\epsilon^2}{k} + S_\epsilon \quad (\text{A.17})$$

In these equations, G_k represents the generation of turbulence kinetic energy due to the mean velocity gradients. G_b is the generation of turbulence kinetic energy due to buoyancy. Y_M represents the contribution of the fluctuating dilatation in compressible turbulence to the overall dissipation rate. $C_{1\epsilon}$, $C_{2\epsilon}$, and $C_{3\epsilon}$ are constants. σ_k and σ_ϵ are the turbulent Prandtl numbers for k and ϵ , respectively. S_k and S_ϵ are user-defined source terms.

The Realizable k - ϵ Model

The realizable k - ϵ model differs from the standard k - ϵ model in two important ways:

- The realizable k - ϵ model contains an alternative formulation for the turbulent viscosity.
- A modified transport equation for the dissipation rate, ϵ , has been derived from an exact equation for the transport of the mean-square vorticity function.

The term “realizable” means that the model satisfies certain mathematical constraints on the Reynolds stresses, consistent with the physics of turbulent flow. [1, section 4.3.1.2] To understand the mathematics behind the realizable k - ϵ model, combine the Boussinesq hypothesis, eq. A.10 on page 53, and the eddy viscosity definition, eq. A.15 on page 54, to obtain the following expression for the normal Reynolds stress in an incompressible strained mean flow:

$$\overline{u^2} = \frac{2}{3}k - 2\nu_t \frac{\partial U}{\partial x} \quad (\text{A.18})$$

Here you see that the normal stress u^2 - which by definition is a positive quantity becomes negative, i.e “non-realizable”, when the strain is large enough to satisfy

$$\frac{k}{\epsilon} \frac{\partial U}{\partial x} > \frac{1}{3C_\mu} \approx 3.7 \quad (\text{A.19})$$

This unphysical behavior is avoided by converting the constant C_μ into a variable that is aware of the values of the normal stresses, correcting the sign and thus *realizing* the model. This adaption improves the model in regions of strong curvature, strong gradients and rotation.

The k - ω Model

The k - ω model is similar to the k - ϵ model, it also takes advantage of the Boussinesq approximation. But instead of deriving a transport equation for the dissipation, a transport equation for the specific dissipation is derived, with specific dissipation defined as:

$$\omega = \frac{\epsilon}{k} \quad (\text{A.20})$$

which results in a change in the eddy viscosity:

$$\nu_t = \frac{k}{\omega} \quad (\text{A.21})$$

The transport equations are given as: [1, section 4.4.1.2]

$$\frac{\partial}{\partial t}(\rho k) + \frac{\partial}{\partial x_j}(\rho k u_j) = \frac{\partial}{\partial x_j} \left[\left(\mu + \frac{\mu_t}{\sigma_k} \right) \frac{\partial k}{\partial x_j} \right] + G_k - Y_k + S_k \quad (\text{A.22})$$

and

$$\frac{\partial}{\partial t}(\rho\omega) + \frac{\partial}{\partial x_j}(\rho\omega u_i) = \frac{\partial}{\partial x_j} \left[\left(\mu + \frac{\mu_t}{\sigma_\omega} \right) \frac{\partial \omega}{\partial x_j} \right] + G_\omega - Y_\omega + S_\omega \quad (\text{A.23})$$

The advantage of k - ω over k - ϵ is that it is easier to implement near wall treatment, it does not overestimate production of turbulence and it handles recirculation better. Unfortunately k - ω has a much bigger sensitivity towards the free-stream velocities and inlet conditions.

The SST k - ω Model

The core idea behind Mentner's SST k - ω model [28] was to merge the advantageous aspects of the k - ϵ and k - ω models into a single model. The two models are coupled together by a blending function which results in a model that is robust in the far field, and still able to model accurately the near-wall region. From Fluent's Theory Guide section 4.4.2.1:

- "The standard k - ω model and the transformed k - ϵ model are both multiplied by a blending function and both models are added together. The blending function is designed to be one in the near-wall region, which activates the standard k - ω model, and zero away from the surface, which activates the transformed k - ϵ model.
- The SST model incorporates a damped cross-diffusion derivative term in the ω equation.
- The definition of the turbulent viscosity is modified to account for the transport of the turbulent shear stress.
- The modeling constants are different."

Round-up of the two-equation models

Because of their robustness, low computational cost and reasonable accuracy for a large range of flows, the two-equation turbulence models have become popular in the CFD-community. They give better results than the algebraic mixing length model and they are very well validated, especially k - ϵ . Negative aspects of the two-equation models are that they treat turbulence/eddy viscosity as an isotropic quantity, and therefore perform poorly when the variations of the diagonal components of the Reynolds stresses are significant, i.e in high shear zones where gradients are strong. Even though the transport equations of k , ϵ and ω are exact, their coupling to the eddy viscosity is based on physical reasoning and phenomenological considerations, so the models are semi-empirical and relies on constants derived from experiments on specific flows. This is a big drawback as it is like creating a model for yesterday's weather.

Reynolds Stress Models

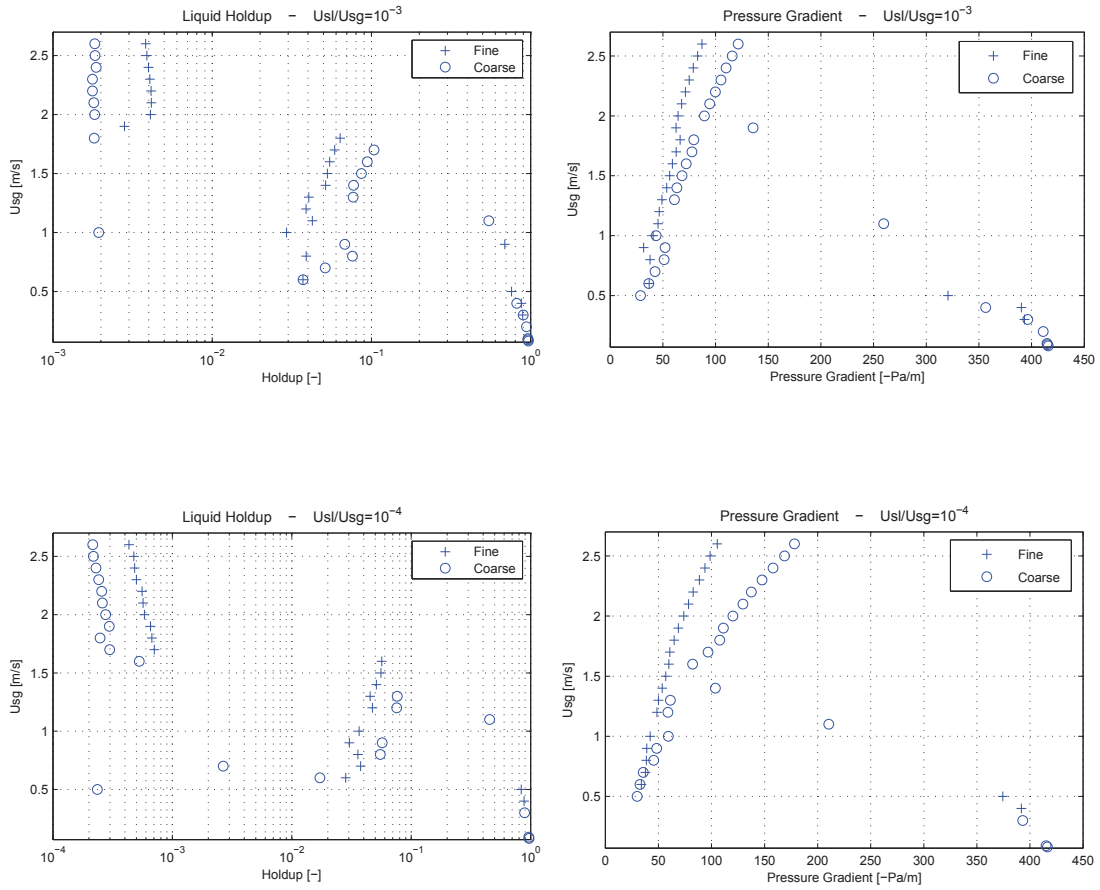
The Reynolds stress model is an advanced RANS-model which does not take advantage of the Boussinesq eddy viscosity hypothesis. RSM solves the closure problem by deriving a transport equation for each of the Reynolds stresses, as well as an equation for the dissipation rate. So for a three dimensional flow, seven new partial differential equations have to be solved. Unfortunately only parts of the transport equations are exact, meaning that some modeling assumptions needs to be made which again leads to uncertainties and accuracy loss of the model. On the bright side, the turbulence is no longer isotropic because all of the Reynolds stresses are computed. This makes RSM a better option than two-equation models when the flow experiences curvature, swirl and rotation i.e combustor flow, cyclone flow or in rotating equipment. The equations with their closure models are long and complex and the reader is guided to articles by Brian Edward Launder for thorough details [24].

The Scale-Adaptive Simulation

Lastly we present the summary of the 2D SAS model we employed; from the theory guide section 2.7:

”The Scale-Adaptive Simulation (SAS) is an improved Unsteady RANS formulation, which allows the resolution of the turbulent spectrum in unstable flow conditions. The URANS simulation produces only the large-scale unsteadiness, whereas the SAS-SST model adjusts to the already resolved scales in a dynamic way and allows the development of a turbulent spectrum in the detached regions. The SAS concept is based on the introduction of the von Karman length-scale into the turbulence scale equation. The information provided by the von Karman length-scale allows SAS models to dynamically adjust to resolved structures in a URANS simulation, which results in an LES-like behavior in unsteady regions of the flow field. At the same time, the model provides standard RANS capabilities in stable flow regions.”

B - LedaFlow Profile Model



C -User Defined Functions

```

#include "udf.h"
DEFINE_PROFILE(Pressure,ft,i) /*Pressure profile*/
{
    real x[ND_ND];          /*this will hold the position vector */
    real y;
    real h;
    real p;
    real a;
    face_t f;

    begin_f_loop(f,ft)
    {
        F_CENTROID(x,f,ft);
        h=0.0685;           /*Diameter of pipe*/
        y=x[1]/h;           /*Non-dimensional height (x[0]=x, x[1]=y)*/
        a=0.25;             /*Non-dimensional liquid height*/
        p=48*9.796555736*(1-y)*h; /*Pressure at the given height*/
        if (y<a)
        {
            p=9.796555736*((1-a)*48+(a-y)*817)*h;
        }
        F_PROFILE(f,ft,i) = p;
    }
    end_f_loop(f,ft)
}

DEFINE_PROFILE(fractionVOF,ft,i) /*Vof profile*/
{
    real x[ND_ND];
    real y;
    real h;
    real p;
    real a;
    face_t f;

    begin_f_loop(f,ft)
    {
        F_CENTROID(x,f,ft);
        h=0.0685;
        y=x[1]/h;
        a=0.25;
        d=0;
        if (y<a)
        {
            d=1;
        }
        F_PROFILE(f,ft,i) = d;
    }
    end_f_loop(f,ft)
}

DEFINE_PROFILE(VelDist,ft,i) /*Velocity profile*/
{
    real x[ND_ND];
    real y;
    real h;
    real v;
    real a;
    face_t f;

    begin_f_loop(f,ft)
    {
        F_CENTROID(x,f,ft);
        h=0.0685;
        y=x[1]/h;
        a=0.25;
        v=1.95/(1-a);
        if (y<a)
        {
            v=1.95*0.0001/(a);
        }
        F_PROFILE(f,ft,i) = v;
    }
    end_f_loop(f,ft)
}

```

```

#include "udf.h"
DEFINE_PROFILE(Pres,ft,i) /*Pressure profile*/
{
    real x[ND_ND]; /* this will hold the position vector */
    real z;
    real p;
    real h;
    real a;
    face_t f;
    begin_f_loop(f,ft)
    {
        F_CENTROID(x,f,ft);
        h=0.0685;
        z=(x[1]*2/h+1)/2;
        a=0.25;
        p=9.796556*h*48*(1-z);
        if (z<a)
        {
            p=9.796556*h*(48*(1-a)+817*(a-z));
        }
        F_PROFILE(f,ft,i) = p;
    }
    end_f_loop(f,ft)
}

/* VOF profile same as 2D */
DEFINE_PROFILE(Vel,ft,i) /*Vel profile*/
{
    real x[ND_ND]; /* this will hold the position vector */
    real z;
    real v;
    real h;
    real a;
    real area;
    real theta;
    real pi=4*atan(1);
    face_t f;
    begin_f_loop(f,ft)
    {
        F_CENTROID(x,f,ft);
        h=0.0685;
        z=(x[1]*2/h+1)/2;
        a=0.25;
        theta=2*acos(1-a*2); /* 1 */
        area=(theta-sin(theta))/(2*pi); /* 2 */
        v=1.65/(1-area); /* 3 */
        if (z<a) /* 4 */
        { /* 5 */
            v=1.65*0.001/(area); /* 6 */
        }
        F_PROFILE(f,ft,i) = v;
    }
    end_f_loop(f,ft)
}

/* 1 Area of a circle segment= 1/2*(theta-sin(theta))*r^2 */
/* 2 where theta is the middle angle in a triangle defining the segment (in radians) */
/* 3 r=a+r*cos(theta/2), leading to the area of the segment in the expression */
/* 4 that has been divided by the total area to give the gas and liquid fraction area. */
/* 5 In the theta equation the liquid height a is divided by r which is half */
/* 6 of the total height therefore multiplied by a factor of two*/

```

1D LedaFlow						1D LedaFlow					
Usl/Usg 0.01%						Usl/Usg 0.1%					
Usg	Holdup	Pressure Gradient	Usg	Holdup	Pressure Gradient	Usg	Holdup	Pressure Gradient	Usg	Holdup	Pressure Gradient
0,750	0,387813	-177,95	1,644	0,006300	-42,54	0,750	0,388165	-178,23	1,765	0,131004	-84,93
0,800	0,373631	-172,85	1,645	0,033851	-49,82	0,800	0,373999	-173,14	1,770	0,123419	-82,39
0,850	0,360556	-168,14	1,648	0,034671	-50,13	0,850	0,360939	-168,45	1,775	0,115277	-79,68
0,900	0,348463	-163,75	1,650	0,035209	-50,34	0,900	0,348861	-164,08	1,780	0,106784	-76,87
0,950	0,337246	-159,63	1,660	0,038133	-51,44	0,950	0,337657	-159,97	1,785	0,096863	-73,59
1,000	0,326811	-155,71	1,670	0,041405	-52,67	1,000	0,327235	-156,06	1,790	0,085733	-69,94
1,050	0,317079	-151,95	1,680	0,045025	-54,01	1,050	0,317515	-152,32	1,795	0,073319	-65,92
1,100	0,307630	-148,17	1,690	0,049384	-55,61	1,100	0,308430	-148,71	1,800	0,061533	-62,18
1,150	0,299458	-144,83	1,692	0,050251	-55,93	1,150	0,299917	-145,23	1,805	0,052869	-59,54
1,200	0,291456	-141,48	1,693	0,050727	-56,10	1,200	0,291924	-141,89	1,810	0,047620	-58,03
1,250	0,283927	-138,28	1,694	0,051230	-56,28	1,250	0,284406	-138,72	1,820	0,040970	-56,26
1,300	0,276832	-135,28	1,695	0,005747	-43,45	1,300	0,277320	-135,73	1,830	0,036860	-55,30
1,350	0,270133	-132,47	1,700	0,005701	-43,55	1,350	0,270630	-132,94	1,840	0,033959	-54,72
1,400	0,263798	-129,84	1,710	0,005605	-43,74	1,400	0,264303	-130,33	1,850	0,031745	-54,36
1,450	0,257798	-127,29	1,720	0,005527	-43,92	1,450	0,258311	-127,80	1,900	0,025210	-53,93
1,500	0,252107	-124,93	1,730	0,136165	-85,90	1,500	0,252628	-125,47	1,950	0,021810	-54,44
1,510	0,251003	-124,48	1,740	0,005385	-44,30	1,550	0,246767	-123,15	2,000	0,019598	-55,31
1,520	0,249875	-124,02	1,750	0,005319	-44,50	1,600	0,239975	-120,59	2,050	0,018005	-56,37
1,530	0,248675	-123,55	1,800	0,005022	-45,48	1,610	0,234597	-118,83	2,100	0,016780	-57,55
1,540	0,247467	-123,07	1,850	0,004787	-46,49	1,620	0,229145	-117,05	2,150	0,015795	-58,81
1,542	0,247226	-122,98	1,900	0,004582	-47,53	1,630	0,223612	-115,24	2,200	0,014981	-60,15
1,543	0,247105	-122,93	1,950	0,004400	-48,60	1,640	0,217993	-113,40	2,250	0,014289	-61,54
1,544	0,009897	-41,30	2,000	0,004243	-49,69	1,650	0,212280	-111,53	2,300	0,013723	-62,97
1,545	0,010024	-41,34	2,050	0,004103	-50,80	1,660	0,206466	-109,63	2,350	0,013237	-64,43
1,550	0,009190	-41,27	2,100	0,003980	-51,94	1,670	0,200541	-107,69	2,400	0,012812	-65,93
1,560	0,008523	-41,32	2,150	0,003860	-53,11	1,675	0,197535	-106,71	2,450	0,012434	-67,45
1,570	0,008042	-41,42	2,200	0,003753	-54,29	1,690	0,188297	-103,69	2,500	0,012096	-69,00
1,580	0,007669	-41,54	2,250	0,003652	-55,50	1,700	0,181910	-101,61	2,550	0,011786	-70,59
1,590	0,007363	-41,67	2,300	0,003558	-56,72	1,710	0,175312	-99,45	2,600	0,011505	-72,19
1,600	0,007105	-41,82	2,350	0,003468	-57,98	1,720	0,168483	-97,22			
1,610	0,006880	-41,97	2,400	0,003384	-59,25	1,730	0,161414	-94,91			
1,620	0,006681	-42,13	2,450	0,003305	-60,54	1,740	0,154073	-92,52			
1,630	0,006503	-42,30	2,500	0,003230	-61,86	1,745	0,150277	-91,28			
1,640	0,006356	-42,47	2,550	0,003157	-63,20	1,750	0,146354	-90,00			
1,642	0,006328	-42,50	2,600	0,003088	-64,55	1,755	0,142298	-88,67			
1,643	0,006315	-42,52				1,760	0,137367	-87,04			

Q3D LedaFlow						Q3D LedaFlow		
Usl/Usg 0.01%						Usl/Usg 0.1%		
High interface level gradient			Low interface level gradient			High interface level gradient		
Usg	Holdup	Pressure Gradient	Usg	Holdup Lowgrad	Pressure Gradient	Usg	Holdup	Pressure Gradient
1,400	0,345755	-167,57						
1,500	0,330307	-165,29				1,500	0,329796	-164,68
1,600	0,308884	-157,53	1,600	0,302491	-156,38	1,600	0,299064	-153,76
1,700	0,282905	-149,02	1,700	0,282350	-150,59	1,700	0,279927	-148,09
1,800	0,267093	-145,87	1,800	0,260166	-139,72	1,800	0,269925	-145,94
1,900	0,247382	-139,05	1,900	0,247224	-141,85			
2,000	0,230015	-133,15	2,000	0,215336	-127,27			
2,100	0,201023	-123,39						
2,200	0,180321	-111,21						

Profile Model LedaFlow						Profile Model LedaFlow					
Usl/Usg 0.01%						Usl/Usg 0.1%					
Grid nodes: 1x75			Grid nodes: 1x2000			Grid nodes: 1x75			Grid nodes: 1x2000		
Usg	Holdup	Pressure Gradient	Usg	Holdup	Pressure Gradient	Usg	Holdup	Pressure Gradient	Usg	Holdup	Pressure Gradient
2,60	0,000216	-178,22	2,60	0,000433	-105,44	2,60	0,001832	-121,44	2,60	0,003823	-87,17
2,50	0,000219	-168,83	2,50	0,000475	-98,75	2,50	0,001839	-115,84	2,50	0,003891	-83,04
2,40	0,000229	-158,03	2,40	0,000483	-93,82	2,40	0,001867	-110,08	2,40	0,003985	-78,87
2,30	0,000242	-147,62	2,30	0,000500	-88,65	2,30	0,001772	-105,16	2,30	0,004059	-75,06
2,20	0,000256	-137,58	2,20	0,000558	-82,72	2,20	0,001772	-99,87	2,20	0,004134	-71,33
2,10	0,000260	-129,57	2,10	0,000568	-78,34	2,10	0,001806	-94,44	2,10	0,004153	-67,83
2,00	0,000276	-120,21	2,00	0,000583	-73,85	2,00	0,001828	-89,42	2,00	0,004093	-64,40
1,90	0,000296	-111,26	1,90	0,000656	-68,81	1,90	0,000121	-135,61	1,90	0,002816	-62,57
1,80	0,000248	-107,81	1,80	0,000674	-64,81	1,80	0,001819	-79,39	1,80	0,063602	-66,33
1,70	0,000298	-96,73	1,70	0,000706	-60,78	1,70	0,103808	-77,51	1,70	0,058839	-62,58
1,60	0,000528	-82,21	1,60	0,056758	-59,83	1,60	0,094283	-72,16	1,60	0,054726	-59,05
1,50	NaN	NaN	1,50	0,055877	-56,95	1,50	0,086518	-68,12	1,50	0,052896	-56,52
1,40	0,000041	-103,64	1,40	0,051035	-53,64	1,40	0,077196	-63,29	1,40	0,051549	-53,64
1,30	0,076305	-61,28	1,30	0,045235	-50,04	1,30	0,076745	-60,96	1,30	0,040440	-49,17
1,20	0,075496	-59,01	1,20	0,047385	-48,62	1,20	NaN	NaN	1,20	0,038860	-46,57
1,10	0,453525	-210,53	1,10	NaN	NaN	1,10	0,546260	-259,65	1,10	0,042551	-45,36
1,00	0,000045	-59,29	1,00	0,036596	-42,25	1,00	0,001939	-43,54	1,00	0,029324	-40,78
0,90	0,057210	-48,30	0,90	0,030344	-39,09	0,90	0,068046	-52,03	0,90	0,687833	-31,70
0,80	0,055145	-45,60	0,80	0,035741	-38,66	0,80	0,076003	-51,22	0,80	0,038996	-37,75
0,70	0,002666	-35,69	0,70	0,037695	-37,78	0,70	0,051324	-42,61	0,70	NaN	NaN
0,60	0,017203	-32,66	0,60	0,028256	-33,89	0,60	0,037270	-36,63	0,60	0,037181	-36,97
0,50	0,000235	-29,90	0,50	0,834558	-374,40	0,50	0,000002	-28,78	0,50	0,758825	-320,63
0,40	NaN	NaN	0,40	0,880962	-391,96	0,40	0,817544	-356,43	0,40	0,874998	-390,28
0,30	0,891047	-393,24	0,30			0,30	0,898191	-396,42	0,30	0,892108	-393,29
0,20	NaN	NaN				0,20	0,941500	-411,10			
0,10	NaN	NaN				0,10	0,961582	-414,71			
0,09	0,964340	-415,22				0,09	0,962550	-415,02			
0,08	0,969538	-416,40				0,08	0,968786	-415,77			

2D Fluent						2D Fluent					
Usl/Usg 0.01%						Usl/Usg 0.1%					
High Holdup Mesh			Low Holdup Mesh			High Holdup Mesh			Low Holdup Mesh		
Usg	Holdup	Pressure Gradient	Usg	Holdup	Pressure Gradient	Usg	Holdup	Pressure Gradient	Usg	Holdup	Pressure Gradient
0,75	0,637540	-193,42	1,50	0,004793	-11,67	0,75	0,633749	-187,07	1,40	0,022874	-15,51
0,80	0,607009	-168,71	1,55	0,004538	-12,29	0,80	0,606096	-168,92	1,45	0,021449	-16,25
0,85	0,589911	-166,97	1,60	0,004600	-13,55	0,85	0,589666	-168,00	1,50	0,019304	-15,74
0,90	0,570501	-172,28	1,65	0,004459	-14,40	0,90	0,572339	-168,79	1,55	0,018684	-16,79
0,95	0,540010	-160,30	1,70	0,004514	-15,05	0,95	0,540533	-158,58	1,60	0,017797	-17,88
1,00	0,522719	-155,65	1,75	0,004501	-16,10	1,00	0,523738	-157,52	1,65	0,017597	-18,97
1,05	0,489057	-139,92	1,80	0,004392	-17,07	1,05	0,488102	-137,37	1,70	0,017084	-19,77
1,10	0,456915	-140,94	1,85	0,004424	-17,97	1,10	0,458977	-141,56	1,75	0,016992	-20,58
1,15	0,439349	-138,13	1,90	0,004326	-18,85	1,15	0,441328	-129,99	1,80	0,016517	-21,69
1,20	0,423143	-114,89	1,95	0,004284	-19,16	1,20	0,420251	-125,44	1,85	0,014794	-20,54
1,25	0,404988	-118,31	2,00	0,004209	-20,13	1,25	0,407730	-121,77	1,90	0,014587	-21,52
1,30	0,381690	-116,22	2,05	0,003980	-21,32	1,30	0,380019	-117,48	1,95	0,014329	-22,88
1,35	0,373916	-120,03	2,10	0,003902	-22,05	1,35	0,372869	-108,06	2,00	0,014186	-24,21
1,40	0,352316	-106,21	2,15	0,004020	-24,20	1,40	0,359757	-110,54	2,05	0,013960	-24,91
1,45	0,337445	-98,34	2,20	0,003854	-25,66	1,45	0,336741	-103,35	2,10	0,013904	-25,59
1,50	0,324974	-94,57	2,25	0,003872	-26,89	1,50	0,320083	-96,69	2,15	0,013717	-27,22
1,55	0,308251	-96,04	2,30	0,004089	-28,22	1,55	0,309211	-92,76	2,20	0,013681	-29,19
1,60	0,277372	-83,79	2,35	0,003853	-29,53	1,60	0,279323	-84,54	2,25	0,013514	-30,14
1,65	0,274043	-84,57	2,40	0,003864	-31,01	1,65	0,268469	-82,46	2,30	0,013359	-29,92
1,70	0,255119	-77,06	2,45	0,003744	-32,25	1,70	0,254847	-80,80	2,35	0,013214	-33,32
1,75	0,220459	-61,89	2,50	0,003907	-33,68	1,75	0,237879	-77,35	2,40	0,013104	-35,32
1,80	0,206480	-65,12	2,55	0,003907	-33,68	1,80	0,208213	-58,96	2,45	0,012945	-33,36
1,85	0,170220	-52,51	2,60	0,003731	-36,11	1,85	0,174746	-55,05	2,50	0,012798	-36,85
1,90	0,021890	-25,62				1,90	0,024404	-25,82	2,55	0,012728	-39,29
									2,60	0,012582	-40,79

3D Fluent						3D Fluent					
Usl/Usg 0.01%						Usl/Usg 0.1%					
High Holdup Mesh			Low Holdup Mesh			High Holdup Mesh			Low Holdup Mesh		
Usg	Holdup	Pressure Gradient	Usg	Holdup	Pressure Gradient	Usg	Holdup	Pressure Gradient	Usg	Holdup	Pressure Gradient
0,75	0,599520	-173,97				0,75	0,599971	-174,93	1,30	0,009656	-24,09
0,80	0,572807	-164,05				0,80	0,572849	-173,87	1,40	0,008931	-25,35
0,85	0,546001	-169,66				0,85	0,546862	-163,74	1,50	0,008167	-24,35
0,90	0,526981	-157,09				0,90	0,528212	-155,71	1,60	0,007355	-28,15
0,95	0,502693	-149,85				0,95	0,509422	-156,01	1,70	0,006431	-28,12
1,00	0,479706	-143,71				1,00	0,480518	-145,69	1,80	0,006431	-32,45
1,05	0,448294	-127,52				1,05	0,451691	-129,80	2,00	0,004232	-39,99
1,10	0,418528	-125,43				1,10	0,427833	-130,64	2,20	0,003679	-48,33
1,15	0,406099	-123,01				1,15	0,407754	-121,29	2,40	0,003983	-51,13
1,20	0,385943	-118,03				1,20	0,387441	-119,22	2,60	0,003992	-60,16
1,25	0,366866	-109,47				1,25	0,367746	-108,33			
1,30	0,343106	-102,46				1,30	0,341897	-106,98			
1,35	0,309745	-96,41				1,35	0,324342	-102,90			
1,40	0,294379	-100,78				1,40	0,292652	-90,11			
1,45	0,266132	-85,69				1,45	0,269812	-92,87			
1,50	0,201426	-65,91				1,50	0,177753	-59,91			
1,55	0,147115	-50,35				1,55	0,145331	-49,96			
1,60	0,149219	-52,62				1,60	0,147909	-52,33			
1,65	0,116492	-43,74				1,65	0,055719	-27,14			
1,70	0,102438	-44,18				1,70	0,027568	-19,54			
1,75	0,070774	-38,93				1,75	0,005113	-15,66			
1,80	0,018494	-30,29									
1,85	0,001094	-15,41									

TD Model											
LL=0.1%											
Blue solution			Green solution			Blue solution			Green solution		
Usg	Holdup	Pressure Gradient	Usg	Holdup	Pressure Gradient	Usg	Holdup	Pressure Gradient	Usg	Holdup	Pressure Gradient
			2,15	0,610731	-140,67	3,85	0,008664	-106,81	5,55	0,007176	-231,04
0,50	0,865905	-69,35	2,20	0,603736	-141,99	3,90	0,008559	-110,04	5,60	0,007158	-235,18
0,55	0,856516	-72,89	2,25	0,596751	-143,27	3,95	0,008462	-113,29	5,65	0,007142	-239,35
0,60	0,847352	-76,26	2,30	0,589773	-144,52	4,00	0,008373	-116,57	5,70	0,007125	-243,55
0,65	0,838387	-79,48	2,35	0,582801	-145,74	4,05	0,008291	-119,86	5,75	0,007110	-247,78
0,70	0,829598	-82,56	2,40	0,575832	-146,92	4,10	0,008215	-123,17	5,80	0,007095	-252,04
0,75	0,820968	-85,52	2,45	0,568865	-148,07	4,15	0,008145	-126,51	5,85	0,007080	-256,32
0,80	0,812481	-88,38	2,50	0,561898	-149,19	4,20	0,008079	-129,88	5,90	0,007066	-260,64
0,85	0,804125	-91,13	2,55	0,554929	-150,27	4,25	0,008018	-133,27	5,95	0,007052	-264,98
0,90	0,795887	-93,78	2,60	0,547954	-151,32	4,30	0,007960	-136,68	6,00	0,007039	-269,35
0,95	0,787757	-96,35	2,65	0,540974	-152,34	4,35	0,007906	-140,13			
1,00	0,779728	-98,84	2,70	0,533984	-153,32	4,40	0,007855	-143,59	3,25	0,015955	-63,65
1,05	0,771790	-101,25	2,75	0,526983	-154,28	4,45	0,007807	-147,09	3,30	0,018838	-63,63
1,10	0,763937	-103,59	2,80	0,519970	-155,20	4,50	0,007762	-150,61	3,35	0,021013	-64,51
1,15	0,756163	-105,86	2,85	0,512940	-156,08	4,55	0,007719	-154,16	3,40	0,023035	-65,68
1,20	0,748461	-108,07	2,90	0,505893	-156,94	4,60	0,007679	-157,73	3,45	0,025017	-67,03
1,25	0,740826	-110,21	2,95	0,498824	-157,75	4,65	0,007640	-161,34	3,50	0,027008	-68,51
1,30	0,733254	-112,30	3,00	0,491732	-158,54	4,70	0,007603	-164,97	3,55	0,029036	-70,10
1,35	0,725740	-114,33	3,05	0,484614	-159,29	4,75	0,007568	-168,63	3,60	0,031121	-71,77
1,40	0,718280	-116,31	3,10	0,477467	-160,01	4,80	0,007535	-172,32	3,65	0,033280	-73,52
1,45	0,710871	-118,24	3,15	0,470287	-160,69	4,85	0,007503	-176,03	3,70	0,035525	-75,36
1,50	0,703508	-120,11	3,20	0,463071	-161,33	4,90	0,007473	-179,78	3,75	0,037871	-77,27
1,55	0,696188	-121,95	3,25	0,013206	-66,58	4,95	0,007444	-183,55	3,80	0,040332	-79,25
1,60	0,688909	-123,73	3,30	0,011719	-71,02	5,00	0,007417	-187,35	3,85	0,042921	-81,31
1,65	0,681666	-125,47	3,35	0,011008	-74,63	5,05	0,007390	-191,18	3,90	0,045657	-83,44
1,70	0,674459	-127,17	3,40	0,010522	-78,01	5,10	0,007365	-195,04	3,95	0,048556	-85,66
1,75	0,667283	-128,82	3,45	0,010152	-81,28	5,15	0,007340	-198,92	4,00	0,051641	-87,96
1,80	0,660136	-130,44	3,50	0,009855	-84,50	5,20	0,007317	-202,84	4,05	0,054936	-90,36
1,85	0,653016	-132,01	3,55	0,009607	-87,69	5,25	0,007294	-206,78	4,10	0,058472	-92,86
1,90	0,645920	-133,55	3,60	0,009396	-90,87	5,30	0,007273	-210,75	4,15	0,062287	-95,47
1,95	0,638847	-135,04	3,65	0,009213	-94,04	5,35	0,007252	-214,75	4,20	0,066429	-98,20
2,00	0,631793	-136,51	3,70	0,009052	-97,22	5,40	0,007232	-218,78	4,25	0,070960	-101,08
2,05	0,624757	-137,93	3,75	0,008909	-100,40	5,45	0,007212	-222,84	4,30	0,075964	-104,12
2,10	0,617737	-139,32	3,80	0,008780	-103,60	5,50	0,007194	-226,92	4,35	0,081557	-107,38

TD Model						TD Model					
LL=0.1%						LL=0.01%					
Usg	Holdup	Pressure Gradient	Usg	Holdup	Pressure Gradient	Usg	Holdup	Pressure Gradient	Usg	Holdup	Pressure Gradient
Cont. Green solution			1,60	0,001001	-20,26	4,70	0,000676	-177,36	3,20	0,024353	-55,11
4,40	0,087875	-110,88	1,65	0,000952	-21,92	4,75	0,000676	-180,86	3,25	0,025690	-56,81
4,45	0,095178	-114,71	1,70	0,000916	-23,58	4,80	0,000675	-184,39	3,30	0,027091	-58,53
4,50	0,103997	-119,03	1,75	0,000889	-25,24	4,85	0,000675	-187,96	3,35	0,028562	-60,30
4,55	0,115387	-124,15	1,80	0,000866	-26,92	4,90	0,000674	-191,55	3,40	0,030106	-62,10
4,60	0,132886	-131,15	1,85	0,000848	-28,62	4,95	0,000674	-195,17	3,45	0,031728	-63,94
Red solution			1,90	0,000832	-30,35	5,00	0,000674	-198,82	3,50	0,033434	-65,83
3,25	0,455816	-161,94	1,95	0,000818	-32,11	5,05	0,000673	-202,50	3,55	0,035229	-67,75
3,30	0,448517	-162,51	2,00	0,000807	-33,90	5,10	0,000673	-206,21	3,60	0,037121	-69,72
3,35	0,441170	-163,04	2,05	0,000796	-35,71	5,15	0,000672	-209,95	3,65	0,039117	-71,74
3,40	0,433771	-163,52	2,10	0,000787	-37,56	5,20	0,000672	-213,71	3,70	0,041226	-73,81
3,45	0,426314	-163,97	2,15	0,000779	-39,44	5,25	0,000672	-217,51	3,75	0,043457	-75,93
3,50	0,418795	-164,38	2,20	0,000772	-41,35	5,30	0,000671	-221,33	3,80	0,045821	-78,10
3,55	0,411206	-164,74	2,25	0,000765	-43,29	5,35	0,000671	-225,19	3,85	0,048333	-80,34
3,60	0,403541	-165,05	2,30	0,000759	-45,27	5,40	0,000671	-229,07	3,90	0,051006	-82,64
3,65	0,395793	-165,32	2,35	0,000754	-47,27	5,45	0,000670	-232,98	3,95	0,053859	-85,02
3,70	0,387953	-165,53	2,40	0,000749	-49,31	5,50	0,000670	-236,92	4,00	0,056914	-87,47
3,75	0,380012	-165,69	2,45	0,000744	-51,38	5,55	0,000670	-240,89	4,05	0,060196	-90,01
3,80	0,371958	-165,80	2,50	0,000740	-53,49	5,60	0,000669	-244,89	4,10	0,063738	-92,64
3,85	0,363779	-165,84	2,55	0,000736	-55,62	5,65	0,000669	-248,92	4,15	0,067581	-95,39
3,90	0,355461	-165,81	2,60	0,000732	-57,79	5,70	0,000669	-252,97	4,20	0,071775	-98,26
3,95	0,346986	-165,72	2,65	0,000729	-59,99	5,75	0,000669	-257,05	4,25	0,076391	-101,28
4,00	0,338334	-165,55	2,70	0,000726	-62,22	5,80	0,000668	-261,17	4,30	0,081521	-104,48
4,05	0,329481	-165,29	2,75	0,000723	-64,49	5,85	0,000668	-265,31	4,35	0,087301	-107,89
4,10	0,320397	-164,95	2,80	0,000720	-66,79	5,90	0,000668	-269,48	4,40	0,093936	-111,59
4,15	0,311045	-164,49	2,85	0,000717	-69,12	5,95	0,000668	-273,67	4,45	0,101767	-115,67
4,20	0,301378	-163,92	2,90	0,000715	-71,48	6,00	0,000667	-277,90	4,50	0,111450	-120,34
4,25	0,291335	-163,21	2,95	0,000713	-73,87	Green solution			4,55	0,124603	-126,10
4,30	0,280835	-162,33	3,00	0,000711	-76,30	1,50	0,001686	-15,29	4,60	0,150586	-135,77
4,35	0,269761	-161,25	3,05	0,000709	-78,76	1,55	0,002091	-15,62	Red solution		
4,40	0,257943	-159,93	3,10	0,000707	-81,25	1,60	0,002432	-16,22	1,50	0,703445	-120,07
4,45	0,245109	-158,26	3,15	0,000705	-83,77	1,65	0,002763	-16,93	1,55	0,696121	-121,89
4,50	0,230771	-156,12	3,20	0,000703	-86,33	1,70	0,003099	-17,71	1,60	0,688837	-123,68
4,55	0,213875	-153,17	3,25	0,000702	-88,91	1,75	0,003444	-18,53	1,65	0,681591	-125,41
4,60	0,190882	-148,35	3,30	0,000700	-91,53	1,80	0,003797	-19,40	1,70	0,674378	-127,11
TD Model			3,35	0,000699	-94,18	1,85	0,004159	-20,30	1,75	0,667197	-128,76
LL=0.01%			3,40	0,000697	-96,86	1,90	0,004539	-21,23	1,80	0,660045	-130,37
Usg	Holdup	Pressure Gradient	3,45	0,000696	-99,57	1,95	0,004939	-22,20	1,85	0,652920	-131,94
Blue solution			3,50	0,000695	-102,31	2,00	0,005358	-23,19	1,90	0,645819	-133,47
0,50	0,865895	-69,34	3,55	0,000693	-105,09	2,05	0,005799	-24,21	1,95	0,638740	-134,97
0,55	0,856505	-72,88	3,60	0,000692	-107,89	2,10	0,006262	-25,26	2,00	0,631680	-136,43
0,60	0,847339	-76,24	3,65	0,000691	-110,73	2,15	0,006747	-26,34	2,05	0,624638	-137,85
0,65	0,838371	-79,46	3,70	0,000690	-113,60	2,20	0,007256	-27,44	2,10	0,617612	-139,23
0,70	0,829581	-82,55	3,75	0,000689	-116,50	2,25	0,007790	-28,57	2,15	0,610599	-140,58
0,75	0,820949	-85,51	3,80	0,000688	-119,43	2,30	0,008350	-29,72	2,20	0,603597	-141,89
0,80	0,812460	-88,36	3,85	0,000687	-122,39	2,35	0,008937	-30,90	2,25	0,596604	-143,17
0,85	0,804101	-91,11	3,90	0,000686	-125,38	2,40	0,009551	-32,11	2,30	0,589619	-144,42
0,90	0,795861	-93,76	3,95	0,000686	-128,40	2,45	0,010195	-33,34	2,35	0,582638	-145,63
0,95	0,787729	-96,33	4,00	0,000685	-131,45	2,50	0,010868	-34,60	2,40	0,575661	-146,81
1,00	0,779697	-98,81	4,05	0,000684	-134,54	2,55	0,011574	-35,88	2,45	0,568685	-147,95
1,05	0,771757	-101,22	4,10	0,000683	-137,65	2,60	0,012312	-37,19	2,50	0,561709	-149,06
1,10	0,763901	-103,56	4,15	0,000683	-140,79	2,65	0,013084	-38,53	2,55	0,554729	-150,14
1,15	0,756124	-105,83	4,20	0,000682	-143,97	2,70	0,013892	-39,89	2,60	0,547745	-151,19
1,20	0,748419	-108,03	4,25	0,000681	-147,17	2,75	0,014738	-41,28	2,65	0,540753	-152,20
1,25	0,740781	-110,18	4,30	0,000681	-150,40	2,80	0,015622	-42,70	2,70	0,533752	-153,18
1,30	0,733206	-112,26	4,35	0,000680	-153,67	2,85	0,016547	-44,15	2,75	0,526740	-154,12
1,35	0,725688	-114,29	4,40	0,000679	-156,96	2,90	0,017516	-45,62	2,80	0,519713	-155,04
1,40	0,718225	-116,27	4,45	0,000679	-160,29	2,95	0,018529	-47,13	2,85	0,512671	-155,92
1,45	0,710811	-118,19	4,50	0,000678	-163,64	3,00	0,019589	-48,66	2,90	0,505609	-156,76
1,50	0,001227	-16,65	4,55	0,000678	-167,03	3,05	0,020699	-50,23	2,95	0,498526	-157,57
1,55	0,001074	-18,56	4,60	0,000677	-170,44	3,10	0,021861	-51,82	3,00	0,491418	-158,35
			4,65	0,000677	-173,88	3,15	0,023078	-53,45	3,05	0,484283	-159,09

TD Model

LL=0.01%

Usg	Holdup	Pressure Gradient
Cont. Red solution		
3,10	0,477118	-159,80
3,15	0,469920	-160,47
3,20	0,462684	-161,10
3,25	0,455407	-161,70
3,30	0,448086	-162,26
3,35	0,440714	-162,78
3,40	0,433289	-163,25
3,45	0,425804	-163,69
3,50	0,418255	-164,08
3,55	0,410633	-164,42
3,60	0,402933	-164,72
3,65	0,395146	-164,97
3,70	0,387264	-165,17
3,75	0,379277	-165,31
3,80	0,371172	-165,39
3,85	0,362937	-165,41
3,90	0,354555	-165,36
3,95	0,346010	-165,23
4,00	0,337278	-165,03
4,05	0,328334	-164,74
4,10	0,319145	-164,35
4,15	0,309670	-163,85
4,20	0,299857	-163,22
4,25	0,289638	-162,44
4,30	0,278917	-161,48
4,35	0,267561	-160,30
4,40	0,255364	-158,84
4,45	0,241983	-156,99
4,50	0,226765	-154,55
4,55	0,208088	-151,03
4,60	0,176595	-143,59

Bibliography

- [1] ANSYS Fluent - <https://www.sharenet.ca/software/fluent12/pdf/th/flth.pdf>.
- [2] ANSYS Fluent - <http://www.ansys.com/products/simulation+technology/fluid+dynamics/ansys+fluent>.
- [3] LedaFlow - <http://www.kongsberg.com/en/kogt/offerings/software/ledaflow/>.
- [4] OLGA - <http://www.sptgroup.com/en/products/olga/>.
- [5] E. Andersen and O. Førde. Simulations and experiments in bubble driven flow. *NTNU*, 2011.
- [6] N. Andritsos and T. Hanratty. Influence of interfacial waves in stratified gas-liquid flows. *AIChE journal*, 33(3):444–454, 1987.
- [7] A. Ashrafian and S. Johansen. Wall boundary conditions for rough walls. *Progress in Computational Fluid Dynamics, an International Journal*, 7(2):230–236, 2007.
- [8] A. Ashrafian, S. Mo, S. Johansen, J. Kjølaas, W. Dijkhuizen, D. Darama, E. Meese, K. Bansal, T. Danielson, and M. Stinessen. Multidimensional modeling of stratified wavy three-phase flows. *Rio Pipeline Conference & Exposition*, September 20-22, 2011.
- [9] A. Baker and N. Gravestock. New correlations for predicting pressure loss and holdup in gas/condensate pipelines. In *Proceedings 3rd Int. Conf. Multi-Phase Flow*, pages 13–20, 1987.
- [10] D. Barnea. On the effect of viscosity on stability of stratified gas–liquid flow—application to flow pattern transition at various pipe inclinations. *Chemical engineering science*, 46(8):2123–2131, 1991.
- [11] D. Barnea and Y. Taitel. Structural and interfacial stability of multiple solutions for stratified flow. *International journal of multiphase flow*, 18(6):821–830, 1992.

- [12] D. Barnea and Y. Taitel. Kelvin-helmholtz stability criteria for stratified flow: viscous versus non-viscous (inviscid) approaches. *International journal of multiphase flow*, 19(4):639–649, 1993.
- [13] D. Barnea and Y. Taitel. Interfacial and structural stability of separated flow. *International journal of multiphase flow*, 20:387–414, 1994.
- [14] D. Barnea and Y. Taitel. Structural stability of stratified flow-the two-fluid model approach. *Chemical engineering science*, 49(22):3757–3764, 1994.
- [15] K. Bendiksen, D. Maines, R. Moe, and S. Nuland. The dynamic two-fluid model olga: Theory and application. *SPE production Engineering*, 6(2):171–180, 1991.
- [16] N. Brauner and D. Moalem Maron. Stability analysis of stratified liquid-liquid flow. *International journal of multiphase flow*, 18(1):103–121, 1992.
- [17] T. Danielson, K. Bansal, C. Djoric, D. Larrey, S. Johansen, A. De Leebeeck, and J. Kjølås. Simulation of slug flow in oil and gas pipelines using a new transient simulator. In *Offshore Technology Conference*, 2012.
- [18] T. Danielson, R. Hansen, and E. Leporcher. Leda: the next multiphase flow performance simulator. In *BHR Group Multiphase Production Technology Conference*, 2005.
- [19] W. Dijkhuizen, A. Ashrafiyan, S. Mo, S. Johansen, E. Meese, K. Bansal, T. Danielson, A. Goldszal, and B. K. Monsen. Multidimensional simulation of multiphase pipe flows with high liquid viscosity. *Presentation at International Conference on Multiphase Flow 2010 (ICMF-2010), Tampa, FL, USA, May 30 - June 4, 2010*.
- [20] A. Goldszal, J. Monsen, T. Danielson, K. Bansal, Z. Yang, S. Johansen, and G. Depay. Ledaflow-1d: Simulation results with multiphase gas/condensate and oil/gas field data. *BHRG Multiphase Production Technology Conference, Edinburgh, UK, 13-15 June, 2007*.
- [21] P. Johansson. Non-unique holdup solutions for inclined two phase flow - artefact or reality? 2012.
- [22] J. Kjølås, S. Johansen, Y. Ladam, R. Belt, T. Danielson, and M. Stinnesen. Modeling of the droplet field in near-horizontal low liquid loading flows. *BHR Group's Multiphase Production Technology Conference in Cannes*, 2011.
- [23] M. Landman. Non-unique holdup and pressure drop in two-phase stratified inclined pipe flow. *International journal of multiphase flow*, 17(3):377–394, 1991.

- [24] B. Launder, G. Reece, and W. Rodi. Progress in the development of a reynolds-stress turbulence closure. *Journal of fluid mechanics*, 68(03):537–566, 1975.
- [25] H. Laux, E. Meese, S. Mo, S. Johansen, K. Bansal, T. Danielson, A. Goldszal, and J. Monsen. Multi-dimensional simulations of slug and slug-like flows in inclined pipes and channels. LedaFlow, XXX.
- [26] H. Laux, E. Meese, S. Mo, T. Unander, S. Johansen, K. Bansal, T. Danielson, A. Goldszal, and J. Monsen. Multidimensional simulations of multiphase flow for improved design and management of production and processing operation. In *Offshore Technology Conference*, 2008.
- [27] R. Lockhart and R. Martinelli. Proposed correlation of data for isothermal two-phase, two-component flow in pipes. *Chemical Engineering Progress*, 45(1):39–48, 1949.
- [28] F. Menter. Two-equation eddy-viscosity turbulence models for engineering applications. *AIAA journal*, 32(8):1598–1605, 1994.
- [29] T. Sira. Hydraulic gradients and shocks in multiphase flow. *IFE Report IFE/KR/F-2007/080*, 2007.
- [30] S. Smith, G. Gregory, and H. Yarranton. Experimental investigation of multiple solutions for liquid holdup in upward inclined stratified flow. *Journal of energy resources technology*, 125:137, 2003.
- [31] Y. Taitel and A. Dukler. A model for predicting flow regime transitions in horizontal and near horizontal gas-liquid flow. *AIChE Journal*, 22(1):47–55, 1976.
- [32] H. Tennekes and J. Lumley. *A first course in turbulence*. The MIT press, 1972.
- [33] A. Ullmann, M. Zamir, S. Gat, and N. Brauner. Multi-holdups in co-current stratified flow in inclined tubes. *International journal of multiphase flow*, 29(10):1565–1581, 2003.
- [34] A. Ullmann, M. Zamir, Z. Ludmer, and N. Brauner. Stratified laminar countercurrent flow of two liquid phases in inclined tubes. *International journal of multiphase flow*, 29(10):1583–1604, 2003.
- [35] F. White. Fluid mechanics. *International Edition, McGraw-Hill*, 1986.